Application of real-time simulation for hydropower plants monitoring

PAR

Michel Sangkyu HAN

EPFL

ÉCOLE POLYTECHNIQUE
FÉDÉRALE DE LAUSANNE

Suisse
2015

Your worth consists in what you are and not in what you have.

— Thomas A. Edison

Remerciements

Avec ces quelques lignes, je tiens à exprimer mes sincères remerciements à toutes les personnes qui ont contribué de manière directe ou indirecte à la finalisation de cette thèse de doctorat.

Ma reconnaissance est en premier lieu tournée vers mon directeur de thèse, le Dr. Basile Kawkabani, qui m'a témoigné de sa confiance en m'offrant l'opportunité d'effectuer ce travail au sein de son groupe. J'aimerais le remercier encore pour sa disponibilité et ses conseils durant les années que j'ai passées sous sa direction.

Ma gratitude est également dirigée vers M. Roland Wetter, qui m'a laissé profiter de sa grande expérience dans le domaine de la métrologie des machines électriques, et sans qui l'organisation des mesures dans la centrale aurait été impossible.

Je désire également remercier le Dr. Christophe Nicolet, membre du jury, ainsi que le Dr. Antoine Béguin pour leur collaboration. Ils ont su me faire profiter de leurs connaissances, expériences et idées durant les réunions. De plus, les mesures finales dans la centrale hydroélectrique n'auraient pas pu aboutir sans leur précieuse aide.

Je tiens à remercier aussi les autres membres du jury, à savoir le Prof. Mario Paolone, Prof. Farhad Rachidi, Prof. Carlos Platero qui ont tous aimablement accepté de consacrer leur temps à la lecture et à l'évaluation du manuscrit.

Ce travail n'aurait pas été possible dans le soutien financier du consortium HydroNET2, ainsi que les contributions de Power Vision Engineering (mise à disposition d'un système de

mesure), Hydro-Exploitation et ALPIQ sans qui les essais dans la centrale de Mottec n'auraient pas été possibles. De plus, le projet a pu être amorcé grâce au système initial de SIMSEN-RT, développé avec la collaboration de VOITH-SIEMENS.

Sur un plan plus personnel, j'aimerais remercier tous mes collègues pour les bons moments passés durant toute la durée du travail. Un tout spécial remerciement à Pedro Silva avec qui j'ai commencé cette thèse de doctorat, et avec qui j'ai partagé les moments difficiles ou sympathiques et surtout avec qui j'ai conclu cette thèse de doctorat.

Je n'oublie pas non plus toutes les personnes qui m'ont soutenu tout au long de ce travail, et en particulier pendant la dernière ligne droite, comme mes collègues ou ami(e)s de l'EPFL ainsi que mes ami(e)s hors campus, qui comptent pour moi. Un grand merci aussi à mes ami(e)s du club de badminton (LUC) avec qui j'ai passé de très bons moments.

부모님께서도 후원을 항상 해주셔서 고맙습니다. 사랑합니다.

Lausanne, 20 Août 2015   HAN Sangkyu Michel

Abstract

The global emission of CO_2 has increased in the sector of power generation from countries outside the OECD, particularly in China which comprises two-third of the share. Meanwhile, OECD countries focus their effort in reducing their emission, where the industry area declined their emission by a quarter.

Consequently, governments set up energy policies where renewable-based energies such as solar or wind energies, are highlighted. The drawback is the dependency of environment factors which generates power variations in the network leading to instabilities and a blackout in the worst case. The use of hydropower is an excellent complement to versatile renewable energy, capable of compensating these fluctuations and even be used as an energy storage. In Switzerland, hydropower is the most available resources and is constantly under development to increase capacity and energy-efficiency. Nevertheless, a lot of effort is put to extend lifetime of power generating equipment as much as possible in order to optimize the best timing for replacement or refurbishment, which requires efficient and flexible tools such as real-time simulations, which are widely used with the rapid development of computation technology.

The objective of this present thesis is the development of a multi-physics model-based real-time monitoring system in SIMSEN for an existing hydroelectric power plant. The concept of such system consists of using a validated model and achieves a real-time simulation taking into account boundary conditions such as water level of upstream reservoir, voltage of power

Abstract

network, but also set point of control system including turbine guide vane opening and the excitation system of generator. The system would enable to detect potential dysfunctions if the behavior of the power plant shows significant discrepancies in the simulation-measurement comparison during the real-time simulation. The study is divided into two main parts, which are the set-up of a test bench and the implementation of the real-time system in the power plant.

The first part describes the methodology for setting-up a small-scale power unit which simulates similar behavior as a large scale one. The model includes the parameters from experimental tests used for parameters identification of synchronous machine. Two validations tests are presented: (i) a load variation (ii) sudden three-phase short circuit. The model validation is achieved comparing offline simulation results with measurement, followed by a validation in real-time with similar tests. The set-up of the test bench is concluded by a demonstration of feasibility in monitoring application by detection of a dysfunction during an opening failure of a circuit-breaker.

The second part explains the modeling of a 72MW hydroelectric power plant, which includes the modeling of hydraulic components such as pipe, surge tank and Pelton turbine besides the modeling of generator. Two measurement campaigns were organized. The first consisted in collecting data in order to validate the present model. The second consisted of implementing the model running in real-time in a general-purpose computer, in the power plant and performed variations of active and reactive powers.

Key words: Real-time simulation, modeling, synchronous machine, hydroelectric power plant, hydraulic modeling, SIMSEN

Résumé

L'émission globale de CO_2 s'est accrue dans le secteur de production d'énergie pour les pays non membres de l'OCDE et plus particulièrement en Chine qui en détient les deux tiers. Entre-temps, les pays membres de l'OCDE ont mis l'accent et leur effort sur la réduction des émissions de CO_2, illustré avec le secteur de l'industrie qui a réussi à réduire d'un quart ces émissions de CO_2.

Par conséquent, les gouvernements ont mis en place une stratégie énergétique en se concentrant sur les énergies renouvelables telles que l'énergie solaire ou éolienne. L'inconvénient de ce type d'énergie est sa dépendance des facteurs environnementaux qui cause des fluctuations de puissances sur le réseau électrique, amenant ainsi à des instabilités, voire un blackout dans le pire des cas. L'utilisation de l'énergie hydraulique est un excellent complément aux énergies renouvelables intermittentes, permettant de compenser ces variations en plus de son utilisation comme stockage d'énergie. En Suisse, l'énergie hydraulique est la plus exploitée dans les centrales qui sont constamment en développement pour accroître leur capacité ou d'améliorer leur rendement. Néanmoins, un effort important est mis sur la prolongation du temps vie, aussi longtemps que possible, des équipements de production d'énergie afin de permettre de déterminer le meilleur moment pour leur rénovation ou remplacement. Ce dernier requiert donc un outil efficace and flexible tel que la simulation en temps-réel qui est largement utilisée avec le développement rapide des technologies de calculs.

Résumé

L'objectif de cette thèse consiste à développer un système de monitoring dans SIMSEN fonctionnant avec une simulation en temps-réel, basée sur un modèle multi-physique d'une centrale hydroélectrique déjà existante. Le concept d'un tel système consiste à simuler en temps-réel un modèle validé en considérant les conditions aux limites telles que le niveau de l'eau dans le barrage en amont, la tension du réseau mais également les points de fonctionnement des systèmes de réglage, comprenant l'ouverture des distributeurs de la turbine et le système d'excitation de la génératrice. Le système pourrait détecter les dysfonctionnements potentiels lorsque le comportement de la centrale montre des écarts importants entre la simulation et la mesure pendant la simulation en temps-réel. L'étude est divisée en deux parties principales qui contient dans un premier temps la mise en place d'un banc test et dans un deuxième temps l'implémentation du système temps réel dans la centrale.

La première partie décrit la méthodologie utilisée pour mettre en place place un groupe de production d'énergie à une échelle de puissance réduite qui, simule le comportement d'un groupe réel. Le modèle comprend les paramètres déterminés à partir de tests expérimentaux d'identification pour une machine synchrone. Les deux cas tests présentés pour sa validation sont : (i) un saut de charge (ii) un court-circuit triphasé brusque. La validation du modèle est effectuée en comparant les résultats des simulations avec les mesures en simulation dite "offline", suivie par une validation temps réel avec des tests similaires. La mise en place du banc test est conclue par une démonstration de faisabilité pour une application de monitoring en détectant la défaillance d'un disjoncteur.

La deuxième partie explique la modélisation d'une centrale hydroélectrique de 72MW, qui comprend des modèles hydrauliques comme les conduites, les cheminées d'équilibre et une turbine Pelton en plus de la modélisation de la génératrice. Deux campagnes de mesure ont été organisées. La première consistait à récupérer des données de mesures afin de valider le modèle considéré. La seconde comprend l'implémentation du modèle, fonctionnant en temps réel sur un ordinateur standard dans la centrale en question et effectuant des variations de puissances active et réactive.

Mots clefs : Simulation temps-réel, modélisation, machine synchrone, centrale hydroélectrique, modélisation hydraulique, SIMSEN

Contents

Contents

List of Figures

List of Tables

1

Introduction

1.1 Situation of energy policies

1.1.1 Energy emission trends

Over the past 25 years, the global emission of CO_2 has increased by more than 50 [%]. The average annual rate of increase between 2000 and 2014 was estimated to 2.3 [%] versus 1.2 [%] in the late 1990s (Figure 1.1). The rapid rise of emission is particularly observed in the power generation sector from countries outside the OECD[1]. The emerging and developing countries have more than doubled their emission coming from electricity and heat generation, especially in China with around two-thirds of this share.

Meanwhile, the total CO_2 emissions from the industry section in OECD countries declined by a quarter although these countries still lead the global emissions in the transportation and buildings sectors. The high level of vehicle ownership in OECD countries justifies the large CO_2 emissions in the transport sector, even though the non-OECD countries doubled their emissions over the past years, resulting from the increase of vehicle ownership and rapid growth of traffic. The building sector is mainly involved by the heating level, which is not

---

[1]Organization for Economic Cooperation and Development
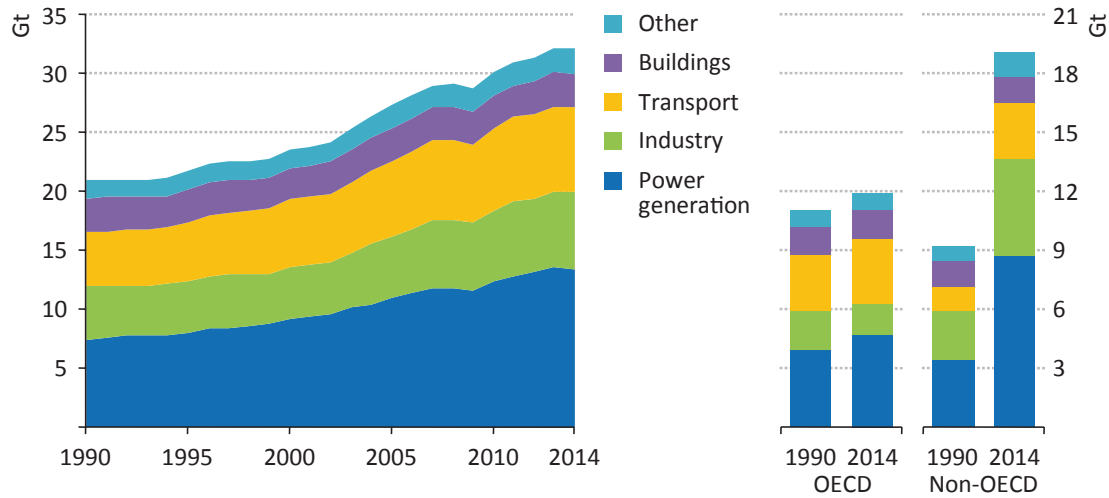
Figure 1.1: Global energy-related CO_2 emissions in gigatonne (Gt) by region and sector [1]

the case for most non-OECD countries since they are located in more temperate climates, requiring a lower level.

1.1.2 Evolution of renewable-based power generation

With the generalization of renewable technologies, their costs are becoming competitive in various countries over the world. In 2014, the power generation capacity was estimated to be enlarged by 128 [GW] from renewable-based technology. Among these renewable energy, 37 [%] is from wind power, almost 20 [%] is from solar power and more than 20 [%] from hydropower. The remaining energy comes from other renewable energy sources, as seen in Figure 1.2.

The growth in wind capacity has kept growing in onshore installations although offshore is expanding rapidly. The largest wind power market remains the China with 20 [GW] of newly added capacity. Germany remains a large market with more than 5 [GW] installed in 2014, however the relatively high cost for offshore wind and delays in the build-up have resulted into delayed projects, biasing the estimation of installed wind power capacity.

Solar photovoltaic (PV) has strongly expended in Asia, and particularly in China and Japan. The expansion of PV in Japan is mainly supported by generous subsidies since the Fukushima incident.

Nuclear power is the worldwide second largest source of low carbon electricity generation after hydropower. In recent years, new nuclear constructions take place in price-regulated market or in markets where government owns the entities and operates the power plants.
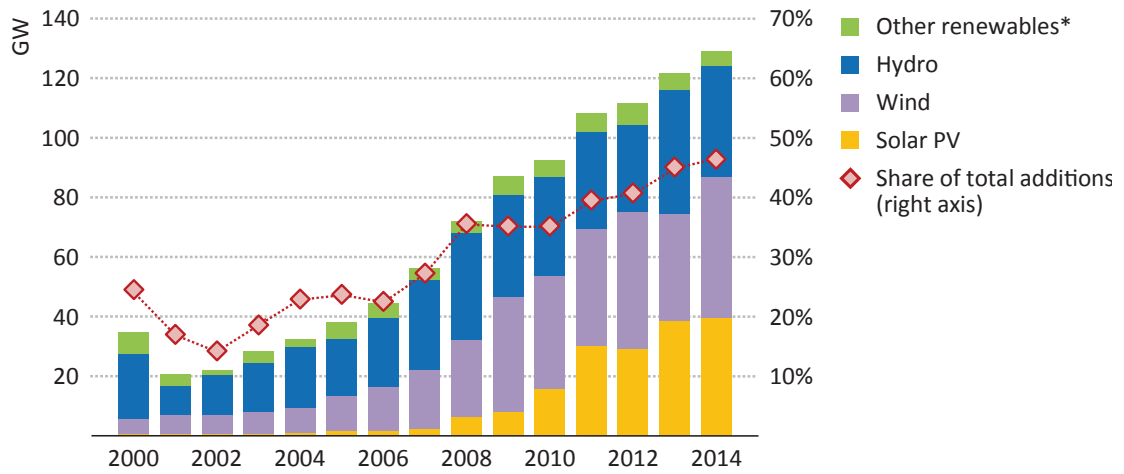
* Includes geothermal, marine, bioenergy and concentrating solar power.

Figure 1.2: Global Renewable-based power capacity [1]

China stays the leader in new capacity additions, with 28 [GW] under construction in 2014
([1]).

1.1.3 Global simulate energy agenda in Switzerland

The Swiss parliament has presented its "Energy Strategy 2050" only two months after the disaster in Fukushima in 2011. The proposal contains modifications in the sectors of transportation and heating in order to fit the European emission standards, and aiming at the same time a rapid change of electricity production.

Since then, Switzerland has participated to the "World Energy Issue Monitor" [2] over the past three years, providing an snapshot of the evolution over time and a high-level perception of energy issues through the impact of an issue on the energy sector (x-axis), the degree of uncertainty related to its impact (y-axis) and the size of the issue bubble represents the degree of urgency that needs to be addressed, as presented in Figure 1.3.

It appears that nuclear has lost weight in term of uncertainty and impact after Fukushima with the abandon of construction of nuclear power plants based on recent technologies.

Electric storage in the hydropower sector is a top priority and a key uncertainty in Switzerland. The water stored in the reservoir has played an important role in power generation for years. However, under the current circumstances, they are no longer profitable. Indeed, the hydropower is the most large and accessible renewable energy source in Switzerland, but the risk is that this potential energy is not harnessed and will hardly be able to compete against other

Figure 1.3: World Energy Issues Monitor 2015 for Switzerland [2]

renewable energy sources, which is highly subsidized. At the same time, the enlargement of storage capacity from existing reservoir lakes will be acknowledged by Swiss citizens.

It is interesting to pay attention that large-scale hydro is not a top action priority in Europe, whereas it is high action topic in Switzerland although electric storage is high uncertainty for both. This discrepancy may come from the need of exploiting the potential of hydropower in Switzerland, whereas Europe perceives electric storage as a tool for intermittent power sources. Consequently, Switzerland has taken an energy-efficiency position in the "need for action" zone.

1.1.4 The importance of hydropower in sustainable development

The desire to move toward green and sustainable energy has therefore driven government and industry to develop renewable-based energy such as solar or wind power. However, these systems cannot guarantee a constant power availability and generation due to the dependency to environmental factors. This intermittent variation of generation constitutes a major issue

Weekly Production Solar
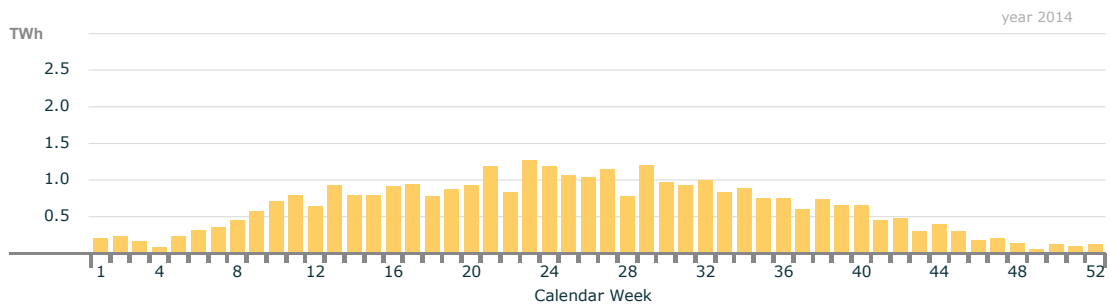
Weekly Production Wind
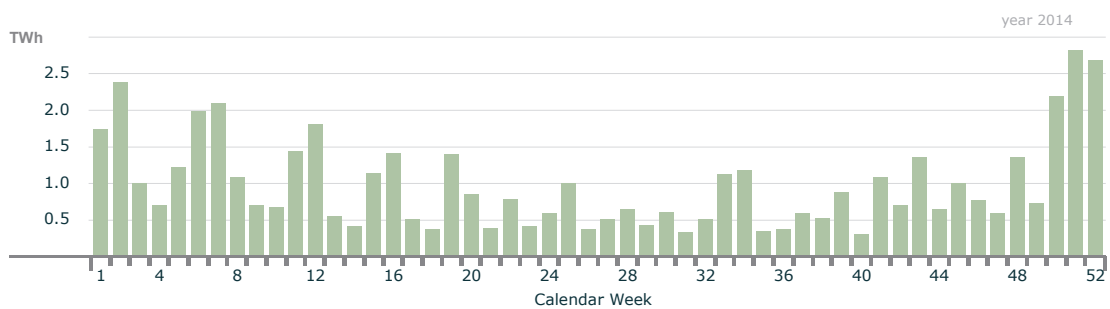
Figure 1.4: Weekly production from solar (top) and wind(bottom) in Germany in 2014 [3]

concerning the dynamic behavior of electric grid, in other words, its stability and reliability. As an example, the electricity production in Germany has recorded an energy fluctuation of 1.2 [TWh] from solar energy against 2.48 [TWh] from wind energy, during the year 2014 (Figure 1.4).

The classification of power generation is categorized in two parts.

- Base load plants - An energy plant devoted to the production of baseload supply. Baseload plants are the production facilities used to meet some or all of a given region's continuous energy demand, and produces energy at a constant rate, usually at a low cost relative to other production facilities available to the system ([10]).

- Peaking load plants - A generating facility operated expressly for the purpose of providing peak energy supply. Peak load plants are typically operated during particular times of day or at times of the year when there is a spike in the demand for energy ([10]).

Considering the intermittency of renewable energy and the peak load criteria, hydropower is the most suitable type of power plant. Indeed, hydropower is a flexible source of power

generation in term of availability and maneuverability for responding to demand fluctuations in active and reactive powers in minutes. Therefore, hydropower is an ideal complement to variable renewables. In addition, pump-storage type of hydro power plants can store energy over seasons or even years depending on the size of the reservoir in order to meet load fluctuations.

The need of hydropower is undeniable and is subject to numerous discussions as seen for the case in Switzerland since the share of energy generation is hydropower. Nevertheless, the investments for the construction of hydroelectric power plants are relatively high, which is profitable with time since it has the longest lifetime among the power plants. Consequently, the standstill due to an upgrade of power capability or breakdown represent a considerable amount of cost according to the scale of the power plant. Various devices are then implemented with the same purpose: protect the electro-mechanical equipment to extend its lifetime, e.g. (i) Power System Stabilizers (PSS): improve the stability of units consecutively to a major electrical fault and reduce inter-area power oscillations; (ii) Protection relays: isolate the generator to prevent serious damages in case of faults; (iii) Monitoring: detect a malfunctioning of a system. Development and design of such systems requires efficient and flexible computation tools.

1.2 Structure of the document

1.2.1 Objective and methodology

The awareness of CO_2 emission against the global warming leads the energy policies to turn toward new energy sources, called renewable. The rapid growth of such technology and its application in the power generation field introduced unstable situations in the power network. Indeed, the versatile production of energy, which mainly depends upon the environment factor, has increased the risk situation where the generation is unable to supply the consumption. In other words, the safe margin has decreased, making the power network potentially unstable. Nevertheless, with the combination of hydropower plants and renewable energy sources, the variation of loads is balanced which improves the reliability of the network.

That being said, the investment cost of such power plants is substantial, depending on the project size. Even though the applied technology has a great maturity with a high level of efficiency, hydroelectric power plants are submitted to various issues, such as components ageing mechanisms ([11]).

- Thermal ageing: This mechanism mainly occurs in the insulation of rotating machines, degrading the electrical and mechanical properties of the insulation when it is exposed

to high temperatures. In addition, temperature cycling can induce mechanical stresses generating deterioration even if the temperature is insufficient to cause damage.

- Electrical ageing: Partial discharges, surface tracking and moisture absorption and transient voltages are considered as electric ageing mechanism. The stress applied to machines insulation induces deterioration leading to faults.

- Mechanical ageing: Mechanical stress is a major contributor to ageing. It is principally produced by relative motions resulting from interaction between mechanical and electromagnetic forces, resonances, intermittent start-up or shutdown and environmental factors that affect the properties.

Such issues are subject to potential risk of breakdowns which may reach 30% of total investment and efforts are placed in systems development of condition monitoring to predict the best timing for maintenance, which is based on model estimation and database used for trend analysis. In order to reduce capitalized losses due to breakdown, as well as the replacement costs, efficient monitoring tools are therefore required to identify abnormalities and failures at their early stage decreasing then the risks.

In this regard, a monitoring system for a hydroelectric power plant is developed in this project. The system is based on real-time simulation model and features the following specifications:

- Simulations performed in SIMSEN on a general-purpose computer;

- Taking into account of boundary conditions measured on the modeled system;

- Monitoring measured quantities in the related model;

- Detection of dysfunctions using a comparative method.

SIMSEN is a time-domain simulation platform developed at EPFL for analyzing multi-physics power systems, including semiconductors and regulation parts under steady-state and transient conditions. Its modular structure allows the built of complex systems and subsystems with an arbitrary topology using libraries of electric and hydraulic models. Moreover, the capability of performing mixed analog-digital simulations leaded to the possibility of interacting with external programs or devices and the development of a real-time extension, SIMSEN-RT, detailed in section 2.2.

The development is organized in two main steps:

i The first part describes the methodology for setting-up a small-scale power unit which simulates similar behavior as a large scale one, yielding a testing platform. A simplified model in SIMSEN is operating to evaluate the real-time capability with a general-purpose PC;

ii The second part explains the modeling of an existing hydroelectric power plant, which includes the modeling of hydraulic components besides the electric installation. The validation of real-time simulation with the plant-related model will prove the feasibility of a monitoring application.
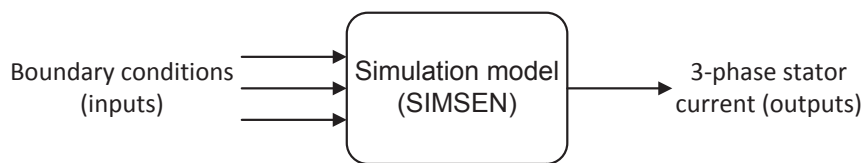
Figure 1.5: Basic diagram of model-based monitoring system

In both parts, the structure of the system remains identical (see Figure 1.5). Indeed, boundary conditions are considered as the inputs of the system and drive the simulation model. The outputs of the monitoring system are the three-phase stator current, in this case, calculated from the model. Therefore, special attention has been focused on the validation with simulation performed in real-time considering boundary conditions as water level of upstream reservoir, voltage of power network, but also set point of control system including turbine guide vane opening and the excitation system of generator of a multi-physics model.

1.2.2 Organization of the document

In this context, the present work is arranged as follows:

Chapter 2 introduces a literature overview of real-time simulation with the recent investigations in various domains of applications. It is followed by an explanation of the concept of real-time and its conditions. The chapter ends with the presentation of the software called SIMSEN.

Chapter 3 presents the applied methodology for setting up a test bench, which simulates the dynamic behavior of a motor-generator unit. In addition, the modeling of the bench is achieved using experimentally estimated parameters. Its validation is carried out using a comparative approach using at first offline simulations results in order to assess the quality of the modeling. Then it is followed by real-time simulations to evaluate the performance

measured data handling, which drives the simulation model. In both situations, two test cases are presented : a load variation and a sudden three-phase short circuit. Finally, a demonstration of a model-based monitoring application is presented to conclude the chapter.

Chapter 4 demonstrates the application of the developed system to a real power plant. A detailed description of the hydroelectric power plant is presented with the modeling of hydraulic main components such as pipe, surge tank and turbine. Some adaptations are then explained such as a simplification of the model for real-time application as well as the development of an interface to make the developed system compatible with the power plant. Then, validations from two measurement campaigns are presented. The first validations consist on the one hand, in evaluating the consistency of results from the simulation models and on the other hand, confirm the accuracy of the simplifications carried out on the validated model for real-time application. The second validations present the results of the power plant model, performed in real-time.

Finally, chapter 5 presents a summary of the presented work. Perspective and improvements are also suggested for further developments.

2

Real-time simulator

2.1 Literature overview

2.1.1 Evolution of real-time simulators

In many contexts, simulation is a numerical resolution for mathematical representation to reproduce real phenomena of the studied system. In power system engineering, dynamic behaviors under steady-state or transient conditions are studied using the simulation, such as electromagnetic transient (EMT). Since mid-1990s, computation technologies have considerably evolved, leading toward physical/analog simulators with sophisticated simulation models, as illustrated in Figure 2.1. And with the emergence of digital systems, the development of simulator worked toward hybrid analogue-digital simulators capable of analyzing these EMT behaviors [12–14]. The drawbacks of this kind of simulators are the high price of the computation hardware and the space that they occupy. Furthermore, skilled technicians were required to handle the device operational.

The development of microprocessors with the floating point representation has created the first custom digital simulators, causing the fading of physical simulators [15]. DSP-based simulators were mainly used for hardware-in-the-loop (HIL) applications [16, 17], but the

limited performance of hardware restrains the possibilities for fast applications which leaded to the supercomputer-based simulators [18, 19].

At the same time, some universities and research institutes investigated the development of a fully digital real-time simulator based on standard computers, commercially available, to compete against the supercomputers which were highly costly. The development of pc-based simulators were a difficult task due to the lack of fast and low-cost inter-computer communication link. This issue was cleared with recent advancements of computer components with the emergence of multi-core processors, which present currently greater performance than a supercomputer equipped with 24-CPU that were existing 10 years ago. Such COTS[1]-based real-time simulations are running under operating systems (OS) such as Windows, Linux and standard real-time OS, making them compatible with power system analysis software tools such as EMTP-RV [20] or Simulink [21], which enable real-time simulations available for power grids, hydropower, systems in all-electric automotive and aircraft.

The last trend consists of building simulation models into a FPGA [22, 23]. Despite some current limitations on implementable model size due to limited number of gates, this approach seems to be promising for the following reasons: (i) Computation time within each time-step is almost independent of system size because of the parallel nature of FPGAs; (ii) Overruns cannot occur once the model is running and timing constrains are met; (iii) The simulation
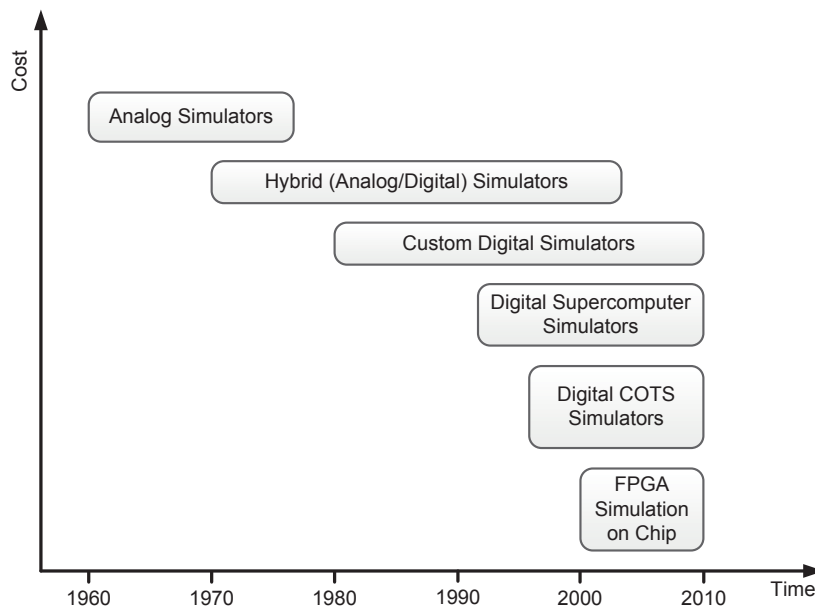
Figure 2.1: Evolution of real-time simulation technologies [4]

---

[1]Commercially Off-The-Shelf

time-step can be very small in the order of 250 [ns].

Regardless the real-time simulator used, it exists three specific categories of applications.

- Rapid Control Prototyping (RCP): The plant controller is implemented in the real-time simulator and is connected to a physical plant. The RCP offers an easy implementation and debug of the prototype. It presents indeed the flexibility of modifying controller parameters or its fine tuning during the test.

- Hardware-in-the-Loop (HIL): A physical controller is connected to a virtual plant, implemented in a real-time simulator. This application is a variation of RCP where the physical plant is replaced by a virtual one, offering therefore the same advantages as RCP. In addition, HIL simulations enable an early testing when test benches are not available or too costly. It also allows the study of the systems under extreme situations, which are unavailable on real hardware.

- Software-in-the-Loop (SIL): SIL is the logical combination following RCP and HIL applications. Both controller and plant are implemented in a single and powerful enough simulator. Since they run on the same device, timing with outside the simulator and inputs/outputs management are no longer critical, thus signals preserve their whole integrity.

2.1.2 Best fitting domain of applications

The high complexity of modern smart grid design demands advanced design and testing approaches. Real-time simulators is a great help regarding to test complex smart grid systems or power system development.

Baek *et al.* presented a method where advanced voltage management system is tested to control reactive power generation in a practical power system. The secondary voltage controller (SVC) has a drawback occurring large transient phenomena shortly after the SVC starts to operate due to the difference of operation statuses before and after the SVC operates. The management program is implemented in a real-time simulator and demonstrates the capacity of the system to solve the issue on a power system in Jeju island in Korea [24]. Ahmidi *et al.* adapted secondary voltage regulation strategies for a distributed network composed of wind farms [25] into a multilevel control system. This actual system presents an optimal multilevel control system which allows the doubly fed synchronous generator based wind farms to participate at reactive power balancing in transmission network. On the other hand Richardot *et al.* proposed in [26] a coordinated voltage control applied to distribution network

capable of managing efficient reactive energy reserve and compare the latter system to the classic secondary voltage control.

Roscoe *et al.* described an implementation method in a HIL environment, which characterizes three-phase AC power systems (generators, loads, controls, protection devices, and switches). The system is realized by using a real-time power-network simulator, which interacts with the hardware through the indirect control of a large synchronous generator and by measuring currents flowing from its terminals [27]. Teninge *et al.* focused on a methodology to model and simulate a medium scale distribution network with several feeders in a real-time multi-core environment [28]. They presented validation results through data of a 20 kV existing medium scale distribution network in France. Sun *et al.* presented a real-time, distributed algorithm that enables the distributed storage units to determine their own charging or discharging amounts, providing power balancing services [29].

Considerable efforts are made to propose State-Space-Nodal (SSN) solvers to improve real-time performance. Indeed, in [30], Dufour *et al.* proposed a solution method that combines SSN analysis for models of electrical systems, leading to [31], where they presented a SSN solver of ARTEMiS for models that features different operations modes and/or models with a high degree of internal redundancy.

In 2012, Sarri *et al.* has introduced a real-time state estimator in [32], applicable for optimal voltage control and fault detection for an active distributed network. An Iterative Kalman Filter (IFF) based algorithm is implemented for states estimation. A comparative evalution with the traditional Weight Least Squares (WLS) is achieved to assess its performance. On larger scale, Vanfretti *et al.* published a toolkit for Wide Area Monitoring systems , compatible with LabView environment. The kit enables a fast full scale prototyping testing in real-time and features data handling of synchrophasor for a specific analysis. At the same time, they present an application of a multitaper spectral estimator [33], focused on mode frequency from the electro-mechanical units in the Nordic grid. The paper gives a special attention on forced ocillations.

Majumder *et al.* proposed in [34], an application of a normalized H_∞ loop-shaping technique for design and simplification of damping controllers in the liner matrix inequalities (LMI) framework. The designed control algorithm is implemented using a rapid prototyping controller, where the performance was validated using a detailed model of multi-machine power system. The simulation model is implemented in multi-processor based PC running in real-time with Linux. Domahidi *et al.* presented a design and real-time implementation of a self-tuning flexible AC transmission system (FACTS) controller for power oscillation damping. The approach demonstrated the feasibility and the performance of an adaptive controller

capable of an online parameters identification, under large disturbances [35].

Yamane *et al.* studied the stability of power hardware-in-the-loop simulation (PHIL) using a smart grid laboratory for modern houses distribution systems [36]. This latter includes multiple energy sources and energy regeneration capability

Real-time simulations are therefore widely used in power systems investigation on different scale levels. Nevertheless, other domains of applications are intensively using such simulators according to the type of applications or the availability of devices. Indeed, considerable investigations are carried out in the development of drive systems. The cost of equipment, the short testing periods restraint developers to use of model-based techniques.

Dufour et Belanger presented an hardware-in-the-loop simulation of a fuel cell hybrid electric vehicle system with several 10 kHz converters, implemented in the RT-LAB simulator. It demonstrates the necessity of using special models of IGBT bridge which implements interpolation techniques within fixed time step in [37]. Based on the same IGBT bridge models, Dufour *et al.* demonstrated technologies designed for hardware-in-the-loop testing of permanent magnet synchronous motor drive systems in fuel cell electric vehicles in [38]. Various motor drive models with different complexities from the basic Park two-axis machine models to detailed finite-element-analysis, are implemented on different hardware such as CPU or FPGA in order to compare performances and precisions.

Similarly, A. Myaing et *et al.* in [39] achieved a comparison study with different behavioral level of IGBT models for FPGA-based real-time simulation (Altera Startix III). Their evaluation is presented using a three-level 12-pulse voltage source converter system driving a squirrel-cage induction motor. They suggested to use behavior model simulation on the early stage of system development, when efficiency is still not considered since such model is fast but comes with a sacrifice of accuracy and details.

As another type of automotive application, Tiegna *et al.* proposed a data-driven predictive control technique to improve the shift quality, i.e. smoothness and efficiency, of vehicles equipped a dual-clutch transmission (DCT) in [40]. Implemented in a FPGA, the effectiveness of the control was assessed using a rapid prototyping platform based on dSPACE, simulating the DCT behavior, in order to guarantee of a real-time environment.

The domain of design and integration of an All-Electric Ship is a challenge, which requires testing the interactions of hundreds of interconnected power electronic subsystems from different manufacturers. Paquin *et al.* tested these interactions using HIL simulations to evaluate the performance of some parts of these very complex systems, allowing to reduce the cost, duration and risks since large test benches or the use of actual equipment are required

for commissioning [41].

Lee *et al.* developed an antiskid brake system (ABS) during an aircraft landing allowing to reduce landing distance and increase safeties [42]. The study of such systems required five degrees of freedom aircraft landing model, where different road conditions could be simulated. The model is interacting with hydraulic brake systems of a real aircraft, which was controlled by the ABS algorithm.

Blànquez *et al.* presented a a real time power plant simulation platform as a tool for education purpose on electrical protections and automatic voltage regulators since any failure during the tests may bring some risk not only for the generator, but also for the reliability of the power grid [43].

At the time of the proposal the present thesis, real-time development have been carried out in [5, 16, 44]. The presentation of this actual real-time layer is referred to in chapter 2.2.

2.2 Requirements for real-time simulation

Simulation is a calculation process attempting to find numerical solutions given a fixed time step from a mathematical model, enabling to analyze or predict the system behavior from a set of parameters and initial conditions. When this procedure is subject to time constraints, it is referred to real-time simulation or online simulation.

2.2.1 General concept

At each time step, simulation executes scrupulously the following sequences:

1. Reading inputs;

2. Applying numerical integration algorithm;

3. Generating results;

4. Holding on for the next step.

As it is illustrated in Figure 2.2.

Considering a time reference T_n and an integration time T_{int}, three situations are distinguished during the simulation procedure, as illustrated in Figure 2.3.

- Case 1 : $T_{int} < T_{n+i}$;

- Case 2 : $T_{int} > T_{n+i}$;

- Case 3 : $T_{int} < T_{n+i}$ but T_{int} has the same time rate as T_{n+i}.

The numerical resolution in case 1 is faster than T_n. The simulation maintains its integration process without any idle time, resulting to a resolution time faster than the given time of simulation. The case 2 illustrates the situation where T_{int} is longer than T_n, and as a consequence, resolution time is longer than the given time of simulation. This kind of instance may occur when the model complexity is too high compared to the computation power or the time step is very short due to very fast transient and T_{int} overflows on T_n. The case 3 has a T_{int} faster than T_n as in case 1. However, the start of the numerical resolution is synchronized with the reference clock T_n. Consequently, the elapsed time of the simulation corresponds to the elapsed time of the reference clock.

The two first situations are referred to as offline simulations, whereas the case 3 corresponds to the real-time simulation in the literature. Indeed, a real-time simulation is assigned to a simulation where time is elapsing at the same rate as a reference clock. This reference clock is usually executed at the same rate as its real counterpart. Therefore, time is an additional constraint that simulation model and computation performance must handle.
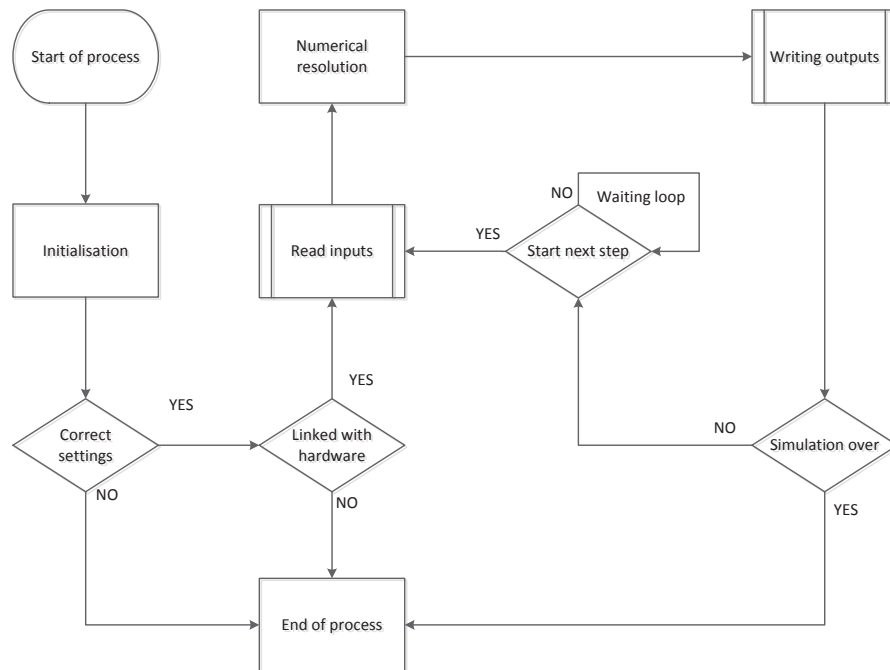
Figure 2.2: Basic functional diagram of real-time simulation process

2.2.2 Timing and constraint

During a real-time simulation, accuracy of computations not only depends upon the precise representation of the system, but also on length of time that results are produced. In fact, in order to be synchronized with the reference clock, computation time must be short enough to perform all the necessary operations for a given time step T_{step}. Further, real-time simulation generally interacts with external devices, thus time for handling inputs and outputs must also be considered while defining T_{step}. Consequently, every simulation step, real-time simulators are bonded to 2.1 with T_{add}, additional time for communication with external devices.

$$T_{step} > T_{int} + T_{add} \tag{2.1}$$

In the case where operations sequences are not achieved within the fixed-time, the simulations are considered as invalid. This instance is commonly referred as "overruns".

Furthermore, carrying out a real-time simulation is one thing, however, performing it synchronously with occurring events is another issue. Indeed, with a time step long enough satisfying Eq. 2.1, event can occur during a time step, as illustrated with the single-phase converter in Figure 2.4a with the switch-on of the thyristor. Consequently, a jitter induces current discrepancies in term of phase and amplitude as seen in Figure 2.4b. Moreover, multiple events can occur during a single time-step and without proper handling from the simulator, only the last one may be considered resulting to invalid results.
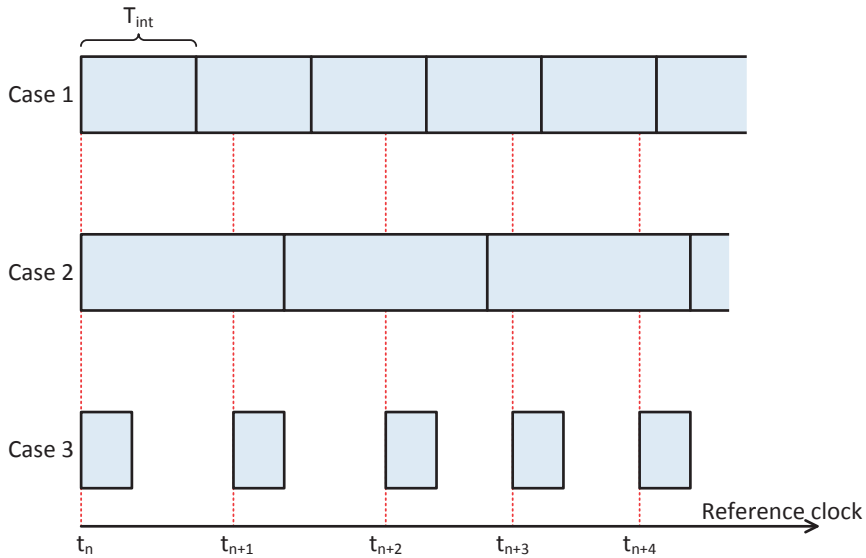
Figure 2.3: Offline simulations techniques and real-time simulation requisites

(a) Rectifier circuit

(b) Comparison of current from real circuit and simulation model
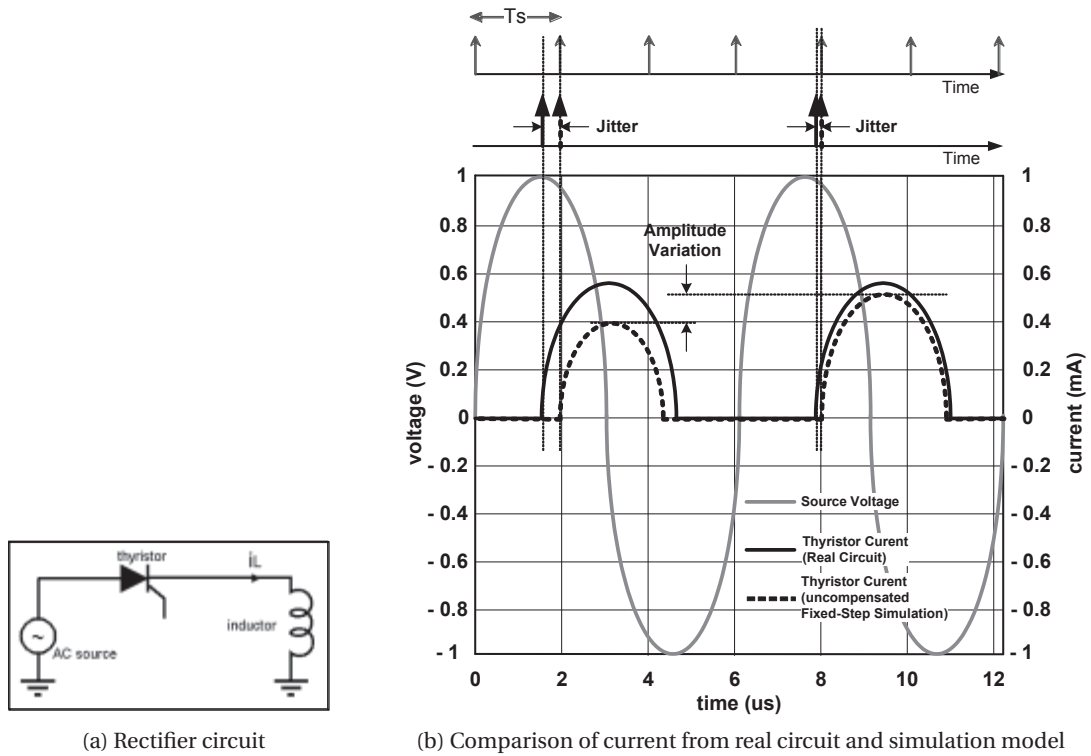
Figure 2.4: Overrun real-time simulation with a given time step ($T_{step}=T_s$) [4]

2.3 Numerical simulator

The simulation software "SIMSEN" for **SI**mulateur **M**odulaire pour **S**ystème **EN**ergétique, is a simulation platform based on modular structure. [9, 45]. The approach of the modular structure enables the fast build of any type of power systems topology and the analysis of dynamic behaviors under steady-state or transient conditions in phase quantities.

2.3.1 General description

SIMSEN has a wide collection of implemented libraries, including components for power networks such as voltage sources, transmission lines, transformers, circuit-breakers and power semi-conductor components with regulator functions. Different type AC electric machines are also available with a hydraulic library of modules, enabling as a result, the modeling and the dynamic response of multi-physics energetic systems.

2.3.2 Mathematical representation

Each element of SIMSEN is represented by an independent sub-system modeled with a set of first-order differential equations in the form of Eq. 2.2.

$$[\mathbf{A}] \cdot \frac{d}{dt} [\mathbf{X}] = [\mathbf{B}] \cdot [\mathbf{X}] + [\mathbf{C}] \tag{2.2}$$

with

- **A** : State global matrix

- **B** : Auxiliary matrix

- **C** : Boundary conditions vector

- **X** : State vector

The connection between different elements generates an equivalent set of equations related to the whole system model, in the same form as Eq. 2.2 due to the identical structure of sub-systems. The numerical resolution is carried out using the fourth order algorithm of Runge Kutte (RK45), which presents a method reasonably simple to implement with a good robustness and accuracy.

2.3.3 Real-time in SIMSEN

Running on a general-purpose computer, the real-time extension available in SIMSEN and referred to as SIMSEN-RT was first developed in [5] to achieve HIL simulations for power systems using hardware regulators. Parameters fine-tuning of regulators and tests under different situations such as emergency shutdown or islanded operation, were therefore applicable. The development was pursued further in [16] using an industrial regulator with a model of a mixed islanded power grid enabling the analysis of their interaction.

2.3.4 Description of real-time layer

Timers

Operation system (OS) such as Windows, is not suitable for real-time applications due to the priority interruption process not dedicated to the real-time simulations, inducing therefore addition latency in the process which can lead to jitters.

Based on the same numerical integration engine as SIMSEN, SIMSEN-RT presents two timer options as reference clock. The first timer features the Windows Multimedia Timer (MMT) from Windows OS. The high priority interruptions called by this latter enables to schedule simulation process as a top priority over other windows tasks, ensuring that all the operations is dedicated to real-time simulations. However, the resolution of time interval cannot be guaranteed under 1 [ms], limiting consequently the time step up to 1 [ms].

The second timer uses the Windows function "Query Performance Counter". The approach retrieves the current value of the counter with a high resolution time stamp (1 [μs]), that is used to estimate the time interval of time step. This method gives the possibility of settling a time step below 1 [ms], however the high priority interruptions are not available as a drawback. In other words, violations of time constraint must be admitted as long as numerical resolution can compensate it afterward, which means jitters can occur, degrading results from the real-time simulation.

Hardware interface

The link between the simulator and the real devices, sharing the same inputs and outputs (I/O), are made through an acquisition board embedding AD/DA converters. The current acquisition board (SORCUS [46]) for SIMSEN-RT comprises a PCI-board with 6 available slots where AD/DA converters modules can be placed. These modules feature 4 differential I/O of ±10 [V] with a 12-bits resolution and communicate with the simulator by means of "RT-element" component, which updates the I/O at the start of each time step.

User interface

A specific user interface is activated as soon as the real-time simulation is starting, giving the opportunity to interact with the simulation in real-time. Figure 2.5 presents the latter interface featuring the following functionalities:

- Manual access to channels inputs and outputs;

- Initialization function for the external hardware device;

- Real-time display of the results;

- Automated or manual activation of disturbances process.

2.3.5 Limit of real-time capability in SIMSEN

The real-time extension in SIMSEN was developed for HIL applications [5, 16] using DC signals. As a consequence, the time resolution of Multi Media Timer (MMT) is perfectly suitable for such applications. By contrast, systems with a slow Electromagnetic Transient (EMT) response such as transient behaviors of electric machines requires a smaller time step, which means the use of the second timer introduced in section 2.3.4. For such applications, the challenge is to select the right integration step capable to simulate the frequency of the fastest transient, i.e. in the order of few hundreds microseconds for electric systems, and determine the complexity or the size of the system model to satisfy Eq. 2.1 along with the fixed T_{step}.

Therefore, a survey is conducted using a computer, which specifications are listed in Table 2.1, to plot the characteristic of computation power against the model complexity as seen in Figure 2.7 in order to use it as a basis for determining the best compromise between simulation accuracy and computing power. It consists of estimating the length of T_{int} for the three given T_{step}, 1.0 [ms], 0.5 [ms] and 0.2 [ms] from the offline simulations, which was carried out for

Figure 2.5: SIMSEN-RT user's interface [5]

different matrix size related to the hydroelectric model of Figure 2.6.
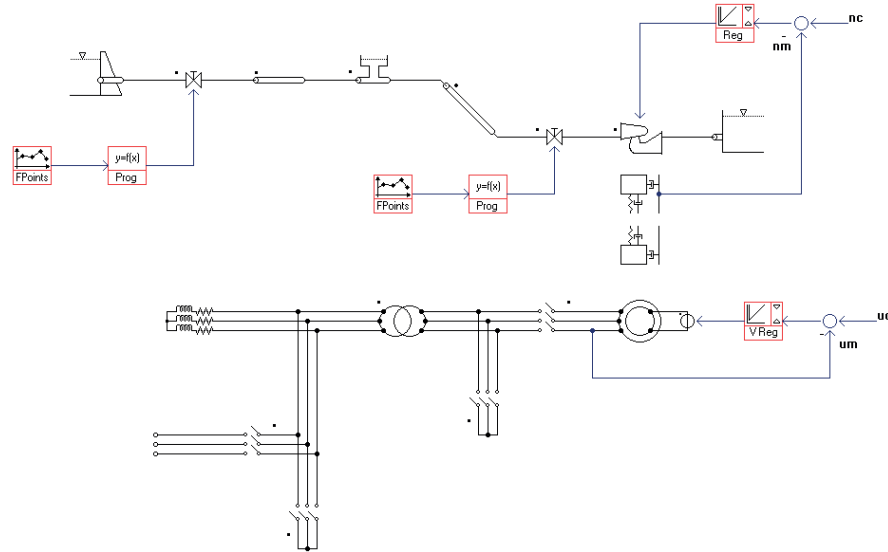
Figure 2.6: Hydroelectric model allowing the variation of complexity used for the survey

The curve resulting from the survey in Figure 2.7 is interpreted as the theoretical limit of T_{step} for a give matrix size since SIMSEN-RT shares the same computation engine. For example, a model with matrix size of 60x60 cannot exceed a T_{step} smaller than 0.2 [ms] without generating overrun situations in real-time, assuming that any communication time is negligible. In practice, a time margin is necessary to considerate additional time spent for communicating with devices and compensate any unexpected interruption from the Operating System (OS).

It is also relevant to note that T_{int} does not vary significantly between different time steps as expected. The slight discrepancies come especially from the short interruptions generated by any background task.

In addition, the quadratic evolution of the curve indicate the rapid increase of computation time with the growth of matrix size. Therefore, the objective is to determine the best compromise between computation speed and complexity of model as mentioned previously.

OS	Windows 7 64-bits
Processor	8x Intel Core i7 @ 3.4Ghz
Random Access Memory (RAM)	16 GB

Table 2.1: Computer specifications used for the survey
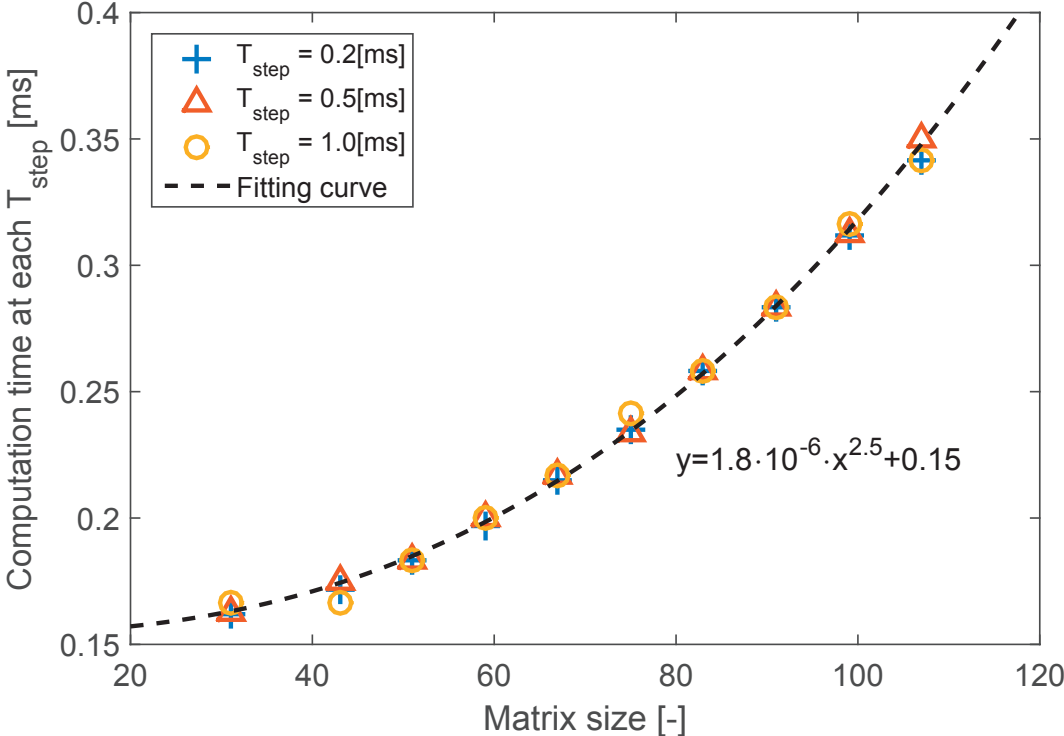
Figure 2.7: Numerical resolution time characteristic for a given model in SIMSEN

3

Real-time simulations for a reduced-scale energy system

3.1 Development of a small-scaled power prototype

This chapter introduces the realization of a real-time simulation on SIMSEN, running in parallel with the reduced-scale power unit. The real-time simulation will feature an integration time suitable for any AC quantity with a frequency of 50[Hz], which involves the issues discussed in section 2.2.2. In addition, the set-up of this prototype is used as a benchmark to emphasize and anticipate eventual issues before the measurement campaign on an existing hydroelectric power plant introduced in chapter 4.

3.1.1 Methodology of the development

The development of the small-scaled power unit follows a systematic approach, separated into three distinct parts as seen in Figure 3.1.

- The "Concept" regroups the technical feasibility where hardware and sensors (type, nature of signals, accuracy and the bandwidth) are selected, based on the application purpose.
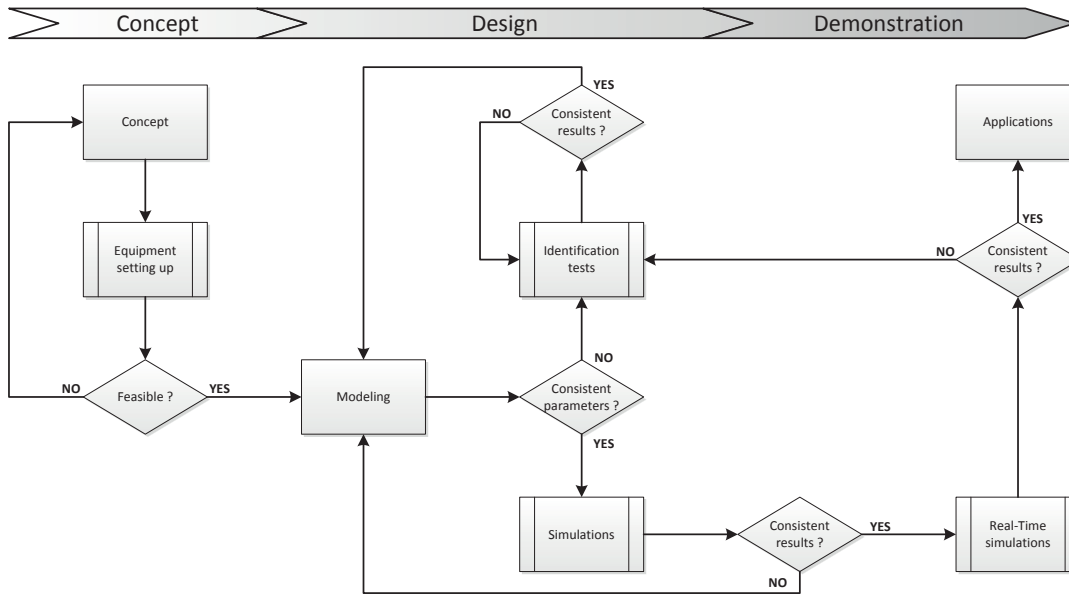
Figure 3.1: Methodology employed for the test bench development

- The "Design" is the modeling of the test bench and it includes typical tests for parameters identification in a electric machine, introduced in appendix A.1.

- The "Demonstration" consists of evaluating the models with experimental validations including offline simulations and followed by real-time simulations. Offline simulations enable to verify the consistency of identified parameters under ideal conditions before testing the simulation model under real-time conditions, where the model is driven by measured boundary conditions, thus enabling the assessment of similar state as the physical plant.

3.1.2   Description of the reduced scale power unit

The test bench enables to emulate the dynamic behavior of an existing power unit in a reduced scale where typical tests such as load variation or load rejection, but also critical situations such as faults can be achieved for study purposes.

The set-up of the unit includes a synchronous generator, with a rotor circuit supplied by an external single-phase voltage source which is manually controlled. The connection of stator terminal to the power network is carried out through a three-phase circuit-breaker. Such type of generator is usually operating in hydroelectric power plants, which has dictated the orientation toward a salient-pole machine, which specifications are reported in Table 3.1.
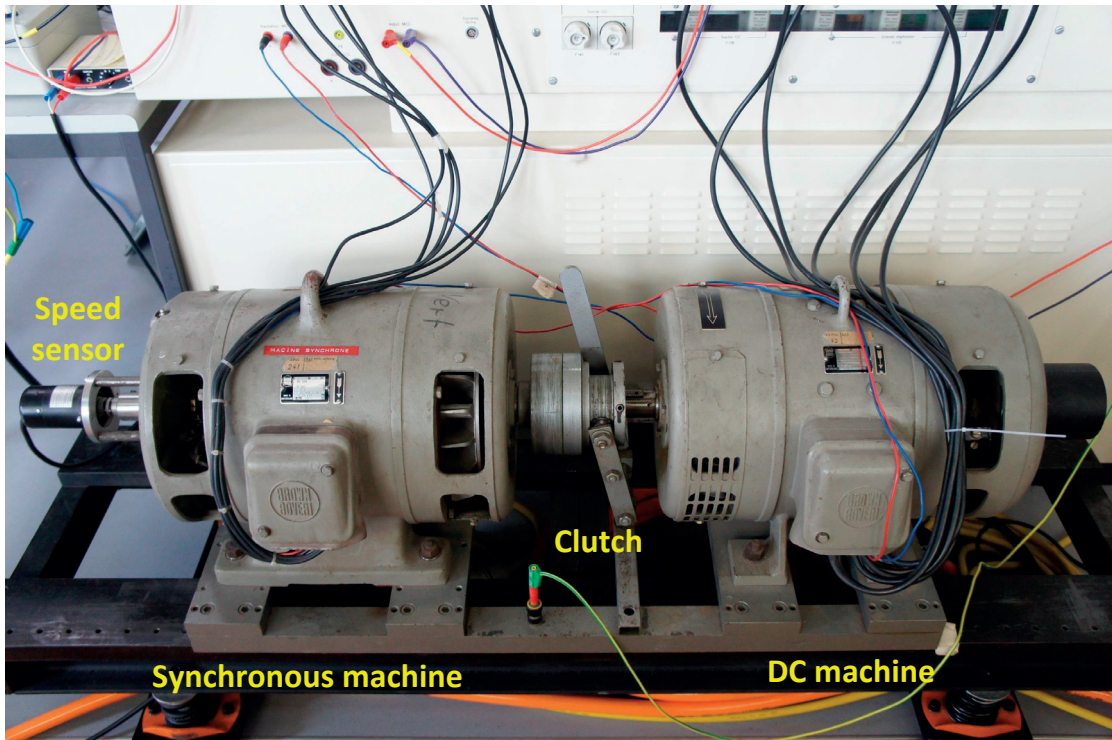
Figure 3.2: Reduced-scale power unit, modeling a the behavior of a generator-turbine group

The prime mover of the generator is a DC machine with a separated excitation system. This kind of machine features a torque that is proportional to the current circulating in its rotor circuit. Consequently, different torque profiles can be implemented in its control system, by regulating the current. As a result, different transient behaviors can be achieved with the test bench, such as start-up, shutdown, load variations, etc.

As seen in Figure 3.2, the two machines are coupled by means of a mechanical coupling, which features a lever for an easy coupling/decoupling.

Synchronous machine		DC machine	
Quantity	Value	Quantity	Value
Rated power S_R	6.25 [kVA]	Rated power $P_{R,DC}$	5.5 [kW]
Rated voltage V_R	380 [V]	Rated voltage $U_{R,DC}$	110 [V]
Rated current I_R	9.5 [A]	Rated current $I_{R,DC}$	50 [A]
Rated frequency F_R	50 [Hz]	Rated excitation voltage $U_{exc,R}$	110 [V]
Rated excitation current I_{fR}	2.8 [A]	Rated excitation current $I_{exc,R}$	2 [A]
Number of poles 2p	4	Rated speed N_R	1500 [rpm]

Table 3.1: Rated parameters of synchronous machine

3.2 Electric machines modeling

The electric machine is a rotating device performing an electromechanical energy conversion. There are different types and sizes widely used in various domain of applications such as transportation or power generation, mainly.

Two operation modes are distinguished, defined by the direction of power flow:

- **Generator** mode: Driven by a prime mover, the electric machine converts the mechanical (kinetic) energy into the electric form;

- **Motor** mode: The electric machine acts as a prime mover, converting the electric energy into the mechanical one.

There are numerous kinds of such rotating machines, such as induction machines, synchronous machines, DC machines (non-exhaustive list) with an operation principle differing to each other. In the context of this work, the modeling of electric machines, based on [6,47–50], is dedicated to a salient-pole synchronous machine, introduced in section 3.2.1.

3.2.1 Salient-pole synchronous machines

Synchronous machines are usually constituted of an armature, identical to other polyphase rotating machines, and a rotor with a single phase winding, excited by a DC current. Due to the
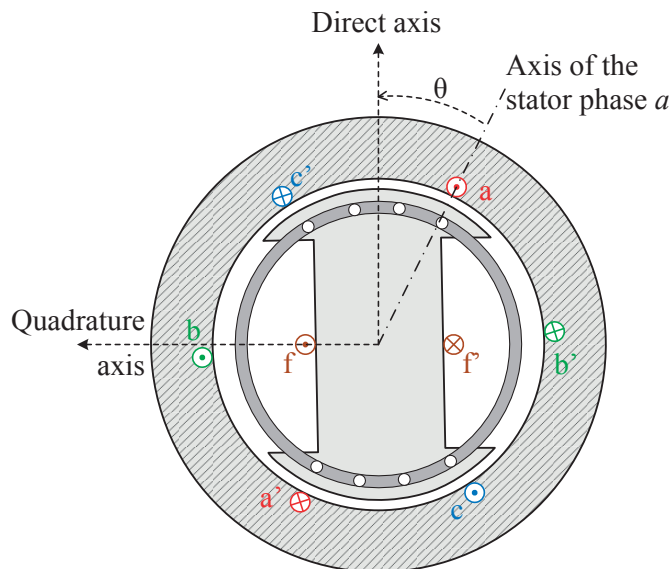
Figure 3.3: Cross-section of a salient-pole synchronous machine of one pair pole [6]

low rotational speed, i.e. 100-750 [rpm], the salient-pole machine is suitable for hydroelectric power plants where they are coupled to Pelton, Francis or Kaplan turbines according to the head characteristics. They are characterized by an asymmetrical geometry of rotor as seen in Figure 3.3, which rotates at the same frequency as the rotating field generated by the power network, i.e. 50 [Hz] in Europe. This synchronous speed is defined as a function of the number of pair poles "p" in Eq. 3.1

$$N = 60\frac{f}{p} \quad [rpm] \tag{3.1}$$

where f corresponds to the frequency of the network in Hertz.

3.2.2 Equivalent circuits of synchronous machines

The modeling of synchronous machine projects the magnetic linked flux generated from the rotor and circulating through the air-gap and stator, on two orthogonal axes shifted by an angle θ against the axis of phase a of stator windings, as seen in Figure 3.3. The direct axis in the alignment of the rotor pole by convention whereas the quadrature axis is perpendicular to the direct axis. The flux projection on the reference frame describes the reactions between fluxes from stator, rotor or damping windings by means of two equivalent electric circuits, as presented in Figure 3.4. As a result, the time domain analysis of dynamic behavior is explained through electric quantities, which leads to the set of equations related to the circuits from Eq. 3.2 to 3.7 in per unit.

$$u_d = r_s i_d + \frac{1}{\omega_n}\frac{d}{dt}\left[x_{ad}\left(i_d + i_D + i_f\right) + x_{\sigma d} i_d\right] - \omega_m \left[x_{aq}\left(i_q + i_Q\right) + x_{\sigma q} i_q\right] \tag{3.2}$$

$$u_q = r_s i_q + \frac{1}{\omega_n}\frac{d}{dt}\left[x_{aq}\left(i_q + i_Q\right) + x_{\sigma q} i_q\right] + \omega_m \left[x_{ad}\left(i_d + i_D + i_f\right) + x_{\sigma d} i_d\right] \tag{3.3}$$

$$u_o = r_s i_o + \frac{1}{\omega_n}\frac{d}{dt}x_o i_o \tag{3.4}$$

$$0 = r_D i_D + \frac{1}{\omega_n}\frac{d}{dt}\left[x_{ad}\left(i_d + i_D + i_f\right) + x_{\sigma Df}\left(i_d + i_D\right) + x_{\sigma D} i_D\right] \tag{3.5}$$

$$u_f = r_f i_f + \frac{1}{\omega_n}\frac{d}{dt}\left[x_{ad}\left(i_d + i_D + i_f\right) + x_{\sigma Df}\left(i_d + i_D\right)\right] \tag{3.6}$$

$$0 = r_Q i_Q + \frac{1}{\omega_n}\frac{d}{dt}\left[x_{aq}\left(i_q + i_Q\right) + x_{\sigma Q} i_Q\right] \tag{3.7}$$

This representation is purely mathematical, which allows to liberate first from the parameters variations over time, such as inductances, induced by the rotation. And secondly, the variables components, i.e. voltages and currents, on each axis are totally decoupled to each other, simplifying thus the study of time domain analysis. The physical quantities are retrieved

(a) Direct-axis   (b) Quadrature-axis
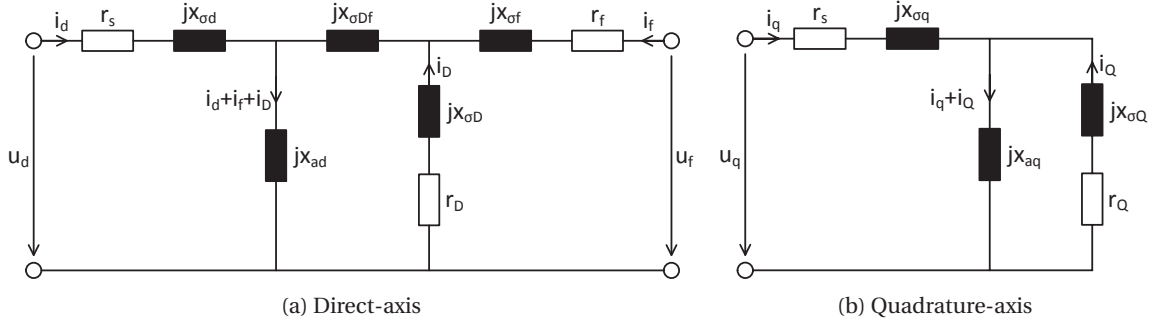
Figure 3.4: Equivalent circuits of synchronous machines

using the mathematical transformation proposed by [51]. The accuracy of the modeling depends upon the elements value in Figure 3.4. These latter are estimated by means of various identifications tests, which are introduced in appendix A.1, performed on the assigned machine. Based on the assumptions that the parameters x_d, x'_d, x''_d, $x_{\sigma d}$, T'_d, T''_d and x_q, x''_q, $x_{\sigma q}$, T''_q related to the direct axis and quadrature axis are known, [52] yields to the relations enabling to calculate all the elements of the equivalent circuits in per unit.

The equations involving the opened-circuit time constants T'_{d0} and T''_{d0}, defined as

$$T'_{do} + T''_{do} = \frac{x_d}{x'_d} T'_d + \left(1 - \frac{x_d}{x'_d} + \frac{x_d}{x''_d}\right) T''_d \qquad ; \qquad T'_{do} T''_{do} = T'_d T''_d \frac{x_d}{x''_d} \qquad (3.8)$$

For a given Canay reactance x_c (see appendix A.1.5), this leads to the preliminary equations as follows.

$$x_{dc} = x_d - x_c \qquad ; \qquad x''_{dc} = x''_d - x_c \qquad (3.9)$$

$$T'_{dc} + T''_{dc} = \frac{x_d}{x_{dc}} \left(T'_d + T''_d\right) - \frac{x_c}{x_{dc}} \left(T'_{do} + T''_{do}\right) \qquad ; \qquad T'_{dc} T''_{dc} = T'_{do} T''_{do} \frac{x''_{dc}}{x_{dc}} \qquad (3.10)$$

$$x'_{dc} = x_{dc} \frac{T'_{dc} - T''_{dc}}{T'_{do} + T''_{do} - T''_{dc}\left(1 + \frac{x_{dc}}{x''_{dc}}\right)} \qquad (3.11)$$

The reactances of the equivalent circuit related to the direct axis are finally obtained using Eq. 3.12 to Eq. 3.14.

$$x_{ad} = x_d - x_{\sigma d} \qquad ; \qquad x_{\sigma f} = \left(\frac{x_{ad}}{x_{dc}}\right)^2 \frac{x_{dc} x'_{dc}}{x_{dc} - x'_{dc}} \qquad (3.12)$$

$$x_{\sigma D} = \left(\frac{x_{ad}}{x_{dc}}\right)^2 \frac{x'_{dc} x''_{dc}}{x'_{dc} - x''_{dc}} \qquad ; \qquad x_{\sigma Df} = \frac{x_{ad}}{x_{dc}} (x_c - x_{\sigma d}) \qquad (3.13)$$

$$r_f = \frac{x_{\sigma f}}{\omega_n T'_{dc}} \qquad ; \qquad r_D = \frac{x_{\sigma D}}{\omega_n T''_{dc}} \qquad (3.14)$$

In a similar approach, the equations related to the model elements of the quadrature axis yield

$$x_{aq} = x_q - x_{\sigma q} \qquad (3.15)$$

$$x_{\sigma Q} = \frac{x''_q - x_{\sigma q}}{x_q - x''_q} x_{aq} \qquad (3.16)$$

$$r_Q = \frac{1}{\omega_n T''_q} \frac{x''_q}{x_q} \frac{x^2_{aq}}{\left(x_q - x''_q\right)} \qquad (3.17)$$

In practice, the leakage reactances of stator windings $x_{\sigma d}$, $x_{\sigma q}$ are assumed as equal ($x_{\sigma d} = x_{\sigma q}$).

3.3 Modeling in SIMSEN

3.3.1 SIMSEN layout of the low power unit for real-time applications

The model of the test bench in SIMSEN is constituted of synchronous machine connected to the 380 [V] power network, represented by a three-phase voltage source. The voltage level estimated from the measurements is applied on the element during a real-time simulation.

The three-phase circuit-breaker is placed between the stator terminals and the infinite bus. Represented by a pure three-phase resistance, which reproduces the opening and closing state of the circuit breaker with respectively a high value and a nil value, this element enables to simulate the synchronization process of the synchronous machine. Indeed, its algorithm is implemented in a macro, a subsystem where various functions can be defined, as detailed in appendix A.2.

The model of synchronous machine is represented by its own element where the equations 3.2 to 3.7 are implemented. A mechanical mass is connected to the machine and corresponds to

the equivalent inertia of the synchronous machine, including the inertia of the prime mover. This element is driven by the setting signal of torque applied on the real DC motor and allows the model to behave as the test bench.

The rotor circuit is supplied from a DC voltage source, which is driven from the measured field current and then converted into an equivalent voltage through a coefficient. This approach avoids the modeling of excitation systems while the dynamic of control system is maintained.

Finally, the element "RTcom" is acting as an intermediary between the acquisition board and the simulation model. Indeed, this element collects data from measured quantities, such as three-phase stator current, speed and air-gap torque[1] and store them in a element called "Output" as seen in Figure 3.6, or can be used to drive the simulation model on the described element above.
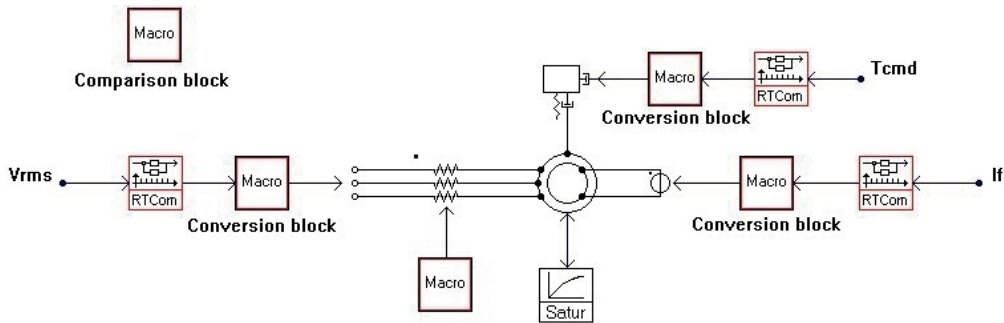
Figure 3.5: Model of test bench in SIMSEN for real-time simulations
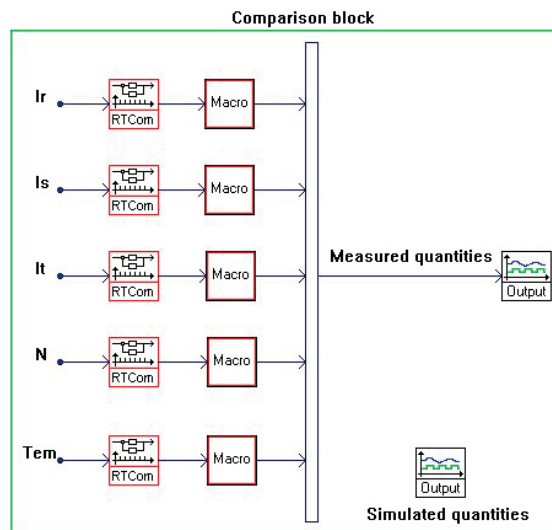
Figure 3.6: Comparison block

---

[1] Air-gap torque estimation device, detailed in appendix A.3

3.3.2 Parameters in the model of synchronous machine

The parameters of the synchronous machine are identified by means of tests described in appendix A.1. The identified parameters are summarized in Table 3.2.

Parameters of synchronous machine			
Resistance of stator winding	r_s	0.045	[p.u.]
Leakage reactance of stator winding	x_σ	0.06	[p.u.]
Synchronous direct reactance	x_d	1.21	[p.u.]
Synchronous quadrature reactance	x_q	0.76	[p.u.]
Direct transient reactance	x'_d	0.16	[p.u.]
Direct sub-transient reactance	x''_d	0.13	[p.u.]
Direct sub-transient reactance	x''_q	0.22	[p.u.]
Direct transient time constant	T'_d	110	[ms]
Direct sub-transient time constant	T''_d	16	[ms]
Inertia	J	0.25	$[kgm^2]$

Table 3.2: Identified parameters of the model of synchronous machine

The calculation of elements in the equivalent circuit of synchronous machine is made with the following assumptions:

- The stator leakage reactance x_σ is identical for both axes, i.e. $x_\sigma = x_{\sigma d} = x_{\sigma q}$;

- The sub-transient time constants are considered as equal, thus $T''_q = T''_d$.

The calculated values are reported in Table 3.3.

Model parameters					
r_s	0.045	[p.u.]	$x_{\sigma f}$	0.0976	[p.u.]
$x_{\sigma s}$	0.06	[p.u.]	r_D	0.0178	[p.u.]
x_{ad}	1.15	[p.u.]	$x_{\sigma D}$	0.506	[p.u.]
$x_{\sigma Df}$	0.0414	[p.u.]	x_{aq}	0.70	[p.u.]
r_f	0.0063	[p.u.]	r_Q	0.207	[p.u.]

Table 3.3: Calculated elements of the equivalent model, based on the identified parameters

3.4 Experimental evaluation of identified parameters

3.4.1 Saturation effect

The parameters listed in Table 3.3 were identified under saturated conditions. Consequently, the SIMSEN model yields simulation results, which would be unsaturated with nominal operations.

This case would be correct for large power machines, whose saturation only appears beyond the rated voltage level. However, such small machine shows important saturation (see Figure A.1), which may induce relevant discrepancies as seen in the top plot of Figure 3.7 under identical state.

The saturation effect is taken account when the model is linked to the element "SATUR". As a result, the amplitude of current is corrected, reducing then the error from 19.67 [%] to 6 [%] as
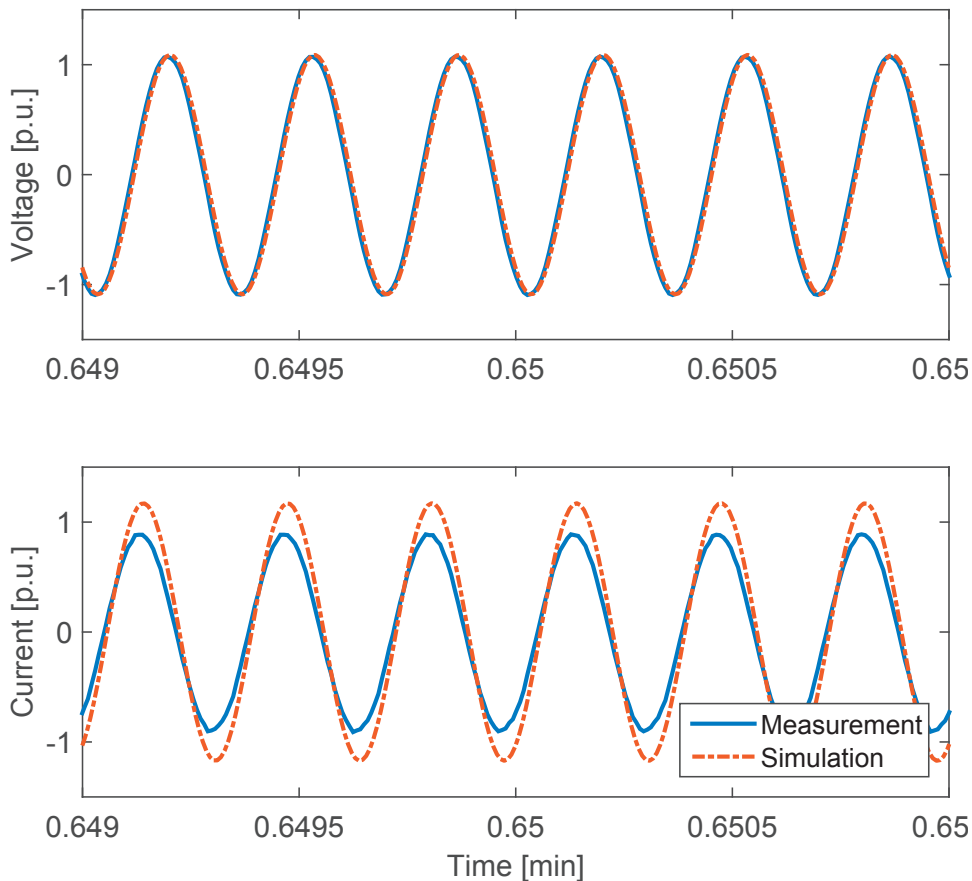
Figure 3.7: Stator current i_r without compensation of saturation with the synchronous machine operating at P=0 [W] and I_f = 0 [A] under the same voltage level.
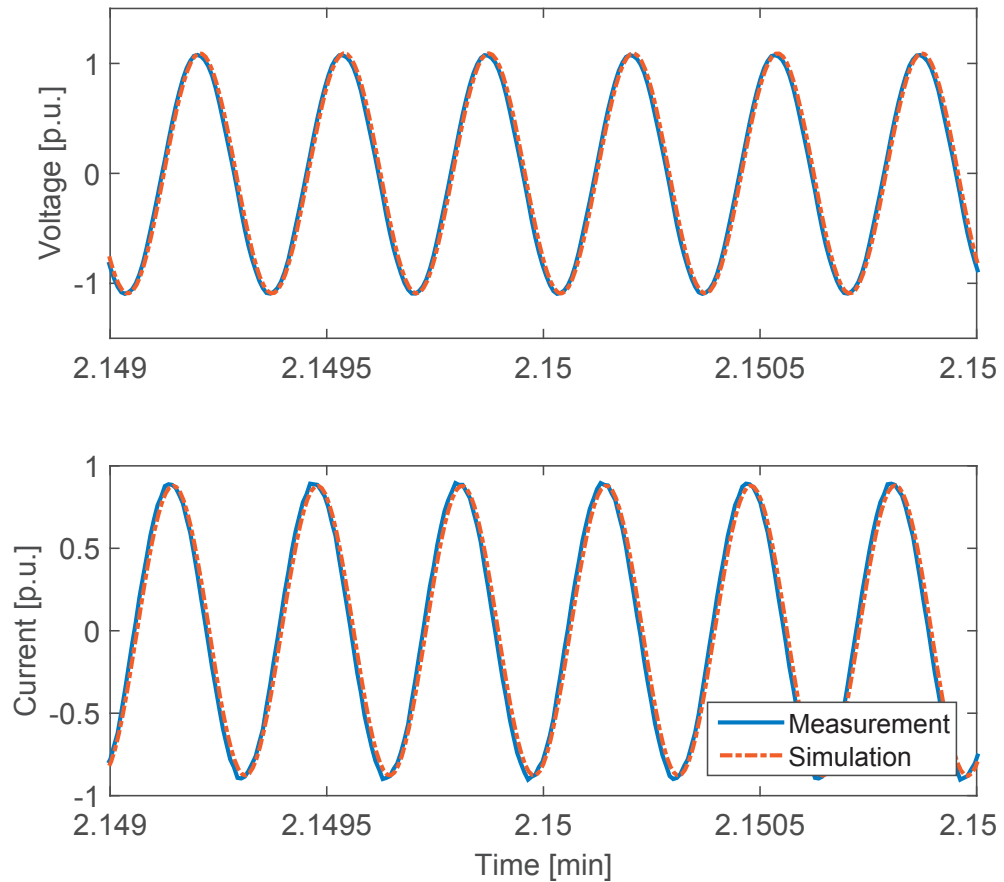
Figure 3.8: Stator current i_r with compensation of saturation with the synchronous machine operating at P=0 [W] and $I_f = 0$ [A] under the same voltage level.

seen in Figure 3.8.

3.4.2 Transient phenomena in electric machines

Validation of model presented in Figure 3.5 is achieved using the comparison between measurements and simulation results. Two test cases are proposed:

1. Torque step - Connected to the network, the synchronous machine operates in steady-state with a power equal to p=0.12 [p.u.] and $\cos(\phi)$=1. A step of torque command signal is applied on the control system of the prime mover. This latter provides then a torque step from 0.12 [p.u.] to 0.42 [p.u.] to the generator.

2. Sudden three-phase short-circuit - The synchronous machine operates under no-load conditions, i.e. nominal voltage induced on opened stator terminals. A sudden three-

phase short-circuit is performed on the stator windings.

Simulation results for torque step test

The results of load variation are presented in Figure 3.9, using the power convention of generator. The unit operates as a generator in steady-state, feeding an active power of 0.12 [p.u.] to the grid. The amplitude of field current is settled to its no-load value so that there is no transfer of reactive power. At t=0.15 [s], the external torque increases to 0.42 [p.u.]. As as result, the rotational speed accelerates, increasing the load angle of the generator. This generates an increase of magnetic coupling stator-rotor illustrated by the air-gap torque in Figure 3.9, which if strong enough slows down the speed and oscillations phenomena begins
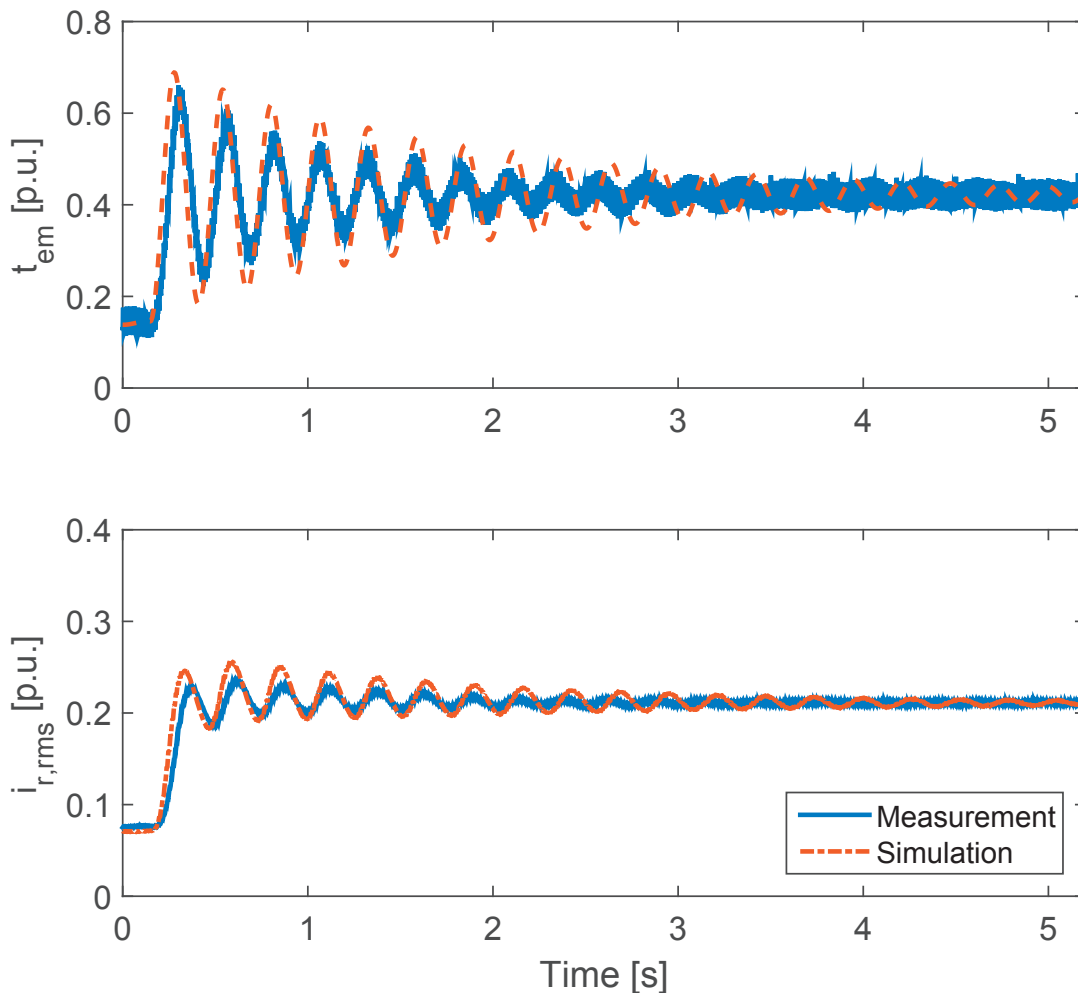
Figure 3.9: Oscillations of torque after a sudden variation of torque and RMS amplitude of stator current, in per unit

around the equilibrium point, until the total stabilization.

The comparison of results confirms the expectation. First, the local mode is verified with the values graphically determined on the air-gap torque: $f_{0,mes} = 3.64$ [Hz] and $f_{0,sim} = 3.79$ [Hz], corresponding respectively to the measured and simulated mode with an error of 4.12 [%]. This mode depends on the operating point before the disturbance and the inertia of the system, which is, as a reminder, the total one including the prime mover and the synchronous machine. Therefore, this comparison validates the correct estimation of the inertia in section A.1. Secondly, as displayed under the RMS amplitude for visibility reason in the bottom plot of Figure 3.9, the stator current shows good agreements. Indeed, the amplitude and oscillation frequency of the simulated current seems to be "tracking" the measurement during the transient state, after the torque step was carried out. In addition, the simulated current is stabilizing toward the same measured value of current in steady-state. Consequently, the
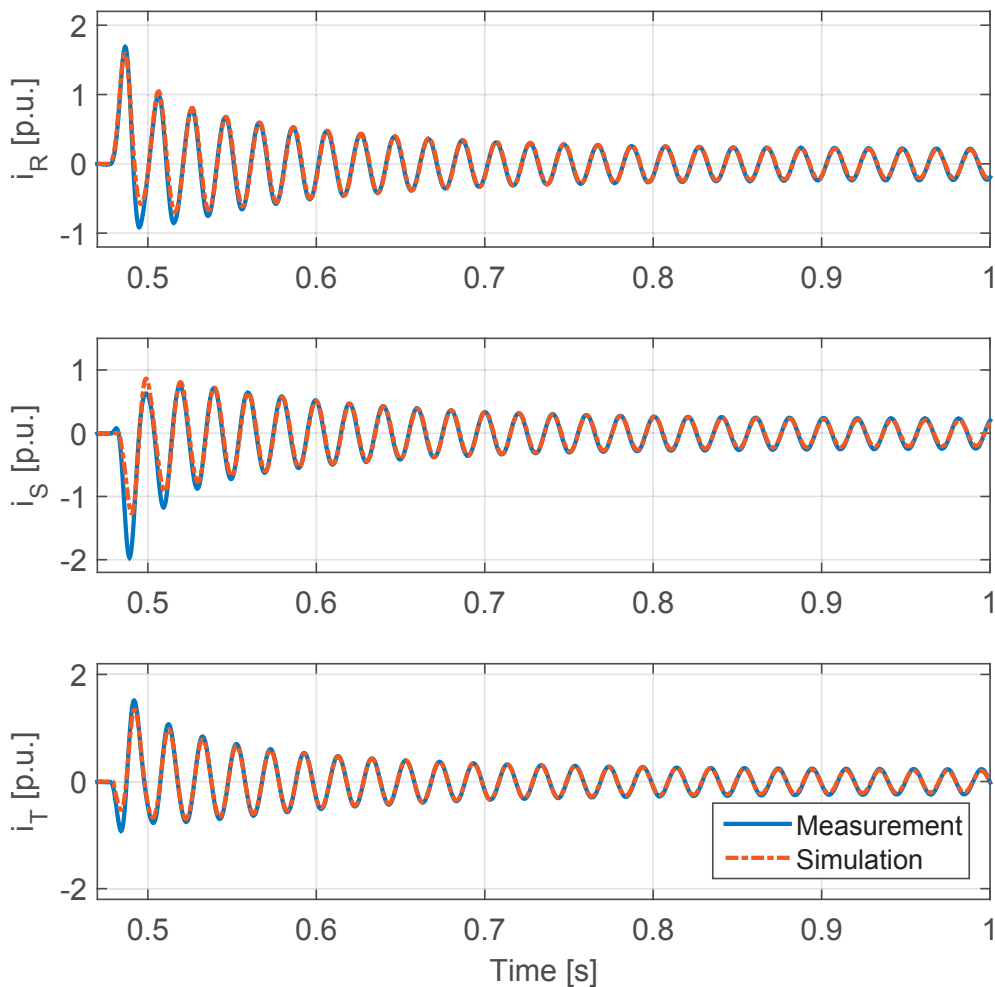
Figure 3.10: Validation of sudden three-phase short-circuited current

simulation model of the unit reproduces correctly the dynamic behavior of the test bench under typical transient cases and in steady-state case.

Sudden three-phase short-circuit test

Figure 3.10 and Figure 3.11 present the sudden three-phase short-circuit performed on the synchronous machine. This test represents the most critical fault that a machine can encounter during the operation, which means that the good agreement complete the assessment of the model.

Figure 3.10 shows that the sudden voltage drop on stator windings generates a high peak current at t=0.47 [s]. The oscillations amplitude are then damped, according to the time constants T'_d and T''_d. Moreover, the asymmetrical component of the transient currents induce a continuous component in the rotor circuit. Figure 3.11 shows the reaction of field current during the transient. This induced component is damped with the stabilization of the stator currents.
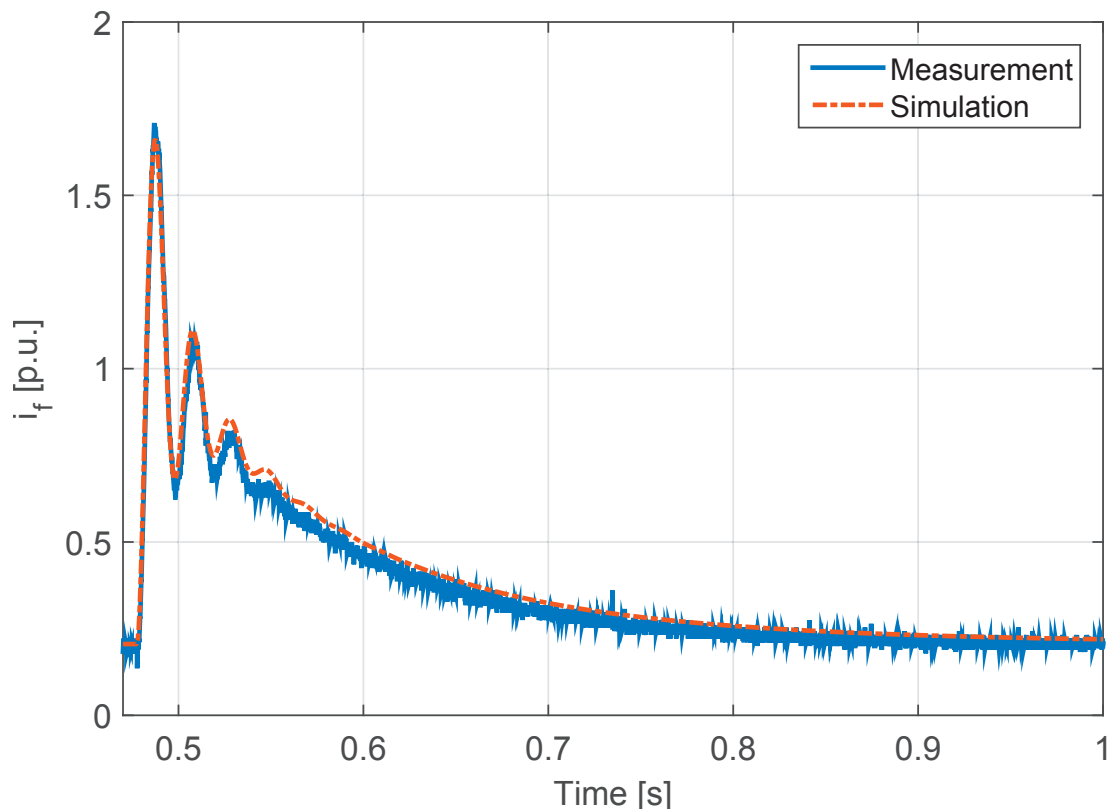
Figure 3.11: Validation of sudden three-phase short-circuited current

In both figures, simulation results show good agreement with measurements. Indeed, the model shows similar current amplitude, especially concerning the damping over time, despite discrepancies on the first peak which depends upon the angular position of rotor. Furthermore, the reaction of rotor circuit was correctly depicted, which attests the correctness of identified parameters.

3.4.3 Real-time simulation scenarios

The offline validations presented a simulation model, which is capable of simulating similar dynamic behavior of the test bench under ideal conditions, i.e. without noise, commutations effect from converters, etc. The following figures show identical test cases but under similar conditions as the ones presented in the offline validation, i.e. step of external torque
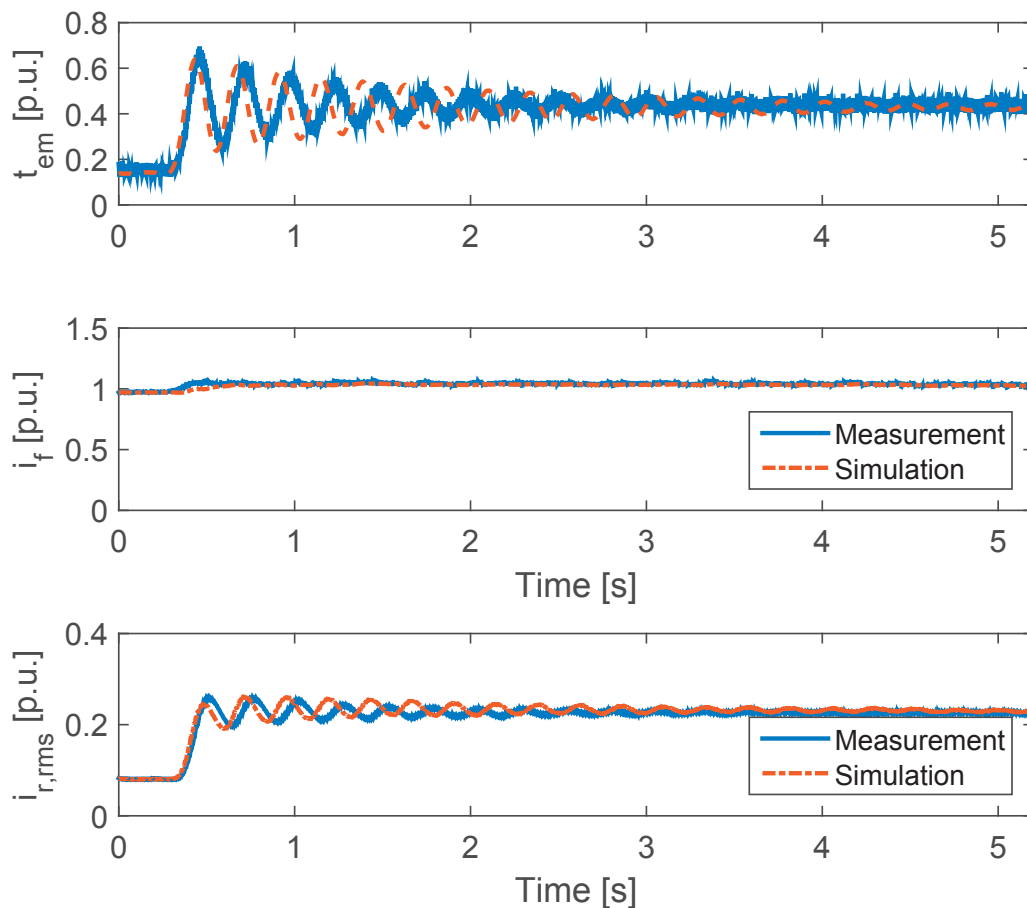
Figure 3.12: Comparison of air-gap torque, field current and stator current during a torque step in real-time
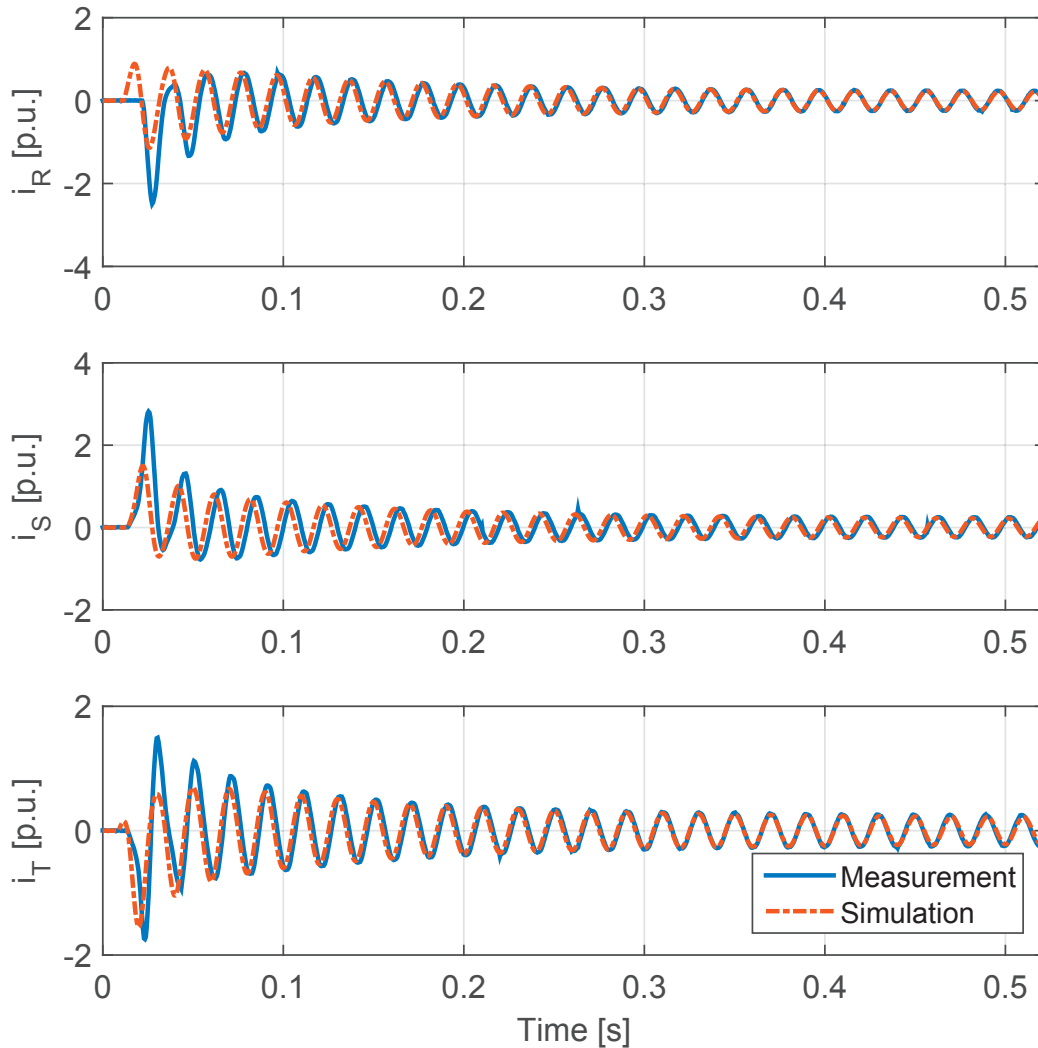
Figure 3.13: Short-circuited stator currents during the sudden three-phase short-circuit in real-time

and sudden three-phase short-circuit. As previously, comparison between simulations and measurements are applied to assess the validity of the system.

The real-time simulations showed good agreement in both test cases, allowing therefore the use of the developed system for monitoring and fault detection applications. It still has to be noted that the sudden short-circuit test case shows significant discrepancies in Figure 3.13 in terms of peak amplitudes after the short-circuit occurs. These amplitudes depend on the angular position of the rotor, which was totally arbitrary and not measurable on the real unit and therefore, the difference of position between the model and the unit justifies these differences. That being said, the damping amplitude shows similar evolution, still enabling the validation of the model.
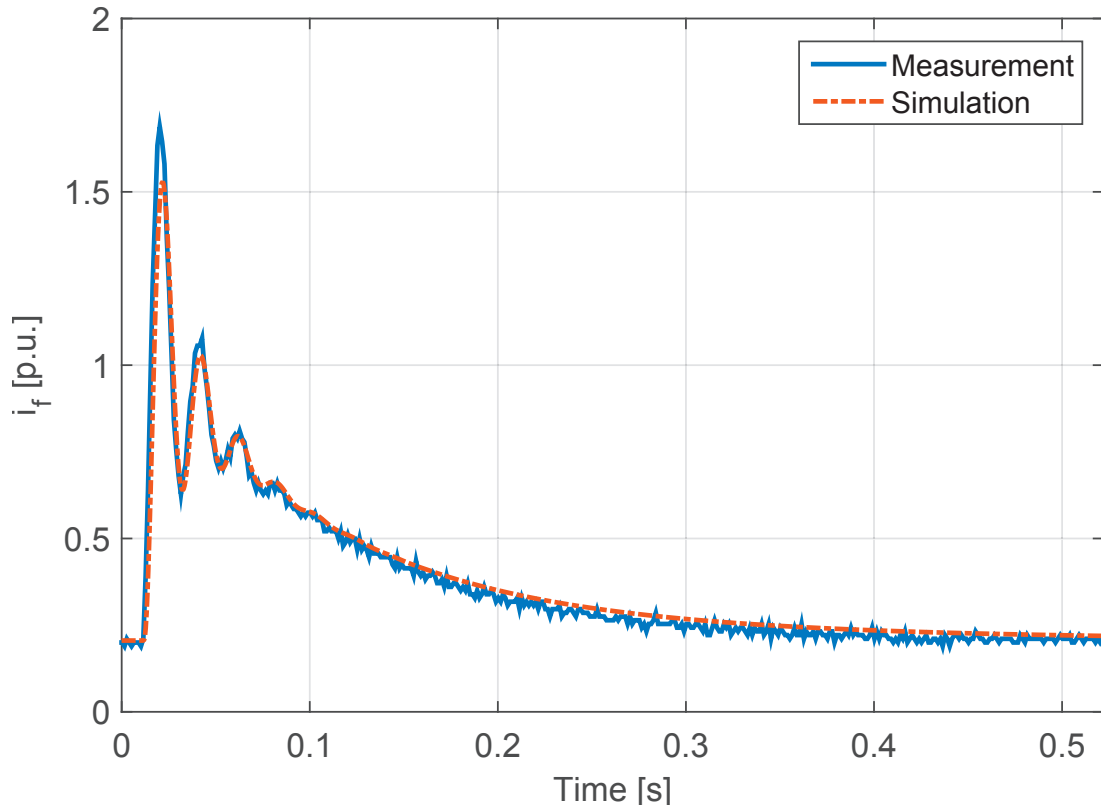
Figure 3.14: Short-circuited field current during the sudden three-phase short-circuit in real-time

3.4.4 Conclusion

Validation tests have remarkably demonstrated the accuracy of the implemented model in SIMSEN. Indeed, identified parameters have been determined with the assumption that the machine is unsaturated when it operates under normal conditions. The linear feature of the equivalent circuit matches greatly for large power machines where saturation usually appears beyond the nominal voltage level. In the introduced case, the saturation occurs in the range of operation. As presented in section 3.4.1, the equivalent circuit in SIMSEN was equipped with the element "SATUR", which takes into consideration the saturation effect and it strongly reduces the discrepancies between simulations results and measurements.

The simulation time step has been settled at $T_{step} = 0.5$ [ms] with a matrix size of 15x15 related to the test bench model. With the mentioned settings, simulation results have demonstrated the good agreement between simulations and reality. The comparison of local mode, currents amplitude and air-gap torque has enabled to validate the implemented parameters. In real-time simulation, greater discrepancies were observed in the case of load variation, due to

small error in boundary conditions. The accumulation of these measurements errors can generate relevant discrepancies if the errors are too large.

In conclusion, the simulation model implemented in SIMSEN enable a real-time simulation with good accuracy. The main issue still remains the identifications of correct parameters and the precision of measured boundary conditions, which are specific for all development of real-time models.

3.5 Model-based monitoring and failure detection

The growth of technology and complex applications have increased recently, resulting to an increase of demand for safety in various domains such as aerospace. The fault detection constitutes fundamental prerequisite for safety and reliability, thus an interest of investigation in advanced systems for fault detection. A fault in a large sense is understood as a malfunction of the system which can lead to harm or breakdown of the studied system due to an undesired operation state. [53, 54] has identified five modern methods of fault diagnosis

1. Hardware redundancy (conventional approach): This kind of system uses arrangement with several layers of sensors aiming to detect and isolate sensor fault. The same variable is measured and then compared from different sensors. Any significant discrepancy is a manifestation of fault;

2. Model-based approach (analytical redundancy): This method exploits the knowledge of the system with a mathematical model of the system, generally implemented into digital simulator, which permits the detection fault or fault identification;

3. Combination of hardware and analytical redundancy: Analytical redundancy replaces the hardware redundancy when this latter cannot be implemented. It enables to suppress some levels of replications as well;

4. Knowledge-based approach: This approach uses the human knowledge of fault and the qualitative reasoning.

5. A combination of all the above (Expert system approach): The combination of all the approaches above are implemented for a complex system enables to support decisions from human knowledge with the diagnosis of quantitative reasoning (analytical and hardware redundancy).
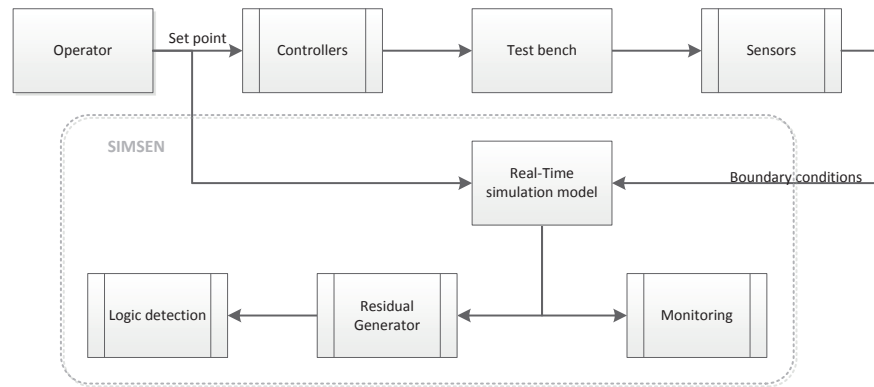
Figure 3.15: Model-based monitoring structure using SIMSEN
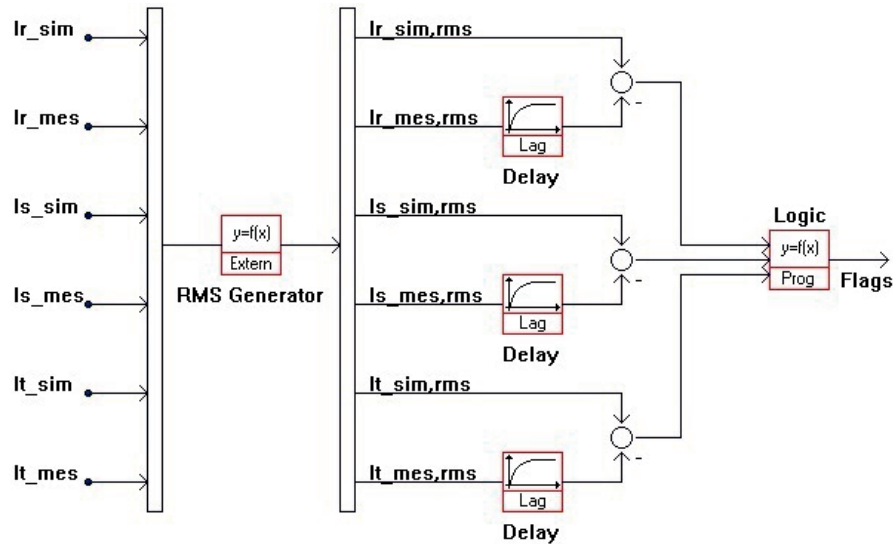
Figure 3.16: Basic residual generator in SIMSEN

3.5.1 Model-based approach fault diagnosis in SIMSEN

As seen in Figure 3.15, the concept of a model-based approach consists of generating residuals, which represents the discrepancies between observers from simulations outputs and signals from sensors, related to the monitored quantities. In the absence of fault, data and simulations show agreement leading to an unbiased residual. Consequently, the model-based approach is established on the knowledge of the normal operations of the system. A direct application consists of carry out a monitoring system for the synchronous machine using the simulation model developed in the previous chapter. The approach suggested in Figure 3.15 demonstrates the feasibility of such application using the real-time simulation from SIMSEN. The implemented residual generator besides the SIMSEN model in Figure 3.5, is a basic fault detection which monitor the three-phase stator current. Indeed, any malfunctioning or fault
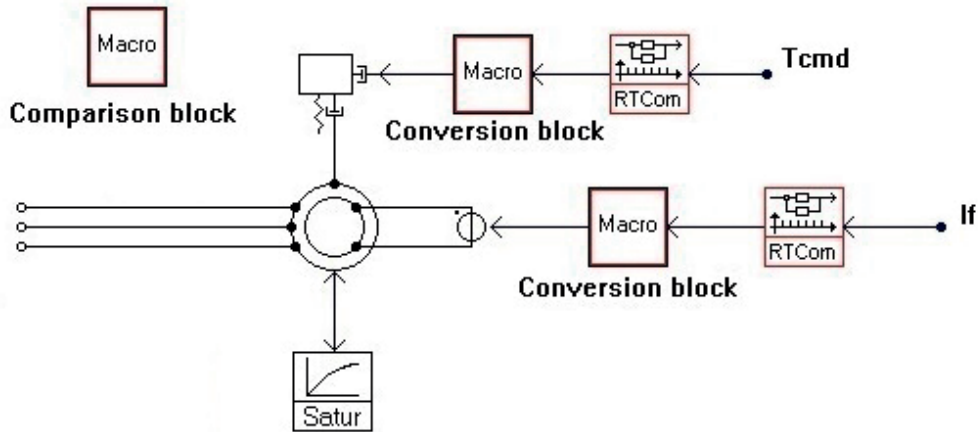
Figure 3.17: Model of SIMSEN used for fault detection

is directly fed back to the current. The residual generator presented in Figure 3.16 calculates the RMS-value of each phase through a dynamic-link library (DLL) function. The currents are then compared to generate the residual on each phase. If the difference becomes too large, a flag is raised to report a fault in the logic element.

The "Lag" element enables to delay the variation of RMS-value of measured currents after the disturbance. This latter gives an interval of time to clear the fault if possible, which would prevent an unnecessary shutdown.

3.5.2 Fault detection scenario

The experiment sets up a two-phase opening failure of a circuit breaker connected to the stator windings. The sequence of demonstration is described as follows: the initial operating point of the test bench is settled at P=-0.14 [p.u.] and Q=-0.32 [p.u] in generator convention. The opening failure is carried out manually and is performed on the phase R and T, i.e. only the phase S is opened. As seen in Figure 3.17, the model used for this application is similar to Figure 3.3. The elements of the synchronous machine with its mechanical mass and its excitation system remain unchanged. The measured field current is still applied on the excitation system through the conversion block, as well as the command signal of the torque, which drives the element of mechanical mass. However, the circuit-breaker has been removed compared to Figure 3.3, making the stator terminals continuously connected to the infinite bus, which is modeled by the three-phase voltage source. This modification is carried out since the real unit is assumed to be providing or absorbing powers from the power network. In addition, the element representing the power network is considered as ideal, thus it is not driven by

the measurement anymore as in the previous model. Indeed, the concept of the model-based fault detection in SIMSEN is to consider the simulation model as a reference. Under normal conditions, this latter reproduces similar behaviors of the real unit. However, when an abnormality occurs, the simulation will continuously operate on the expected operating points while the real plant will show signs of malfunctions such as pulsations, unbalanced stator currents, etc. Hence, it is necessary to avoid the simulation model to behave exactly as the unit.
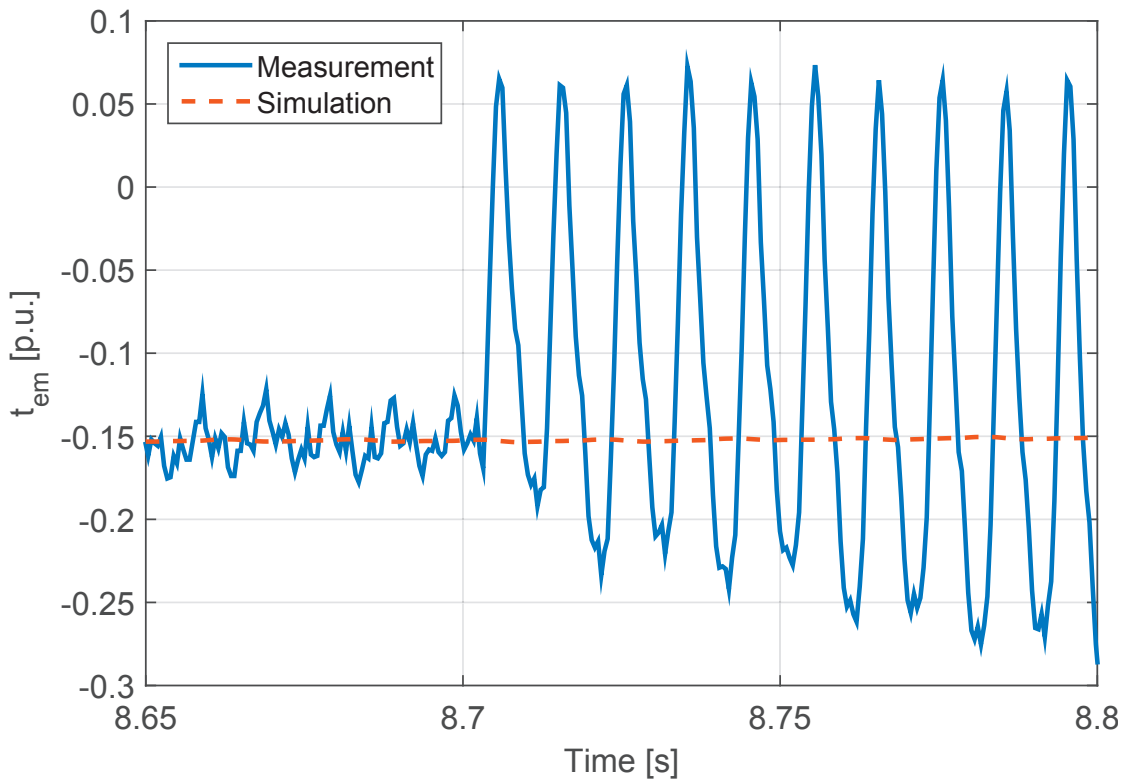
Figure 3.18: Air-gap torque before and after failure

The opening of the phase S at t=8.7 [s] has generated an unbalance distribution in the machine, which means the conditions of voltages and currents in all phases are no longer symmetrical. Consequently, the currents in the phases R and T pulsate at 50 [Hz] in opposition of phase. Considering the currents as phasors, this phenomenon creates a negative sequence component in the currents with an opposite direction of rotation to the positive sequence, inducing a negative sequence torque. As a result, the summation of positive sequence torque generates a constant torque while the interaction of positive and negative sequences induces a torque pulsating at a frequency of 100 [Hz], which is measured with the torque measurement device (see Appendix A.3) and seen in Figure 3.18.

The residuals for each phase throughout the experiment are presented in Figure 3.20. The logic to detect the fault consists of indicating the malfunctions when the residuals exceed the threshold, which is settled arbitrarily at 1 [A] for each phase, the failure is detected after 700 [ms] for the phase where the failure occurred. The residual of the two other phases has increased but not significantly to be detected by the logic.
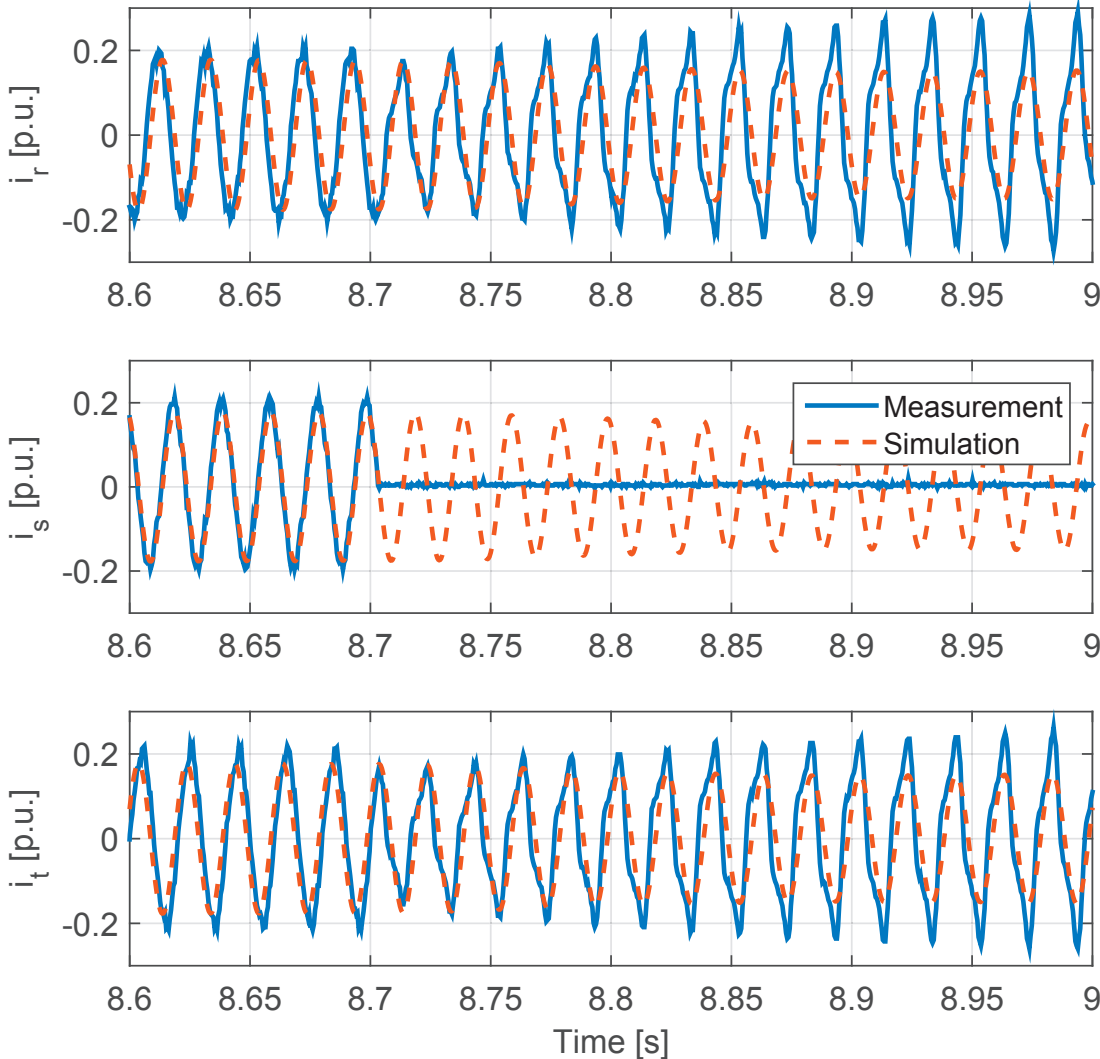
Figure 3.19: Three-phase current before and after failure
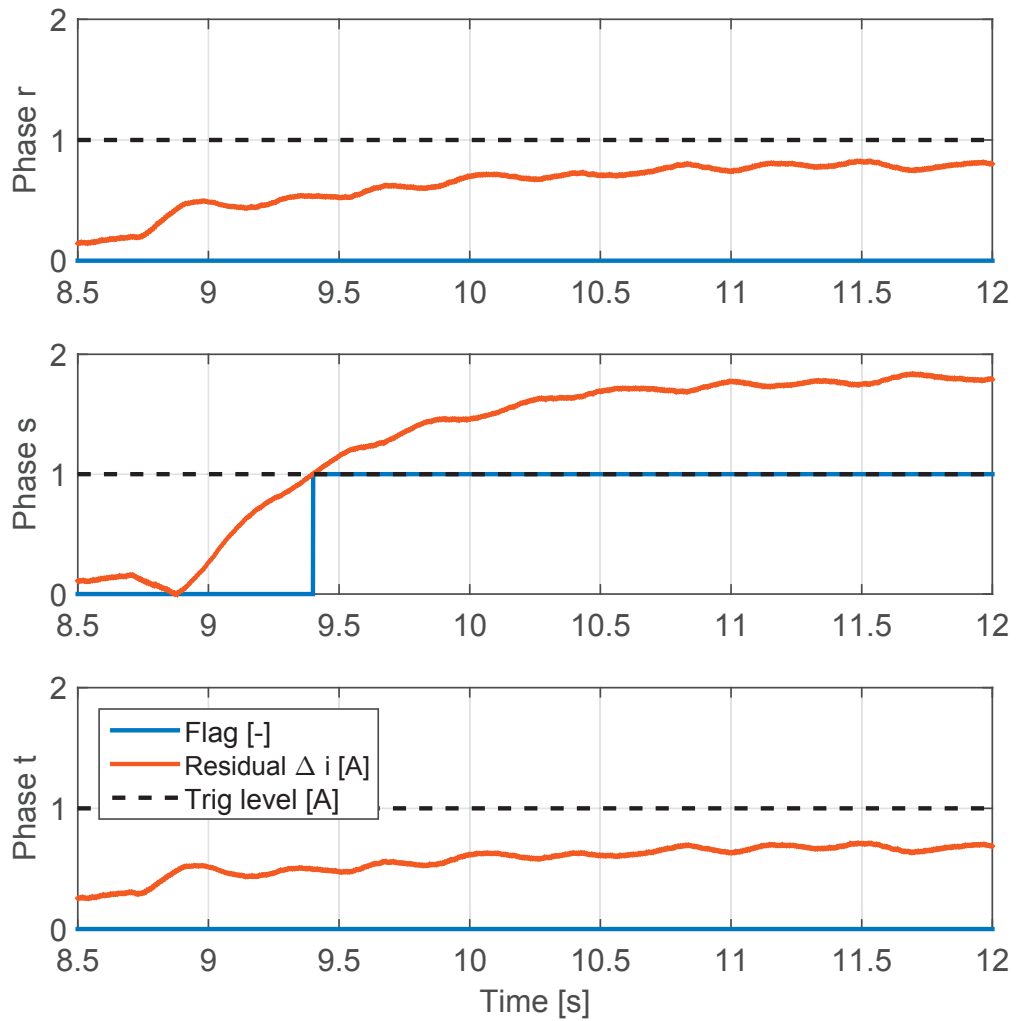
Figure 3.20: Detection sequence of the failure

3.5.3 Conclusion

The example of application using the simulation models in SIMSEN and running in real-time has demonstrated the feasibility of monitoring applications as well as a basic failure detection. Further investigations in detection process would permit an advanced and smart fault detection using the flexibility features of SIMSEN. Furthermore, monitoring application is also a possibility by observing quantities although the example has emphasized the usage in fault detection.

The simulation platform featured an easy logic implementation with the available functions, which can be modified easily as well. The use of DLL file expand the possibility by applying specific compiled functions, which are not available in SIMSEN.

4

Real-time simulations for a real hydroenergy system

4.1 Hydroelectric power plant

Located in the southern Swiss Alps in the Val d'Anniviers, the society "Forces motrices de la Gougra SA" operates three power plants which generate a total power of 650 GWh and 30 GWh of pumping per year since 1954. This energy source comes from hydraulic resources situated in the Val d'Anniviers and in the valley of Turtmann (or Tourtemagne). The exploitation of
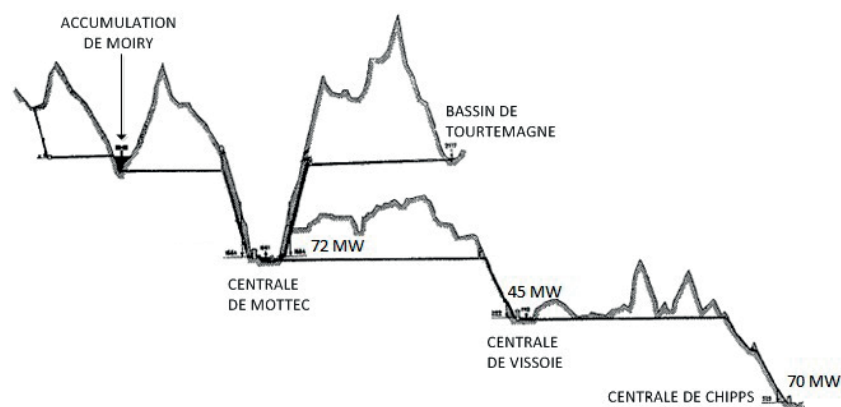
Figure 4.1: Gougra power stations

this energy is sub-divided between 3 power stations : Mottec, Vissoie and Chipps, which are operating in series along the Navisence river (Fig. 4.1). The development of real-time simulation is dedicated to the uppermost upstream power plant : Mottec. Inaugurated in 1959, this latter is a pump-storage station which generates an annual production of about 125 [GWh] with three units of 24 [MW].

(a) View from above of the whole plant   (b) Photo of power house
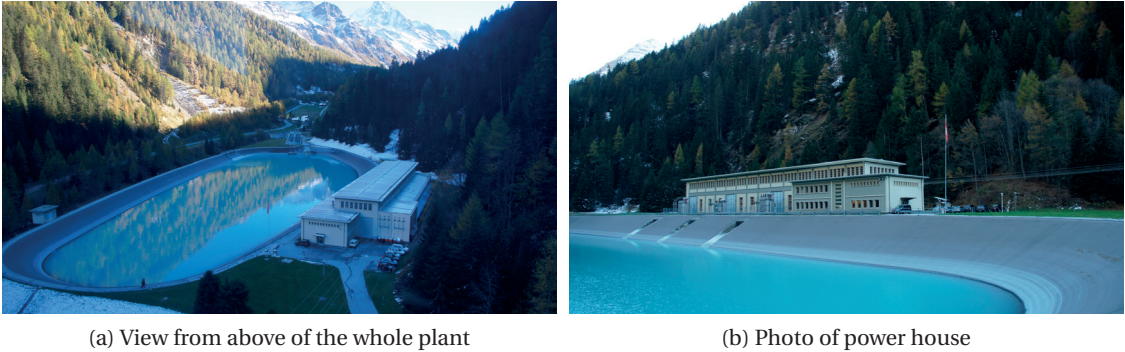
Figure 4.2: Photos of Mottec power plant
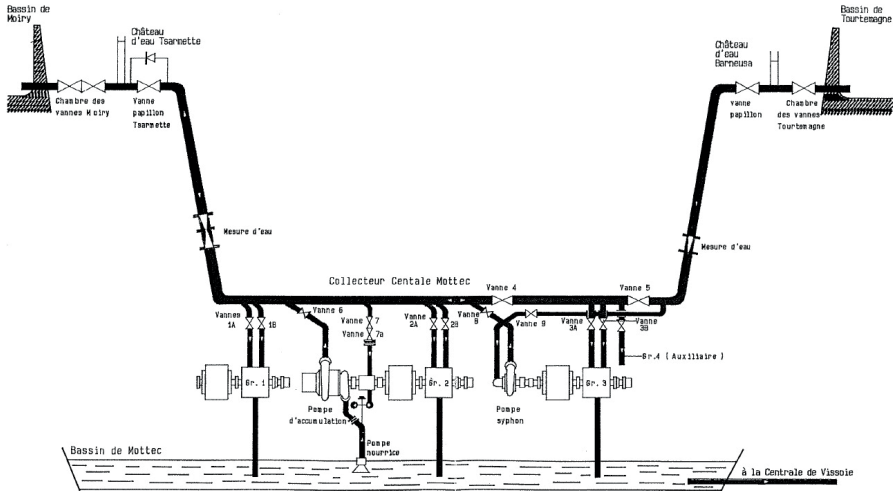
Figure 4.3: Layout of Mottec [7]

4.1.1 Modeling of Mottec

The whole installation is composed of a hydraulic installation including the upstream reservoir and the pipeline, which are feeding water to the power house and the installations inside the power house, where the electromechanical energy conversion is carried out by the rotating motor-generators.

Hydraulic installations

The power house of Mottec is connected to two upstream reservoirs:

- **Moiry**: Water coming from Moiry is held by an arch-type dam of 148 [m] high, 610 [m] wide. With a total capacity of 77 millions [m^3], the water level can fluctuate between 2150 [masl] and 2249 [masl][1].

- **Turtmann**: With a maximum and minimum level of 2177 [masl] to 2164 [masl], respectively, water coming from the glacier of Turtmann is collected with an arch-type dam of 30 [m] high and 110 [m] wide in a reservoir with a capacity of 780'000 [m^3].

The Turtmann reservoir possesses the greatest potential quantity of water, which exceeds its limited capacity. The water is therefore pumped through the power house of Mottec to Moiry reservoir and is used as a water storage.

Each adduction system comprises a gallery, a surge tank and a penstock. The adduction system of Moiry includes specifically a gallery of 3380 [m] long with a diameter of 2.4 [m] which succeeds to Tsarmette surge tank, comprising a lower and a higher expansion chambers in order to protect the upstream gallery and stabilize significantly backward pressure variations due to waterhammer effects caused by a disturbance occurred in a turbine. A penstock of 1180 [m] long, which diameter varies between 2.10 [m] and 1.5 [m] is feeding the power house of Mottec to drive the groups. The water is finally discharged into the downstream reservoir of Mottec with a minimum and maximum water level of 1561 [masl] and 1552 [masl], respectively.

Power house of Mottec

The power plant regroups three units with a Pelton turbine and a motor-generator with the characteristics reported in Table 4.1. Each unit rotates at a nominal speed of 750 [rpm] on a horizontal axis as seen in Figure 4.4. The Pelton turbine comprises two runners with an average diameter D_{ref} of 2 [m] (see Figure 4.10a), which are controlled by two injectors on each. The motor-generator is a salient-pole synchronous machine which is mechanically coupled to the turbine and whose rotor circuit is fed by a DC generator connected on the same shaft.

---

[1]The unit "masl" means **m**eter **a**bove the **s**ea **l**evel.

Generator				Pelton turbine			
Apparent power	S_R	29	[MVA]	Power	P_R	24	[MW]
Stator voltage	U_R	9.0	[kV]	Speed	N_R	750	[rpm]
Stator current	I_R	1860.4	[A]	Discharge	Q_R	4	$[m^3/s]$
Frequency	F_R	50	[-]	Head	H_R	656	[m]

Table 4.1: Rated parameters of machines
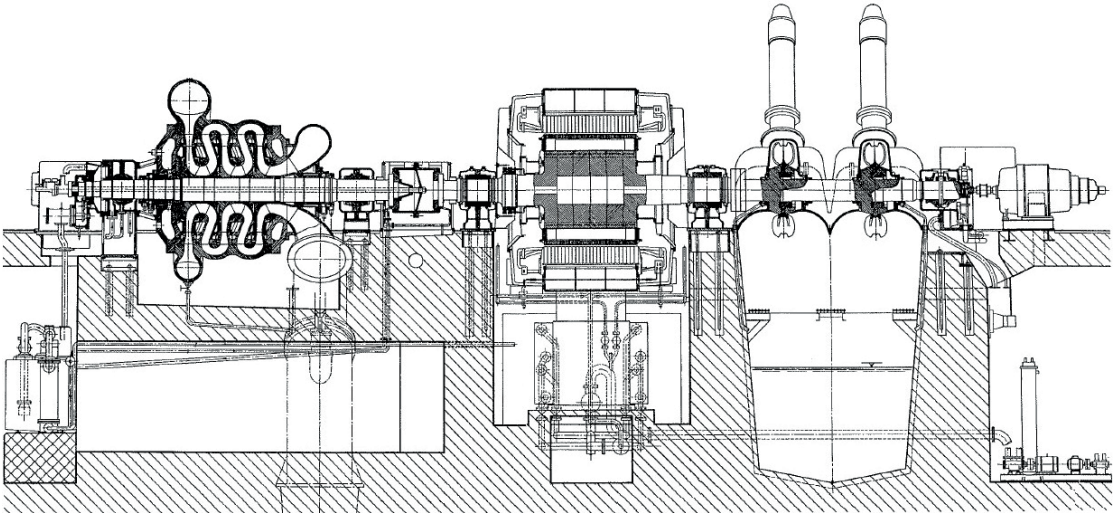
Figure 4.4: Cross-section of unit 2 with a three stages storage pump [7]

Figure 4.5: Ternary unit 3 of Mottec power plant

As it was mentioned above, the modeling of Mottec power plant is especially focused on the adduction system of Moiry-Mottec that is connected to the unit 3 in the power station, since the test cases introduced further operate under the following state:

- Water coming from Moiry reservoir drives the Pelton runners of unit 3 which operates normally with the generator connected to the power network.

- The remaining groups are out of service to prevent any disturbances on the operating unit during the measurement tests.

The modeling of the system in SIMSEN is illustrated in Figure 4.6, with the hydraulic and electric sides of the model considered for this study and based on the description in [7].
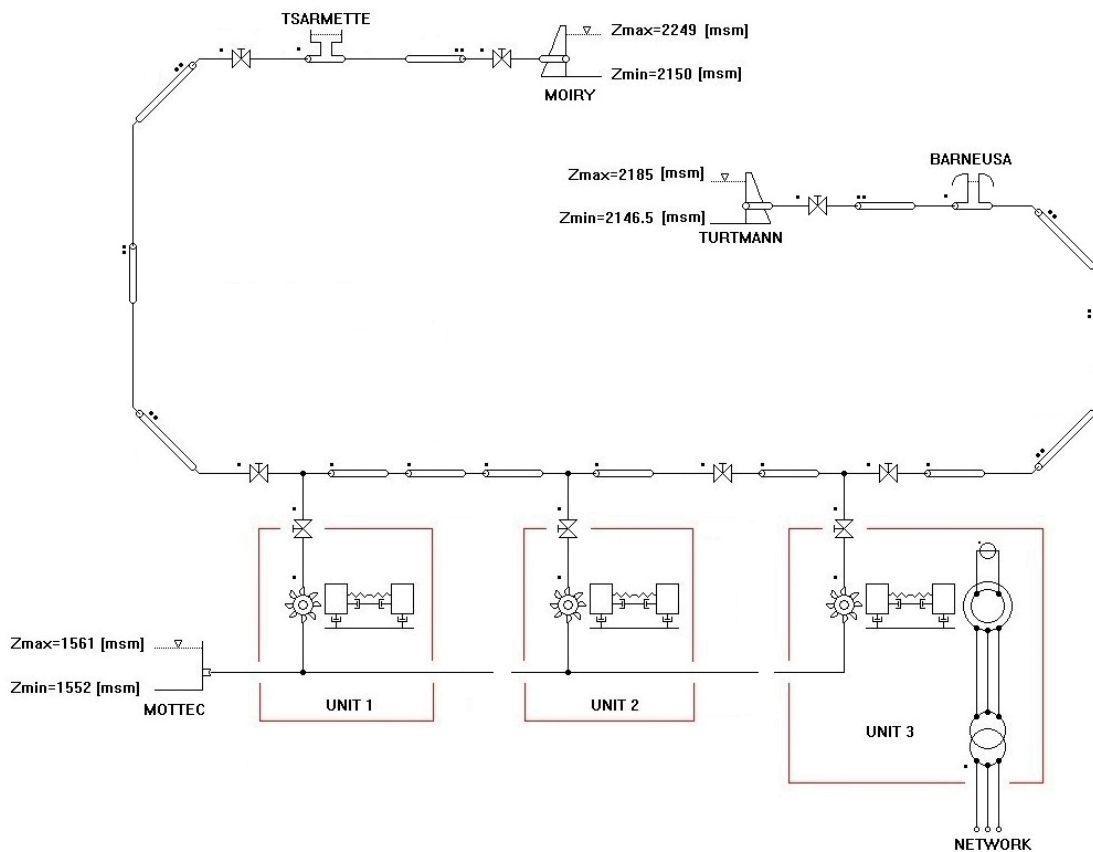
Figure 4.6: Moiry-Mottec simulation model in SIMSEN

4.1.2 Hydraulic system modeling

The one-dimensional hydraulic modeling introduced in [8] enables the mathematical description of dynamic behavior of the hydraulic systems. This approach is based on the following

(a) Pipe model of length dx   (b) Equivalent circuit of pipe with length dx
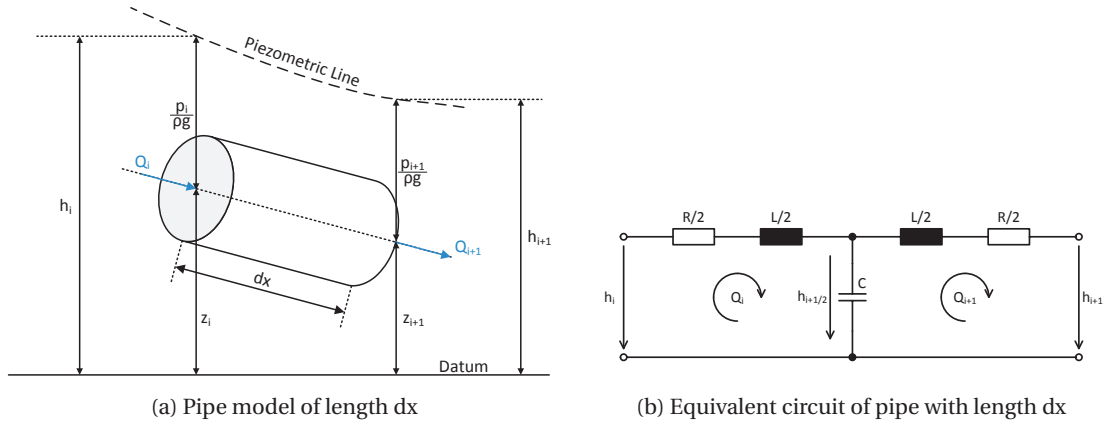
Figure 4.7: Pipe modeling [8]

assumptions, establishes electrical equivalent circuits for different hydraulic components such as valves, surge tanks and turbines.

- The flow is normal to a cross-section;

- Pressure, flow velocity and density are uniform in a cross-section;

- The convective terms are neglected.

Pipe

The model of the pipe of length L is composed of n_b sections of elementary elements of pipe filled of water and with length dx, as represented in Figure 4.7a. The one-dimensional momentum and continuity balance equations Eq. 4.1 yield the behavior for an elementary component.

$$
\begin{cases}
\dfrac{\partial h}{\partial t} + \dfrac{a^2}{gA} \cdot \dfrac{\partial Q}{\partial x} = 0 \\[3mm]
\dfrac{\partial h}{\partial x} + \dfrac{1}{gA} \cdot \dfrac{\partial Q}{\partial t} + \dfrac{\lambda |Q|}{2gDA^2} \cdot Q = 0
\end{cases}
\tag{4.1}
$$

By assuming that

$$
R = \frac{\lambda |Q|}{2gDa^2} \qquad\qquad L = \frac{1}{gA} \qquad\qquad C = \frac{gA}{a^2}
\tag{4.2}
$$

where the coefficient λ, the hydraulic resistance R, the hydraulic inductance L and the hydraulic capacitance C correspond respectively to the local loss coefficient, energy losses, inertia and storage effects. The form of Telegrapher's equations can be dedicated leading to an

(a) Model of Butterfly-type valve   (b) Equivalent circuit of valve
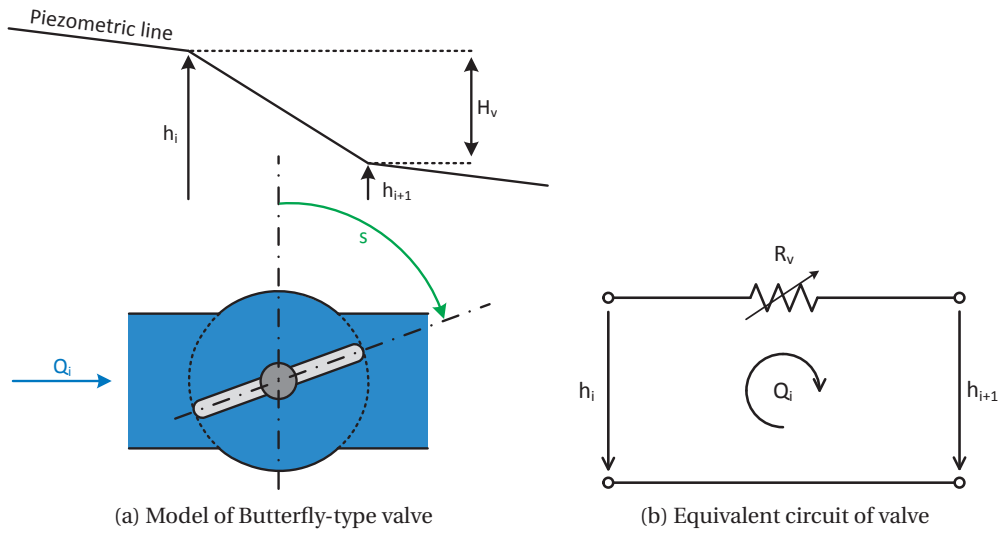
Figure 4.8: Valve modeling [8]

equivalent representation with a T-shaped circuit as seen in Figure 4.7b.

The equations relative to the circuit in Figure 4.7b are based on the Kirchoff's law. It is interesting to note that the analysis of this approach consists of wave propagation issues in a transmission line by considering the voltage and the current as the head and water discharge.

Valve

A valve is a device which regulates the flow by opening, closing or partially obstructing the flow according to the position "s" of the obturator. Moreover, the valve generates head losses which are calculated as

$$H_v = \frac{K_v(s)}{2gA^2} \cdot Q_i^2 \tag{4.3}$$

$K_v(s)$ is a head loss coefficient characterized by the position of the obturator. In one-dimensional modeling, the valve is represented by a hydraulic resistance as seen in Figure 4.8 where the value is function of the obturator position and the discharge.

$$R_v = \frac{K_v(s)}{2gA^2} \cdot |Q_i| \tag{4.4}$$

(a) Model of a surge tank　　　(b) Equivalent circuit of surge tank
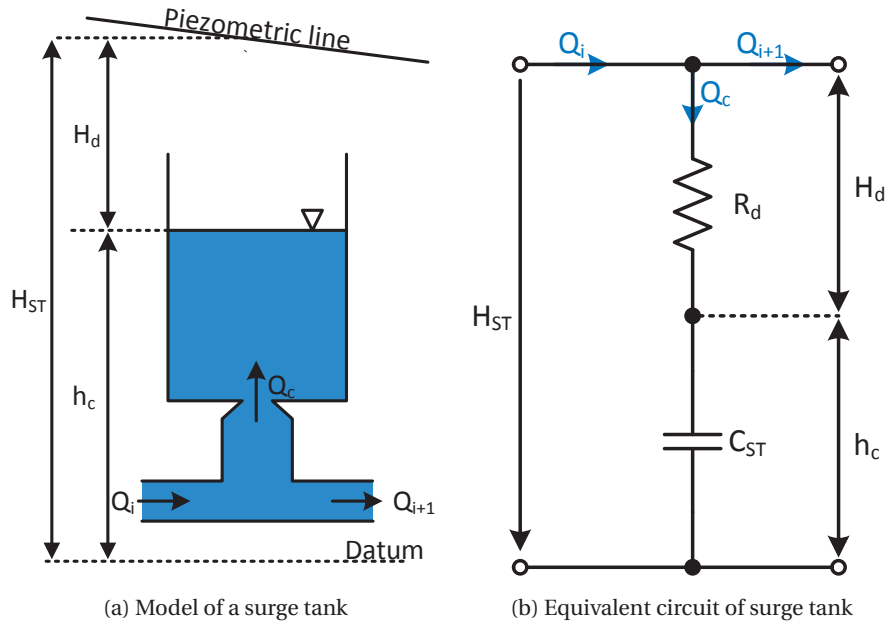
Figure 4.9: Surge tank modeling [8]

Surge Tank

A surge tank is a water storage device used for stabilizing any fluctuation of head (water hammer effect) and protecting the upstream gallery. The tank is a chamber characterized by great amount of volume (Figure 4.9a) which allows the conversion of the kinetic energy of the discharges into a potential energy (head). The sudden change of cross-section during the back and forth motion of the water is subject to energetic losses which is represented by a hydraulic resistance R_d in the equivalent circuit where the expression is given by:

$$R_d(Q_c) = \frac{K_d(Q_c)}{2gA^2} \cdot |Q_c| \tag{4.5}$$

with K_d the head loss coefficient and Q_c the discharge incoming in the surge tank. The head losses dissipated in the component is calculated by

$$H_d = \frac{K_d}{2gA^2} \cdot Q_c^2 \tag{4.6}$$

The capacitive behavior of the tank is represented by a capacitance C_{ST} in Figure 4.9b and is directly correlated with the cross-section of the device. The head of the T-junction is expressed as:

$$H_{ST} = h_c + R_d(Q_c) \cdot Q_c \tag{4.7}$$

with

$$Q_c = Q_i + Q_{i+1} \tag{4.8}$$

$$\frac{d}{dt} h_c = \frac{Q_c}{A(z)} \tag{4.9}$$

Pelton turbine

The Pelton wheel is an impulse type water turbine. It converts the kinetic energy of water flow into mechanical energy, as opposed to the reaction turbines that use kinetic and potential (pressure) energy.

High-speed streams of water coming from injectors are controlled by nozzle leadings to drive the wheel by pushing the buckets as illustrated in Figure 4.10a. The turbine induces a drop of head which is modeled by a resistance in the equivalent circuit in Figure 4.10b.

$$R_t = \frac{1}{\sum\limits_{i=1}^{N_{inj}} \frac{1}{R_{inj}}} \tag{4.10}$$

The resistance considers all N_{inj} injectors available in the turbine into a single equivalent one. Each injector is considered as a resistance given in Eq. 4.11 and depends upon the

(a) Model of Pelton turbine

(b) Equivalent circuit of Pelton turbine
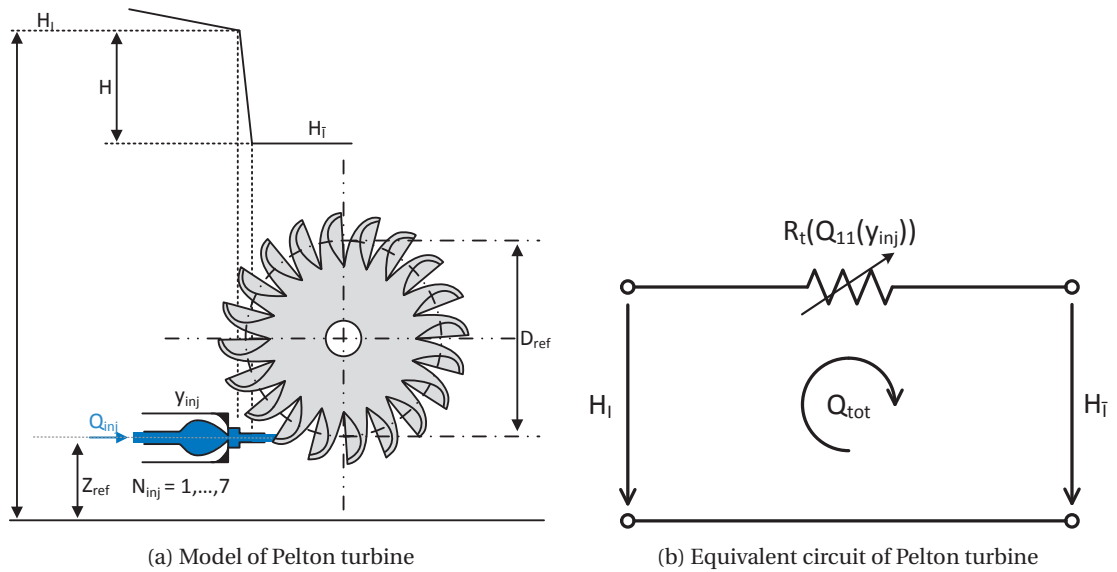
Figure 4.10: Pelton turbine modeling [8]

characteristic in Figure 4.11.

$$R_{inj} = \frac{|Q_{inj}|}{Q_{11}^2 \left(y_{inj}\right) D_{ref}^4} \qquad\qquad Q_{tot} = \sum_{i=1}^{N_{inj}} Q_{inj} \qquad (4.11)$$

The influence of injector contribution on turbine efficiency is neglected by considering a single equivalent injector in the case of a multi-injectors wheel.

The model converts the head drop H into a mechanical torque that is expressed as:

$$T = K_t \cdot \sum_{i=1}^{N_{inj}} T_{11} \left(N_{11}, y_{inj_i}\right) \cdot D_{ref}^3 \cdot H \qquad (4.12)$$

where K_t is a coefficient that considers the unsteadiness of the torque during its operation.

(a) Injector discharge characteristic (b) Torque characteristic
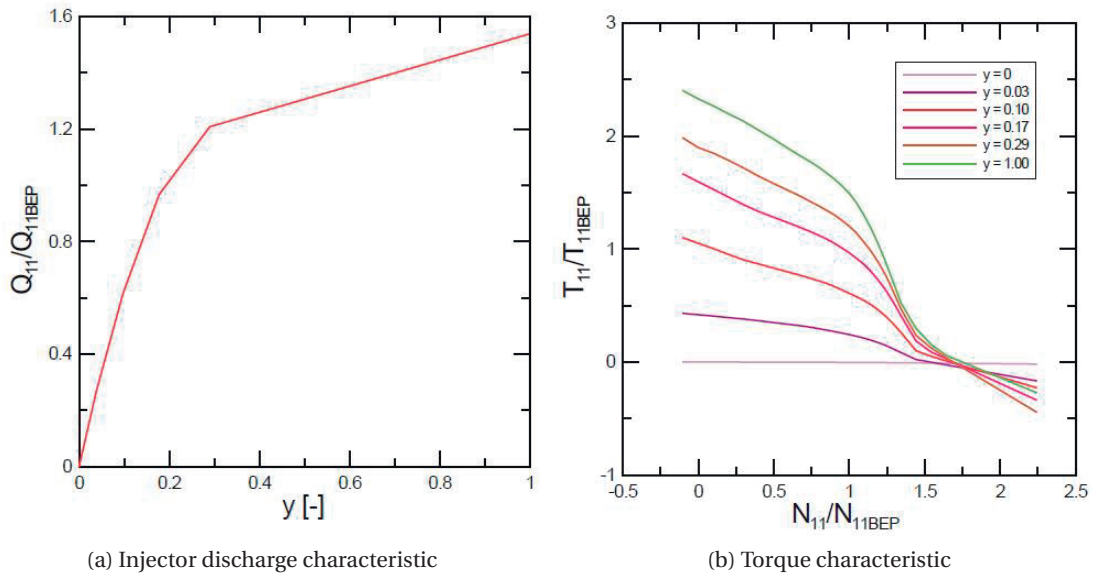
Figure 4.11: Typical single injector characteristics of Pelton turbine [8]

4.1.3 Real-time feasibility of Mottec Model

The model of the Mottec power plant from Figure 4.6 featured a matrix size of 321x321, which involves a real-time feasibility survey based on the Mottec model in SIMSEN. This survey is more important since a new general-purpose computer is dedicated to Mottec implementation, which specifications are reported in Table 4.2. This real-time feasibility is achieved using similar approach as in section 2.3.5, which consisted of characterizing the computation power against the matrix size.

The plot shows "Computation time at each T_{step} [ms]" on the y-axis versus "Matrix size [-]" on the x-axis, with a legend "Model of Mottec" and "Fitting curve", and the equation $y=9.25\cdot10^{-8}\cdot x^{2.93}+0.03$.
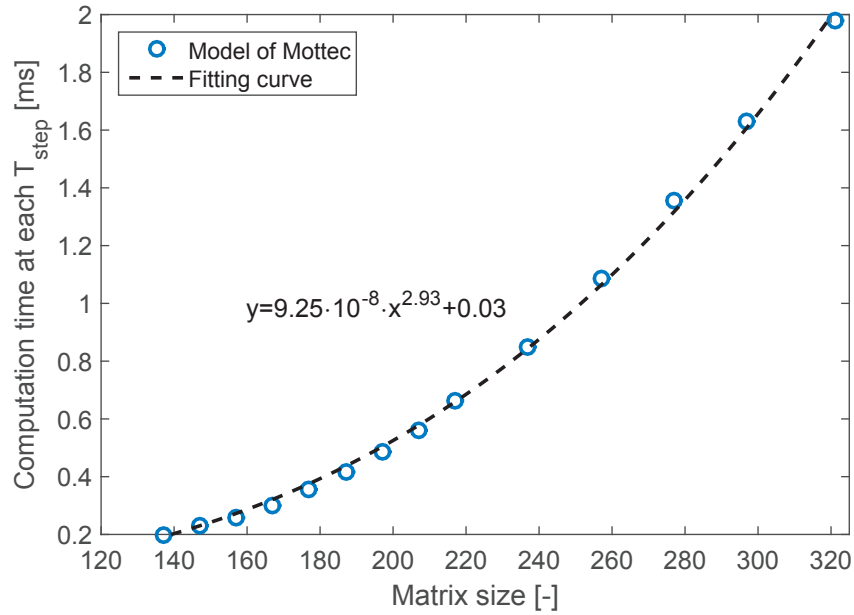
Figure 4.12: Performance of SIMSEN with the model of Mottec

As observed in Figure 4.12, the computation time takes 4 times longer against the settled integration step T_{step}=0.5 [ms] resulting to the situation where the duration of simulation is longer than the fixed simulation time. Under these circumstances, the use in real-time of the related model is then not applicable unless simplifications are carried out in order to improve the calculation performance. Figure 4.12 indicates that the limit of real-time feasibility is fixed to a model which matrix would be below a size of 200x200 and would induce a substantial gain of time.

System	Parameter
OS	Windows 7 64-bits
Processor	12x Intel(R) Xeon(R) CPU E5-1650 0 @ 3.2Ghz
Random Access Memory (RAM)	16 GB

Table 4.2: Specifications of general-purpose computer which is dedicated to the real-time simulation performed in Mottec

Simplification approach of hydraulic models

Since the model of electric components cannot be simplified, the approach of model simplification is applied on the hydraulic model of pipes. This latter component owns a model, which

(a) Without Adaptation   (b) With Adaptation
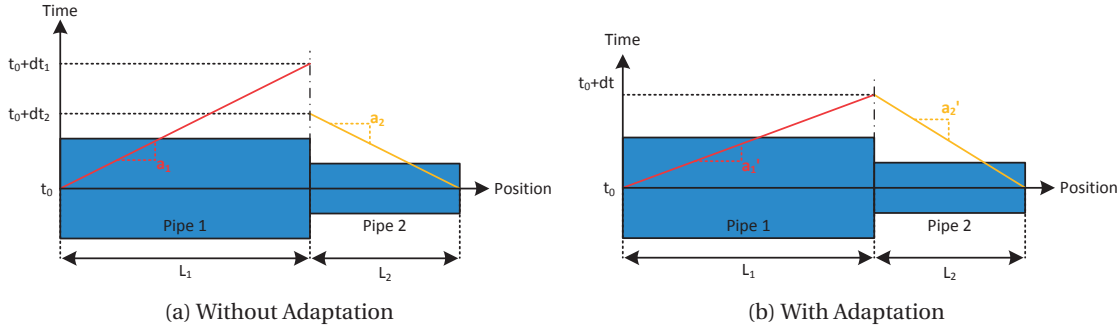
Figure 4.13: Illustration of wave speed adaptation [9]

accuracy is characterized according to the number of discretized length dx, as introduced in section 4.1.2. The procedure reduces the complexity of the pipe model by decreasing the number of dx, inducing the reduction of the general size of the matrix. Nevertheless, this simplification involves adaptation such as the wave speed of the pressure, which is defined in Eq. 4.13. The adjustment is an essential step in order to ensure the continuity of wave propagation at the intersection of two models of pipe as illustrated in Figure 4.13, which means the condition $dt = dt_1 = dt_2$ must be respected.

$$\frac{dx_i}{dt_i} = \pm a_i \quad , i=1,2,... \tag{4.13}$$

The procedure of simplification is carried out as follows:

1. Calculate the pipe wave speed a_i

2. Select a time basis dT

3. Calculate spatial discretization of the pipes $dx_i = a_i \cdot dT$

4. Compute number of elements of each pipe $N_{b_i} = \dfrac{L_i}{dx_i}$

5. Adapt the wave speeds a_i by a_i' and round N_{b_i} into a natural number

The application of the presented procedure on the original model of Mottec power station has resulted to a reduction of matrix size of 119x119. The simplified model has therefore enabled a gain of computation time by a factor 10 according to Figure 4.12. The new model owns an adequate computation cost with a sufficient time flexibility for real-time simulations. The results simulated in the simplified and the original models are compared in section 4.2.2 in order to validate the simplified model and confirm its accuracy.

4.2 Measurement campaign for model validation

Before the implementation of real-time system, a measurement campaign has been organized, which objectives are as follows:

- Collect measurement data from electric and hydraulic quantities in order to validate the model through offline simulations.

- Familiarization with unit system, i.e. behavior of control systems, nature of measurement signals, limits of operations in order to anticipate the required adaptations for the implementation of real-time system in SIMSEN.

4.2.1 Description of instrumentation

The measurements have been achieved using two different acquisition systems, see Figure 4.15a and Figure 4.15b. The hydraulic quantities such as head of penstock, head of surge tank and nozzle positions of turbine injectors with mechanical quantities such as power and rotor speed, were measured from the acquisition system of the power plant while the electric quantities from the generator such as stator voltages, stator currents and field current were recorded using a transient recorder with a sampling rate settled at 2 [kHz].

This partial use of the system involved the lowest risk of unexpected practical issues during the measurements. Indeed, the recording with the acquisition system of the power plant is not suitable for the acquisition of electrical quantities since it features a sampling rate of 10 [Hz], which is perfectly adequate for hydraulic quantities but not sufficient for the electrical time constants. On the other hand, the implementation of an external acquisition device without a perfect knowledge of the acquisition system would give a preparation too demanding, which would also trouble the station operator. Therefore, this solution enabled to implement all the required sensors for electric quantities within the given time.

The implementation of measurement instrumentation is presented under the format of wiring scheme in Figure 4.14. The stator quantities of the synchronous machine is measured by means of voltage and current transformers ($N°1$ and $N°2$) due to the high level of amplitude of electrical quantities on the phases. Moreover, the use of these devices enable a galvanic separation, preventing damages of sensors in the cases of faults. The line voltages and the phase currents are therefore measured by their respective transducers ($N°2$ and $N°5$) connected to the secondary side of their respective transformers. Three "short-circuiters" ($N°4$) as seen in Figure 4.15c are placed between the current transformer and the transducers. This enables to isolate the transducers from the circuit for eventual handling by short-circuiting

61
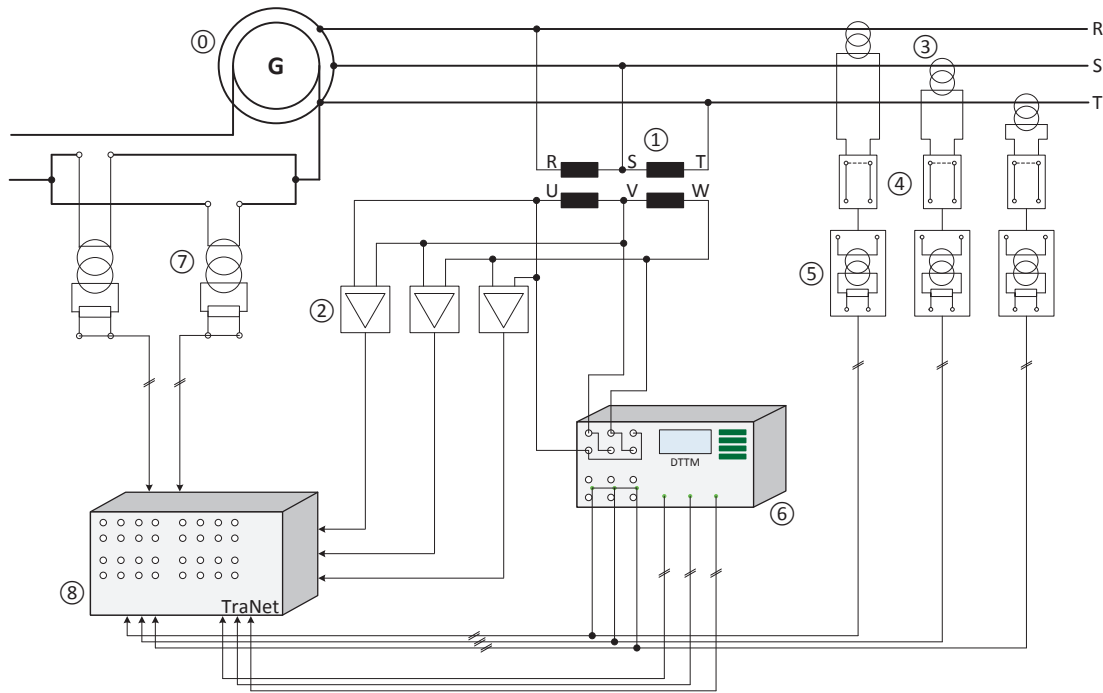
Figure 4.14: Wiring scheme of the campaign

$N°$	Device	Specifications
0	Generator	Rated voltage/current : 9000 [V_{RMS}]/1960 [A_{RMS}]
1	Voltage transformer	Ratio : 9000:110 [V_{RMS}]
2	Voltage transducers	Range : 800 [V_{RMS}], Output : ±10 [V]
3	Current transformer	Ratio : 2000:1 [A_{RMS}]
4	Short-circuiters	-
5	Current transducers	Range : 2 [A_{RMS}], Output : ±10 [V]
6	DTTM	Range : 50, 500 [V_{RMS}]/5 [A_{RMS}], Output : ±10 [V]
7	Current transducers	Range : 1000 [A], Output : 8 [V]
8	Transient recorder	16 differential inputs of ±10 [V]

Table 4.3: List of devices from Figure 4.14

the secondary side of the current transformer without carrying out the full standstill of the generator.

The DTTM device ($N°$6) uses the measurement signals of stator voltages and stator currents to estimate the the air-gap torque as detailed in appendix A.3. The current transducers for DC current ($N°$7) are directly implemented on the rotor circuit as seen in Figure 4.14. The accessible portion of the circuit comprises two identical cables in parallel, the total field current is obtained by summing the signals from the transducers placed on each cable as

seen in Figure 4.15f. Finally, all the output signals from the described sensors are all directly connected to the transient recorder ($N°8$), where signals conversion are carried out to obtain the real value of measurements.
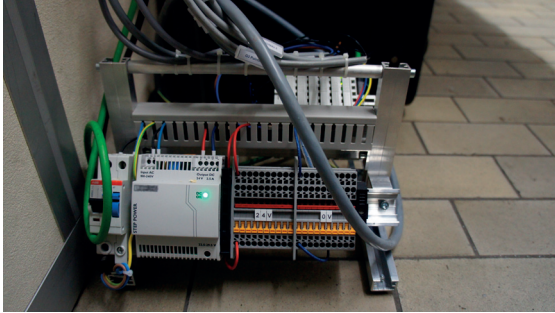
(a) Acquisition system for hydraulic quantities
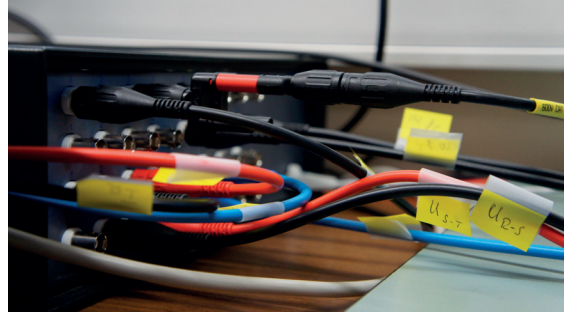
(b) Transient recorder
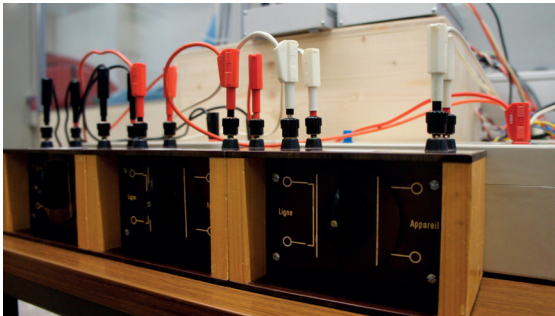
(c) Short-Circuiters
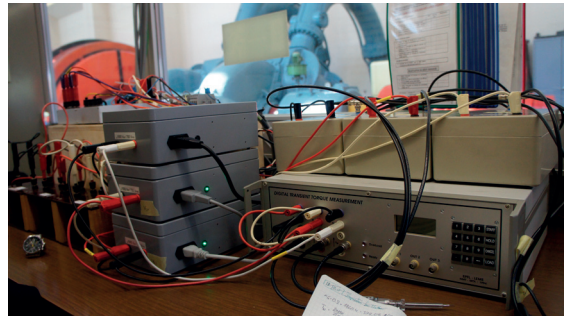
(d) Voltage and current transducers with the DTTM
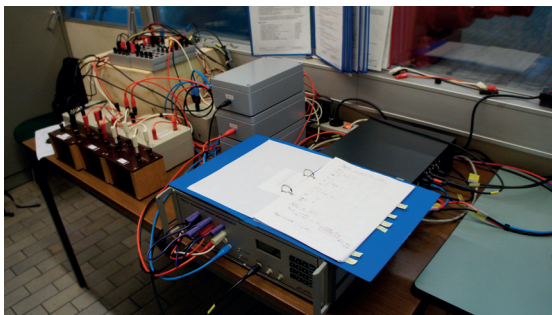
(e) Overall view of sensors installation
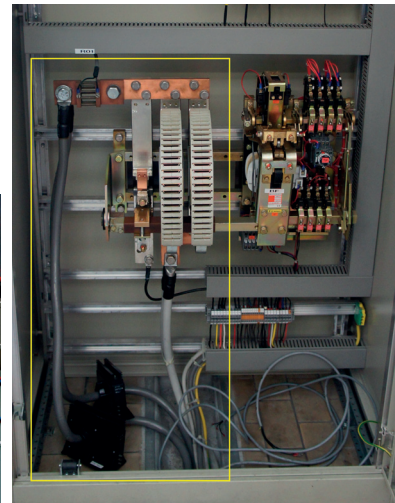
(f) Rotor circuit with the two current transducers

Figure 4.15: Installation of various measurement instruments

4.2.2 Offline validation using experiment data

As mentioned previously, the test cases are performed on the group 3 of the power station, which is fed by Moiry reservoir, with the other units at standstill. The water level evaluated the day of the test is 2240 [masl] and was deduced from the pressure measurement on the surge tank, considering the height of the reservoir against the power station. Two test cases are presented with the generator convention in the following subsection to validate the model :

1. Load variation: The unit is operating at an initial operating point with P=4.5 [MW] and Q=1.5 [MVar]. At t=3.2 [min], the position of injectors changes to reach a turbine power P=22 [MW] in 60 [s] for emulating a sudden increase of load. Then, the group operates in steady-state until the stabilization of Tsarmette surge tank.

2. Load rejection: The unit is stabilized initially at the nominal power P=24 [MW] with a power factor $\cos(\phi)$=1. With the generator connected to the power network at t=1 [min], the injectors is closed in 60 [s], forcing the turbine power $P \approx 0$ [MW] while the field current reaches its no-load value, inducing a reactive power $Q \approx 0$ [MVar]. The initial state of the group is restored 20 [s] after the load rejection.

The validation of the simulation model of Mottec is performed under similar conditions as it would be in real-time. Indeed, the use of the collected data of the boundary conditions in the SIMSEN simulations by means of an external function, which reads and assesses the data as in a real-time simulation, enables to obtain identical operating states as the physical plant and the transient behavior as well. The boundary conditions used in the simulation are:

- Nozzle position of injectors: The position of injectors defines the mechanical power which is feeding the generator before being converted into electric power.

- Three-phase voltage of the network: The voltage RMS-value is calculated from the line voltages before applying in the model as the test bench model in chapter 3, whereas the frequency of the network is assumed as constant and settled at the nominal value, 50 [Hz].

- Field current: The field current assesses the variation of reactive power in the SIMSEN model by transforming the measured values into voltage level before being applied to the model.

This kind of simulations offer not only the possibility to validate the model, but also allow to observe the behavior of the simulation with real data and thus issue such as the signal noise, can be anticipated and adapted with a filter.

Load variation

As seen in the top plot of Figure 4.16, the measured position of the four injectors increase at t=3.2 [min] from 14 [%] to 63 [%] within 60 [s], inducing an increase of mechanical power transmitted to the generator moving from P=4.9 [MW] to 22 [MW] as seen in the middle plot
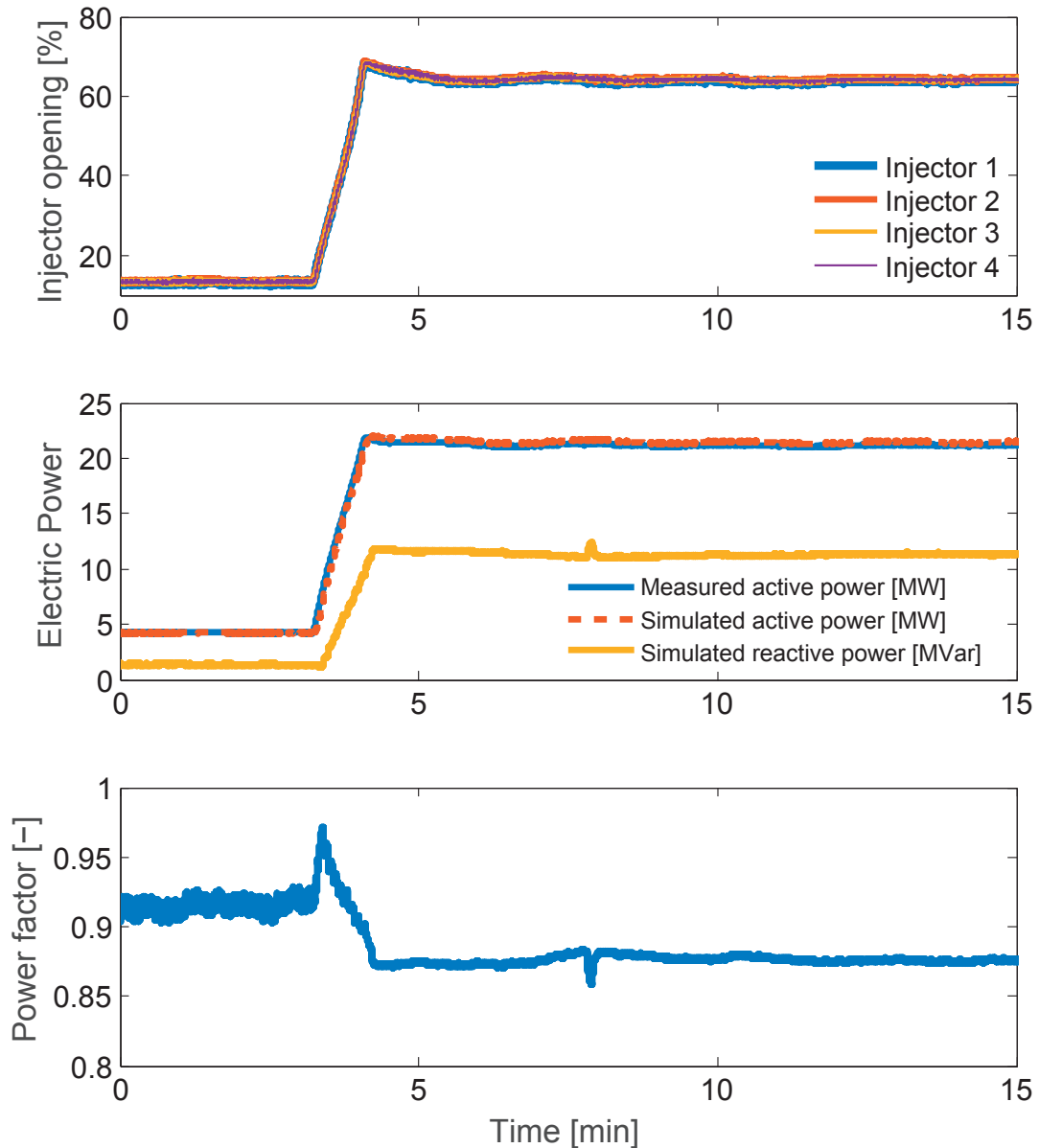
Figure 4.16: Transient behavior of unit 3 in term of powers resulting from injectors opening; Injectors opening (Top); Increase of active power due to the increase of turbine power and increase of reactive power by the control system in order to maintain the power factor (middle); Power factor of unit 3 estimated from the simulated powers (bottom)
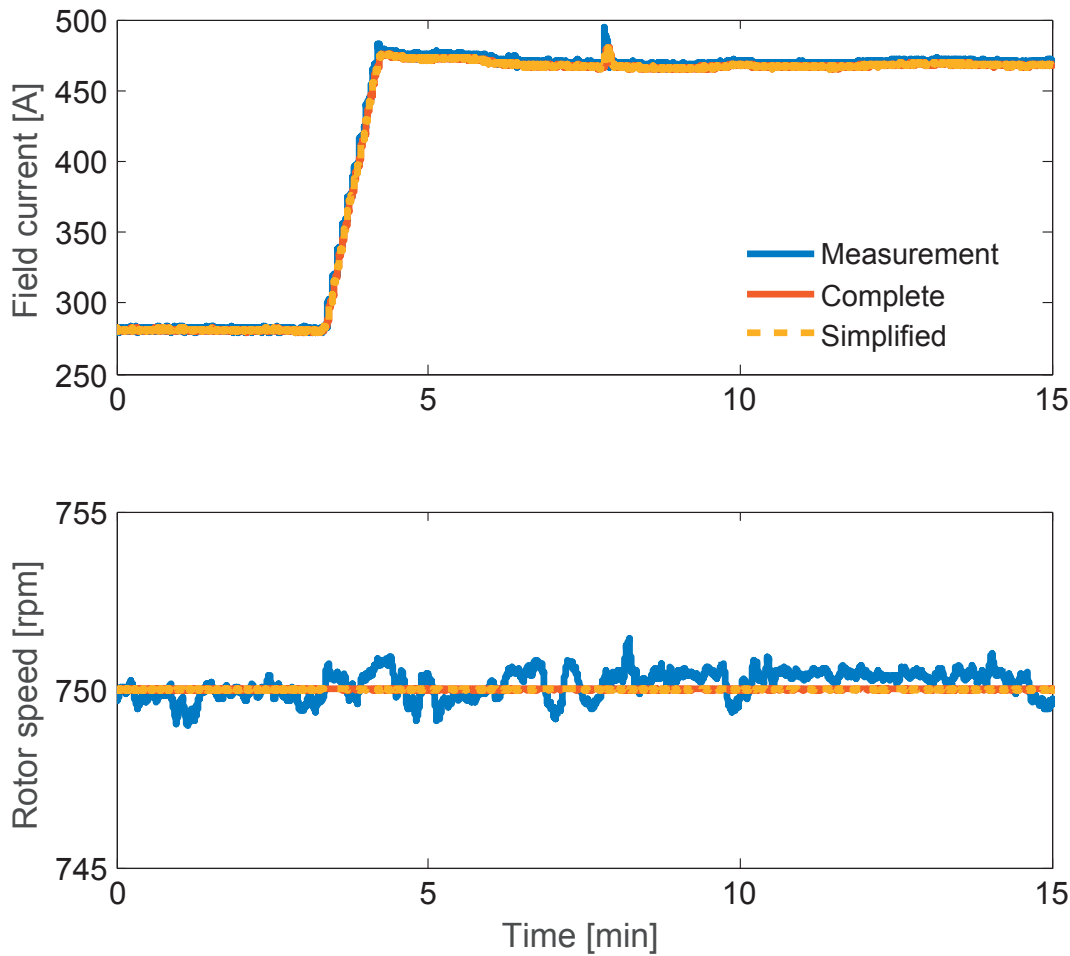
Figure 4.17: Comparison simulation-measurement during the load variation test: Increase of field current to increase the reactive power (top); Rotor speed of unit 3 which is not disturbed by the variation of active power and remained constant (bottom)

of the same figure. The control system of the power plant increases the field current (Figure 4.17) at the same time, inducing a modification of reactive power from 1.26 [MVar] to 11.23 [MVar] in order to maintain the power factor as constant as possible, settled at $\cos(\phi)$=0.9 as seen in the bottom plot of Figure 4.16. With a voltage level of the network fixed at 8.8 [kV], measured on the stator windings, the rise of active and reactive powers induce an increase of intensity of stator current as seen in Figure 4.19 moving on from 300 [A_{RMS}] to 1560 [A_{RMS}].

On the hydraulic side, the injectors opening induces a waterhammer effect in the penstock, starting from an increase of water discharge, which induces a drop of head according to mass oscillations as seen in Figure 4.18. The related head fluctuations is absorbed by Tsarmette surge tank as the discharge of unit 3 remains constant from t=5.45 [min].
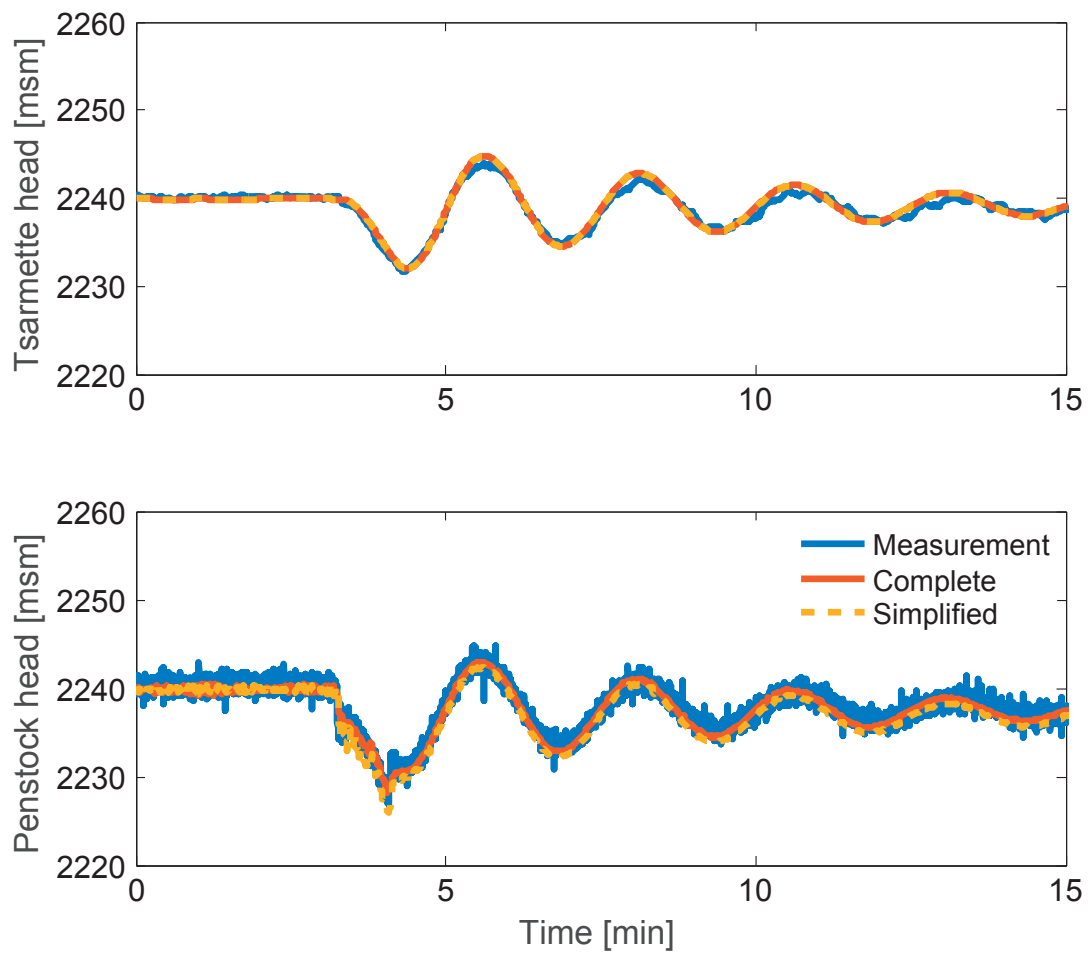
Figure 4.18: Comparison simulation-measurement during the load variation test: Head of surge tank (top) and penstock head (bottom) generated by the injectors opening
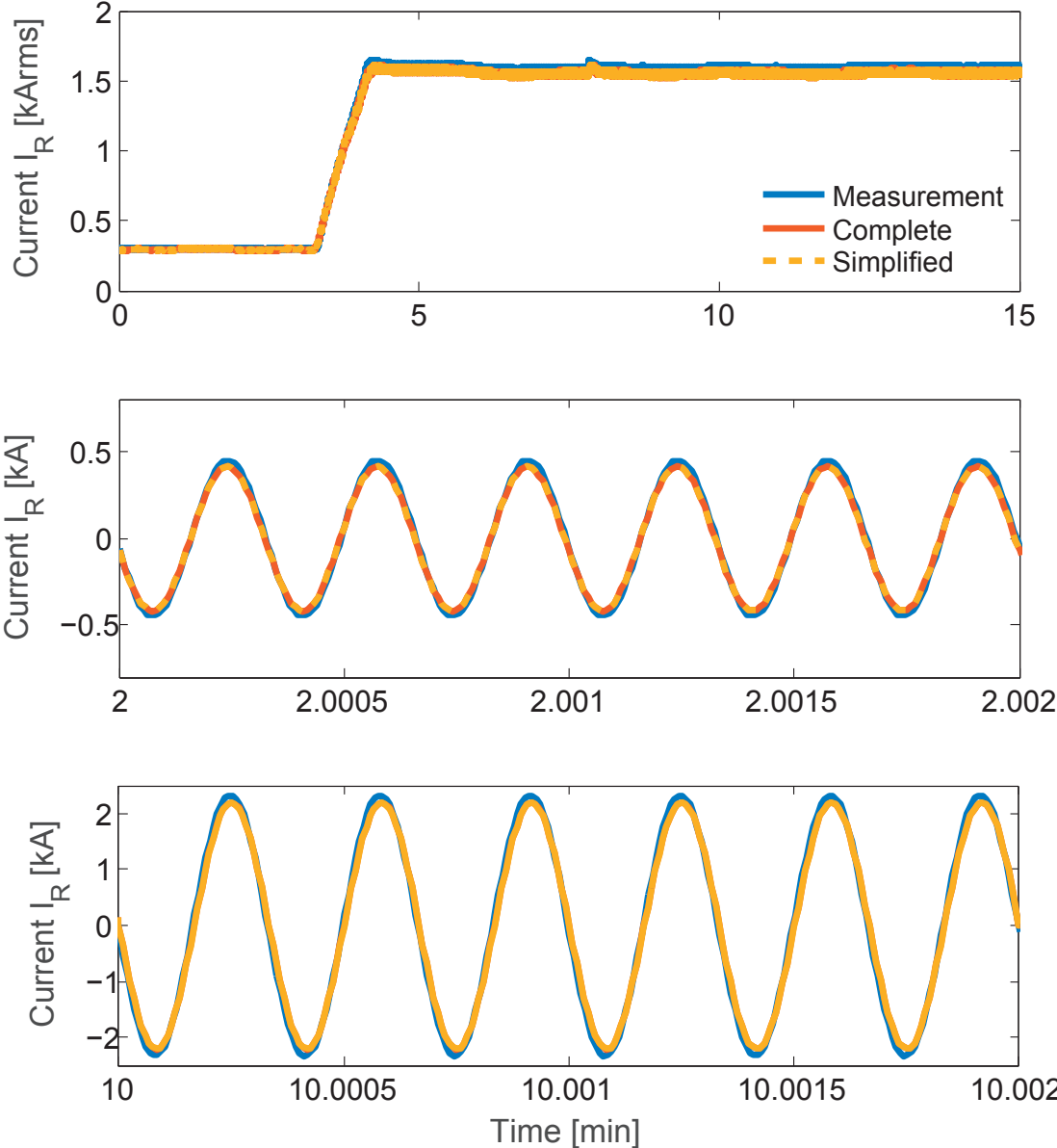
Figure 4.19: Current of phase "R" circulating through the stator windings during the load variation; RMS-value of current during the test (top); Zoom of the current before the injectors opening (middle); Zoom of the current after the power increase (bottom)

load rejection

With a voltage level of 8.8 [kV], the unit operates at P=24 [MW] with a $\cos(\phi)$=1, i.e. Q=0 [MVar]. The power factor was handling from 1 to 0.9 by modifying incrementally from 380 [A] to 350 [A] as seen in Figure 4.21, at the moment when the load rejection procedure triggered.
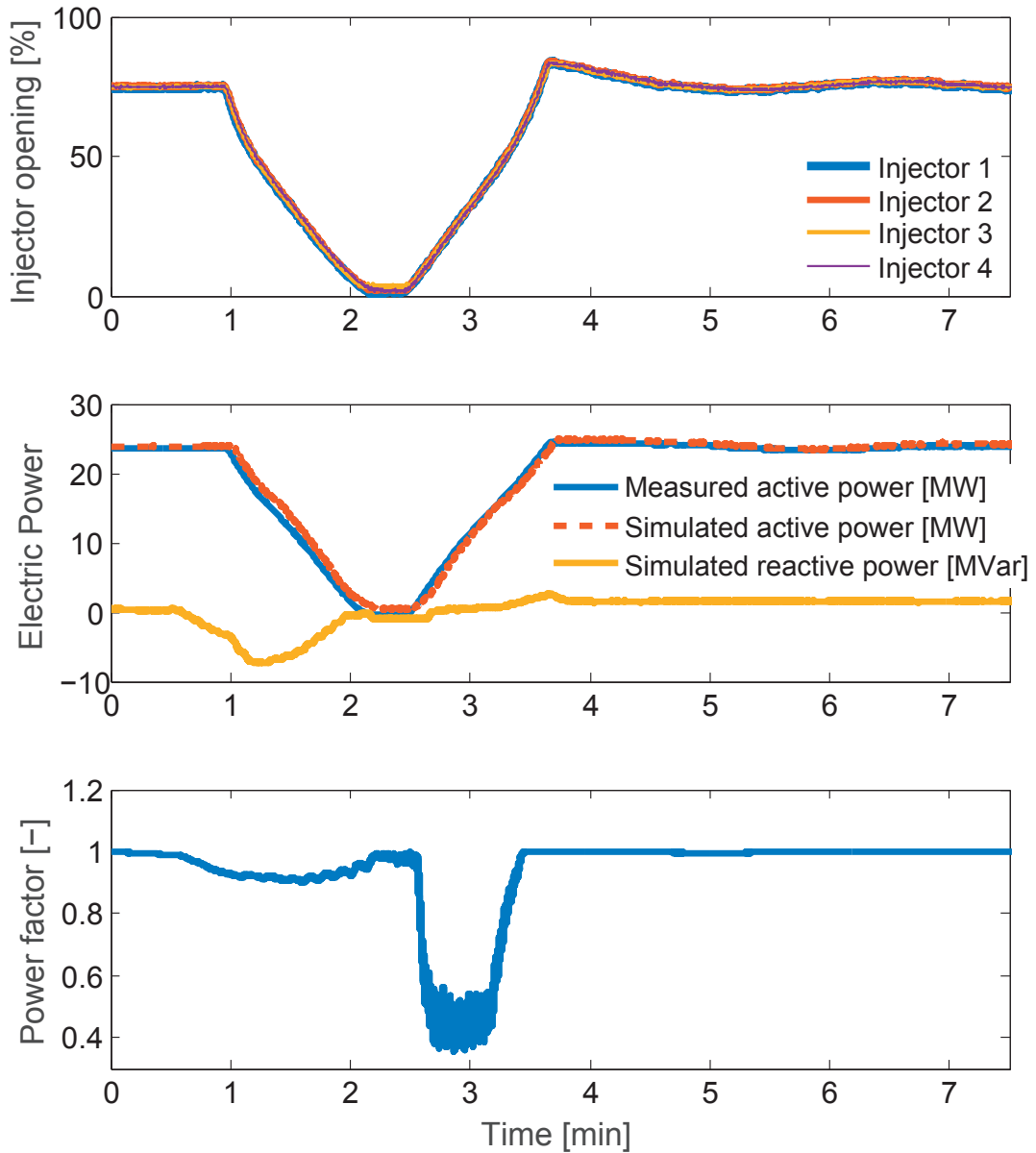
Figure 4.20: Transient behavior of generator powers of unit 3 during the load rejection and immediate recovery to the initial state before the event; Nozzle position of injectors (top); Powers evolution of unit 3 during the event (middle); Estimated power factor from simulated powers (bottom)
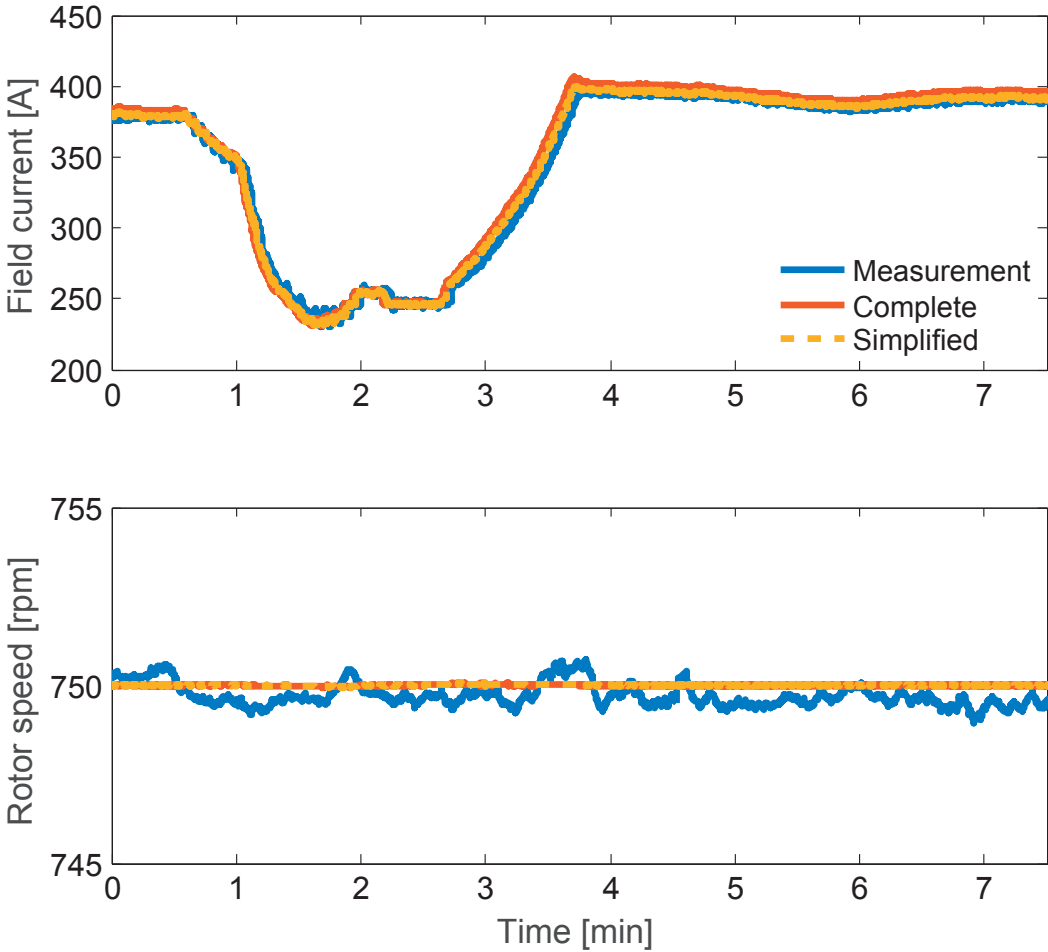
Figure 4.21: Comparison simulation-measurement during the load rejection test: Behavior of the field current during the load rejection (top); Rotor speed of unit 3 (bottom)
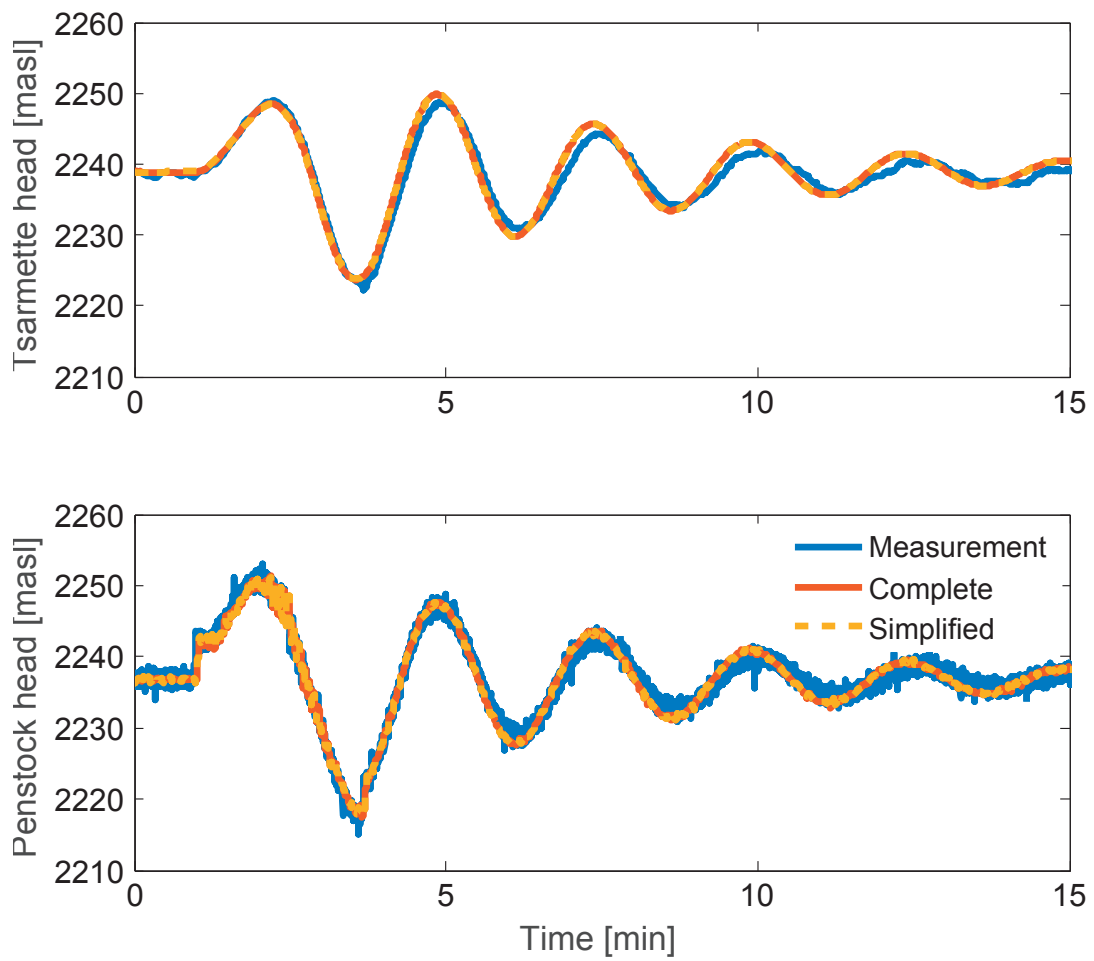
Figure 4.22: Comparison simulation-measurement during the load rejection test: Head of Tsarmette tank (top) and penstock (bottom)
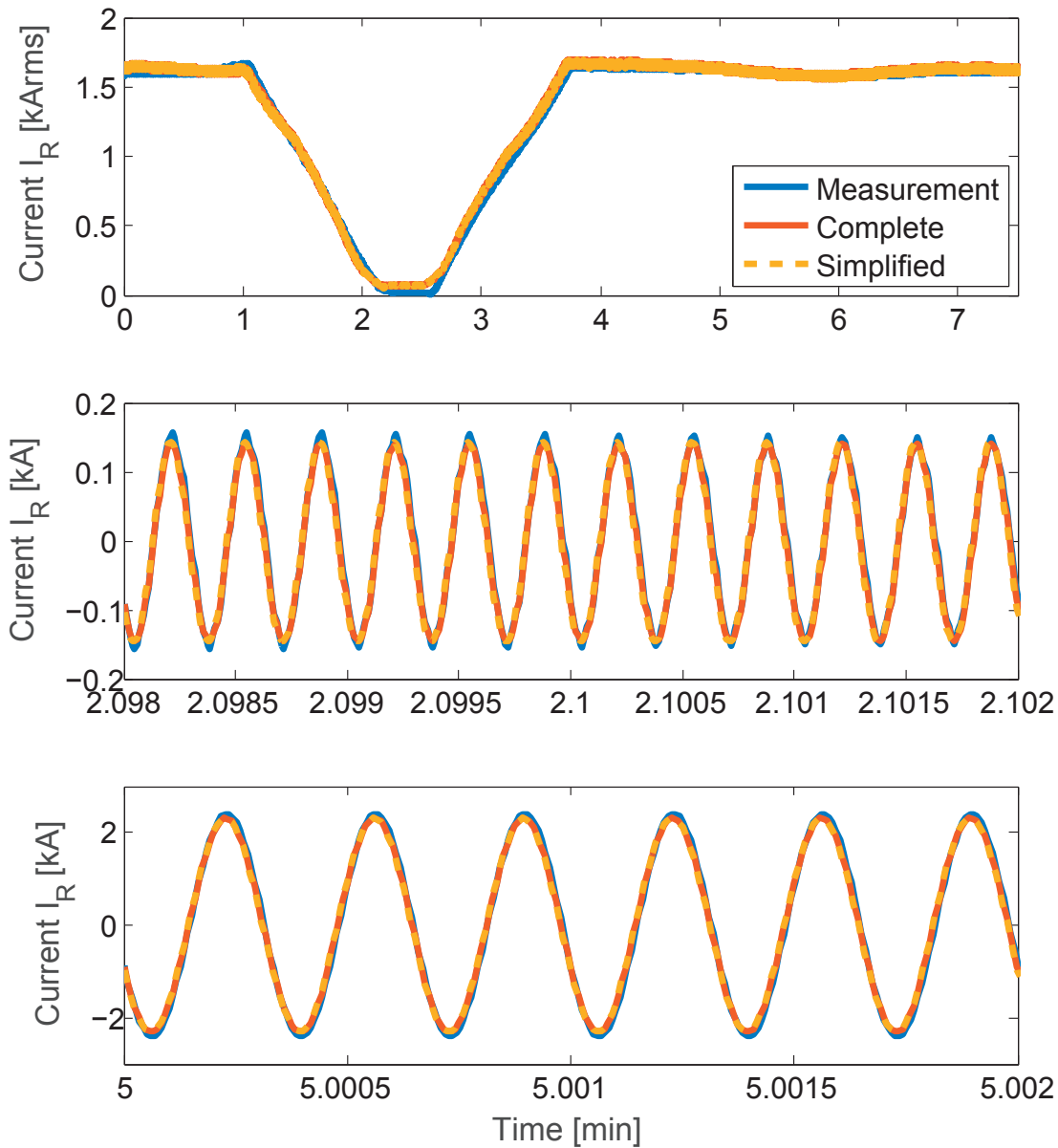
Figure 4.23: Evolution of stator current in the phase "R" during the load rejection; RMS-value of current during the test (top); Zoom of the current when the powers are nil (middle); Zoom of the current after the recovery (bottom)

The field current is therefore brought down to its no-load value, measured at 250 [A] with an overshoot induced by the regulator of the control system. The injectors closing fell down from 0.75 [%] to 1.6 [%], which corresponds to a turbine power approximately nil for 20 [s] before the unit recovers to its initial state of operation. The sudden reduction of water discharge during the closing of injectors generates a rise of head in the penstock, which is propagating

to the surge tank with a delay, leading to the waterhammer effect as seen in Figure 4.22. The premature opening of injectors before the stabilization of Tsarmette tank emphasized the head drop with an amplitude of 34 [m] against 9 [m] in the first peak of the oscillation at 2.23 [min]. The fluctuations of the hydraulic energy is absorbed by the surge tank as the nozzle positions are constant, enabling a fast stabilization of the hydraulic installation.

The transient behavior of the currents flowing the stator windings have similar behavior as the active power with an initial amplitude of 1.6 [kA_{RMS}].

4.2.3 Conclusion

The good agreement between simulations outcomes and measurements attests of the model precision. Indeed, the hydraulic model considered for this study has correctly reproduced the waterhammer effects in the penstock after a variation of power in the turbine as expected. The validation of hydraulic model is especially emphasized with the agreement of the dynamic of the surge tank with the correct modeling of the component for the amplitude and frequency oscillations and with the timing of the beginning of fluctuations, which corresponds to the modeling of the penstock with the approximation of the speed of wave propagation.

The modeling of electric installation has demonstrated the correctness of the model with the comparison of the currents circulating through the stator windings with Figure 4.19 and Figure 4.23, which maximal error was estimated to 3.2 [%] on the amplitude. Additional test cases are available in appendix B.2.

The use of measured data has enabled the hydraulic power station to carry out offline simulations under similar conditions as a real-time simulation. Indeed, the use of the data from the measured boundary conditions has ensured the exact procedure of each variation of power, which allowed the model to be under the same conditions as the physical plant. Moreover, the noise from the sensors and sampled by the acquisitions systems did not alter the simulations outcomes, permitting thus to perform real-time simulations without eventual filters.

Furthermore, the simplification applied on the hydraulic system showed identical results with the complete model with a gain of time of a factor 10. Therefore, the simplified model is applicable in real-time with the certitude that the results will show good agreements as long as the boundary conditions are identical.

4.3 Measurement campaign for real-time implementation

The second measurement campaign has the objective of testing the real-time simulations using SIMSEN running on a standard computer with a complete model of Mottec power plant for:

- Achieving real-time simulations under real conditions;

- Testing the the real-time simulations for hours.

Real-Time interface of SIMSEN

The real-time layer of SIMSEN presented in chapter 2 presents some major drawbacks and was inadequate for the use in the power plant. Consequently, a new real-time equipment has been provided by Power Vision Engineering Sàrl (PVE) for the tests and then adapted for implementation in the power plant. This development was motivated by

- SIMSEN-RT introduced in chapter 2 could not ensure the real-time condition using the Mottec model with a time step below 1 [ms].

- The acquisition card SORCUS did not feature enough exploitable channels for all measured quantities.

- Even all the channels were available, the price of one SORCUS I/O module is significantly more expensive than the whole new hardware.
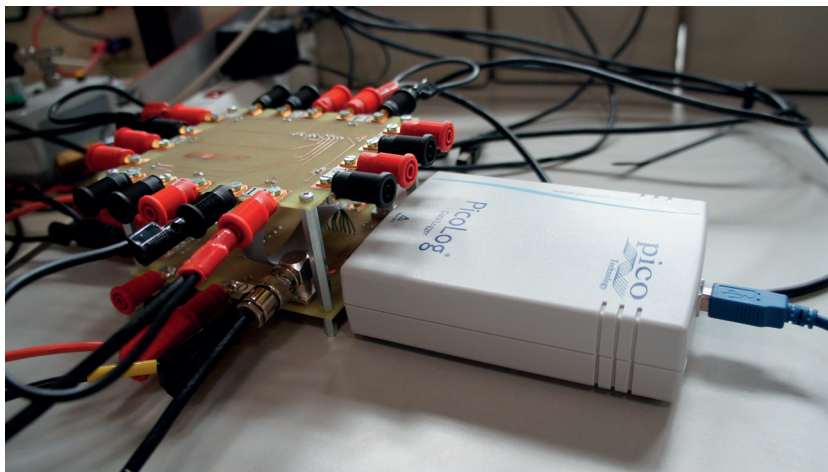
Figure 4.24: Acquisition card PicoLog1216 data logger

Consequently, the development of the new real-time layer involves a new acquisition device, the data logger "PicoLog-1216" as seen in Figure 4.24. This device also ensures the real-time in SIMSEN without modifying the simulation time characteristic in Figure 4.12 since the resolution engine remains the same.

Parameters	Specifications
Sampling rate	Up to 1MS/s
Analog inputs	16 per data logger
Bandwidth	Up to 70 [kHz]
Input type	Single-ended, unipolar
Input Range	0-2.5 [V]
Resolution	12 bits
PC connection	USB 2.0

Table 4.4: Specifications of PicoLog1216 in Figure 4.24

However, this acquisition device owns unipolar voltage inputs comprised between 0-2.5 [V]. This specification makes the acquisition of AC signals in voltage and the current signals not possible without an intermediate device which will adapt them to fit the device inputs.

The interface presented in Figure 4.25, is directly plug into the the PicoLog with the D-sub connector. Two PCBs are mounted on two stages which are connected each other by means of a ribbon cable, in order to include all the 16 inputs. The design of the circuit, detailed in B.1, is specifically made for the implementation of this campaign with a passive circuit. The calibration and the conversion coefficient are carried in the simulation tool.

(a) Top view

(b) Side view
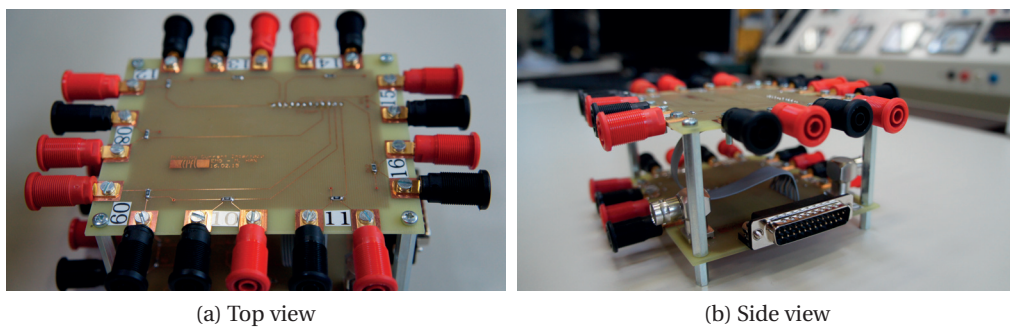
Figure 4.25: Interface for the PicoLog with passive circuits in order to fit the input range

4.3.1   Description of SIMSEN-RT instrumentation

The wiring scheme of the second measurement campaign remains identical, especially with the devices implemented during the first test, i.e. $(N°0 - N°8)$. The observable differences come from the connection to the computer $(N°11)$ via the PicoLog $(N°10)$, which interface $(N°9)$ gathers the signals from the transducers and the signal from the acquisition system of the power plant.
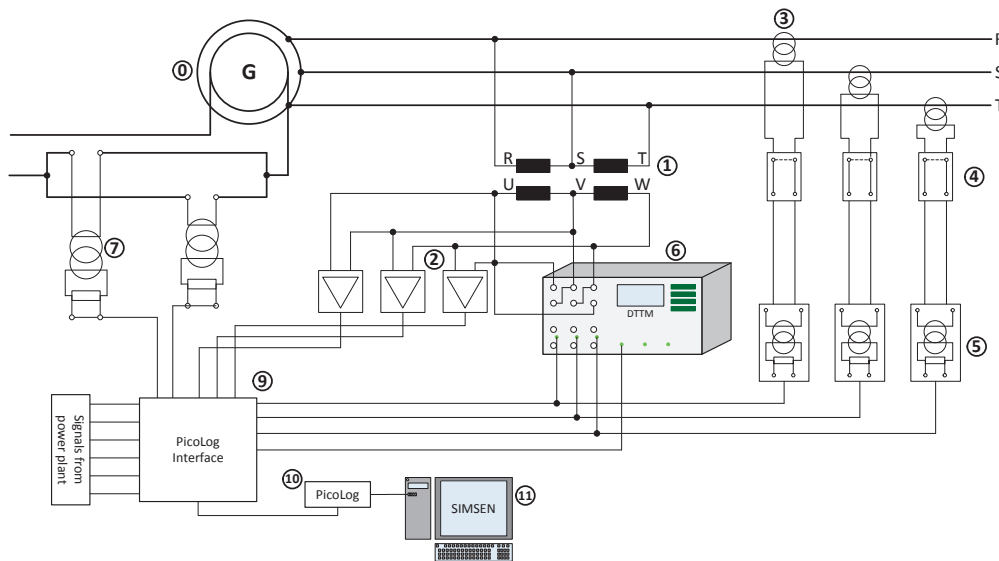
Figure 4.26: Wiring scheme for the implementation of SIMSEN running in real-time

$N°$	Device	Specifications
0-8	-	Specifications listed in Table 4.3
9	PicoLog interface	7 voltage inputs for AC signals, 9 current inputs signals up to 25 [mA]
10	PicoLog data logger	Specifications reported in Table 4.4
11	General-purpose computer	Specifications reported in Table 4.2

Table 4.5: List of devices from Figure 4.26

To sum up, the PicoLog device samples 7 electric quantities such as the stator voltages, the stator currents and the field current from the transducers. The other quantities such as the 4 nozzle positions of injectors, the head of the surge tank and the penstock, the speed and the reactive power are measured by the power plant system, but their signals are acquired by PicoLog.

4.3.2 Real-time validation of Mottec model

The tests of this measurement campaign are performed under identical conditions, i.e. unit 3 connected to a voltage level of 8.8 [kV] power network through the generator mechanically coupled to the Pelton turbine, supplied from the Moiry reservoir with a water level measured at 2158 [masl] at that day. The selected test case enables to evaluate the real-time simulations in SIMSEN, which was achieved without any interruptions during 100 [min]. The sequence is divided into two parts as follows, due to the quantity of data for convenient display:

- 0-40 [min]: Unit 3 operates in steady-state with P=3.5 [MW] and Q=0 [MVar]. At t=13 [min], the turbine injectors open to increase the power at P=11 [MW] and it is maintained until the end of the test.

- 40-100 [min]: While the power remains constant, the reactive power is modified from 0 to -3 [MVar] at t=42.6 [min], followed by a change from -3 [Mvar] to 4.5 [Mvar] at t=73.15 [min].

The modified model for real-time simulation is presented in Figure 4.27, without the hydraulic installation of Turtmann nor the units 1 and 2 for a better visibility. This latter is driven by four boundary conditions in order to verify the outputs, i.e. the three-phase stator current as previously. Indeed, The measured three-phase voltage is read through an interface represented with a macro element. Its values are then applied on the three-phase voltage source to obtain the similar voltage level. Field current is also applied on the excitation system of the model
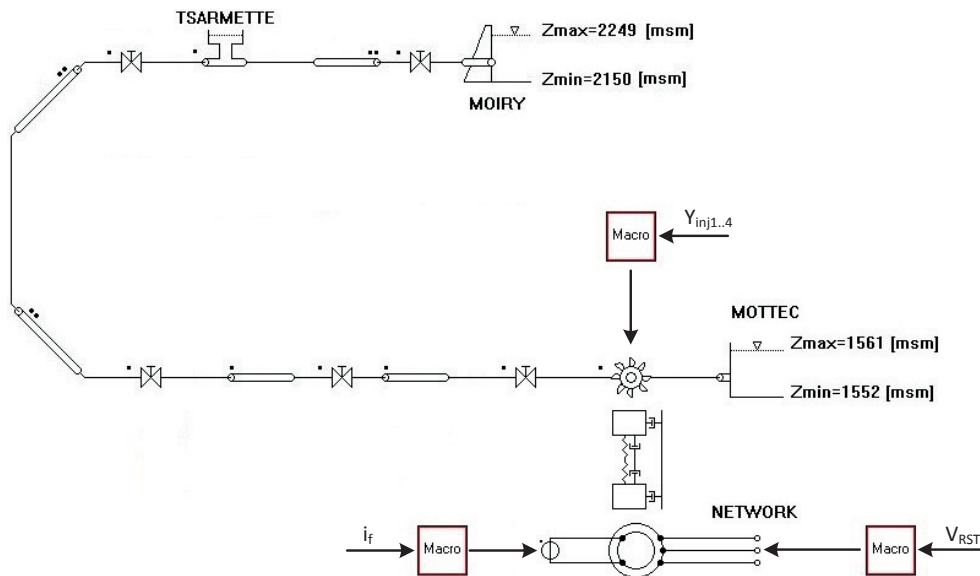
Figure 4.27: Modified schematic drawing for real-time application

from the measured value. This quantity enables to reproduce the excitation state of the generator, which is verified with the reactive power. The active power is regulated from the turbine model, which is driven by the nozzle position of the injectors. The fourth considered boundary condition is the water level in the Moiry reservoir. This quantity is not measured throughout the simulation since it does not fluctuate significantly during the measurement campaign. Therefore, its value is estimated ($H_0 = 2161.48$ [masl]) for the initialization before the start of real-time simulation.

Variation of active power (0-40 [min])
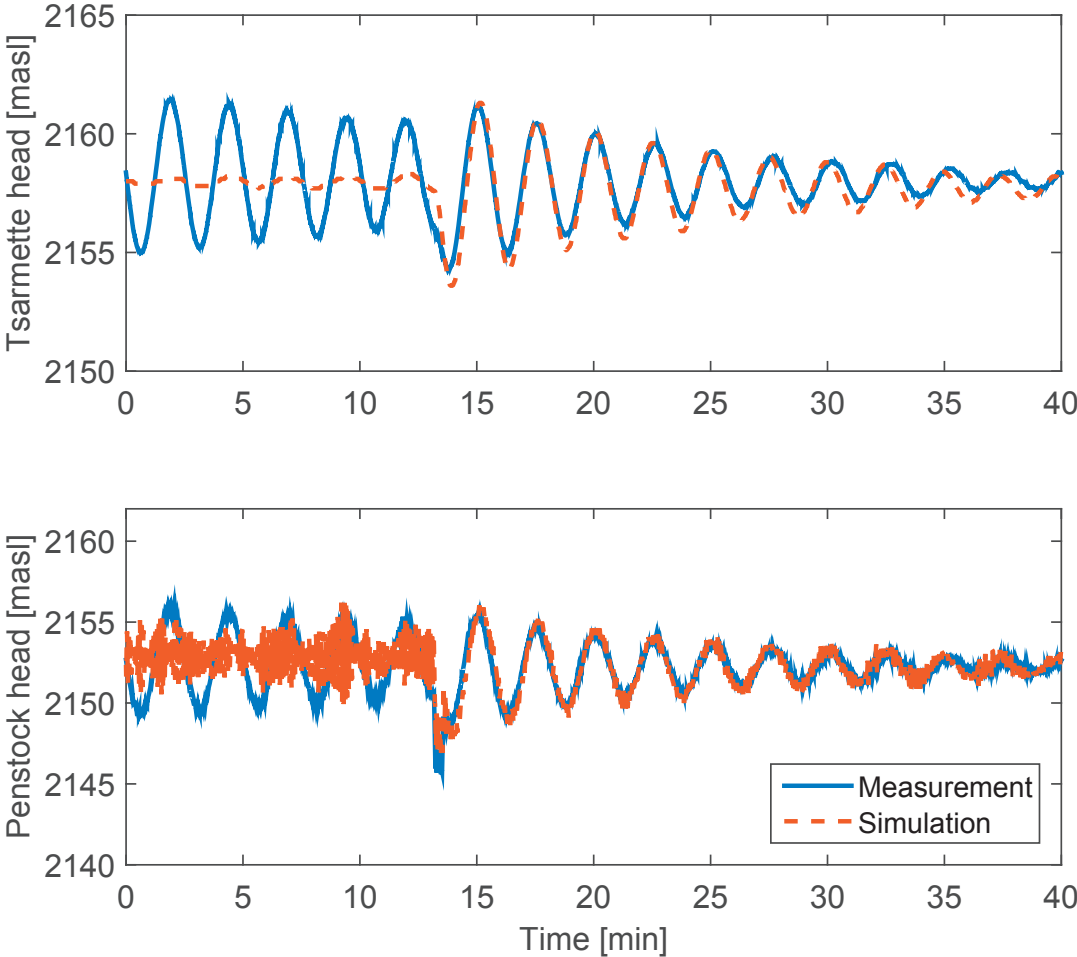
Figure 4.28: Surge tank(top) and penstock(bottom) heads
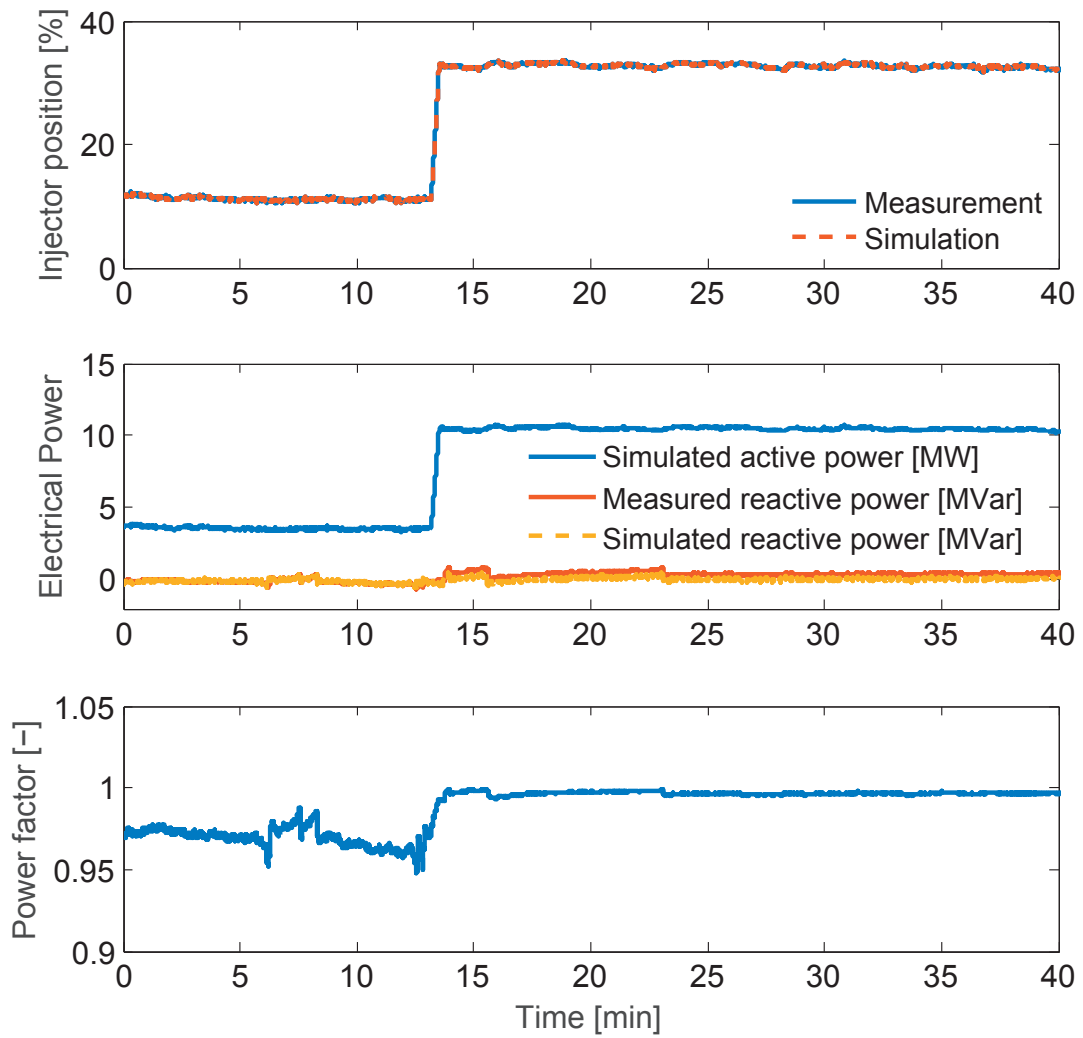
Figure 4.29: First part of the test with a power step from 4.5 [MW] to 11 [MW]; Injector position (top); Electric powers of the generator with measured reative power (middle); Estimated power factor from simulated powers (bottom)
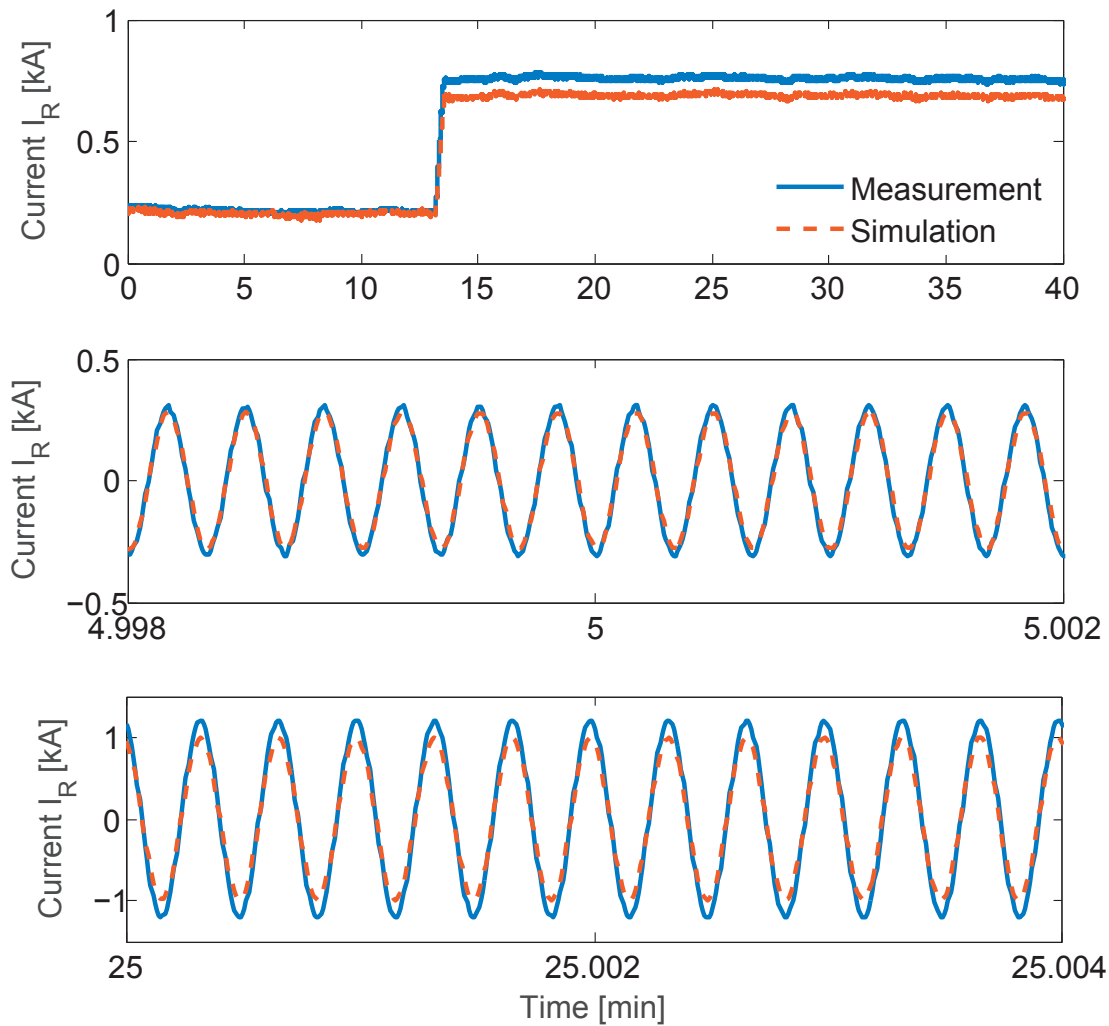
Figure 4.30: Stator current in the phase "R"; RMS-value of current (top); Zoom of the current before modification of power (middle); Zoom of the current after step of power (bottom)

The variation of active power induces a modification of power factor, which is initially settled to 1 as observed in Figure 4.29. Consequently, control system of the generator will react in order to maintain this factor equal to 1 by acting on the field current justifying the increase of the intensity on the top plot of Figure 4.31.

It is to be noted first that the presented test case was performed before the complete stabilization of Tsarmette from previous tests, due to a tight schedule as observed in Figure 4.28. Therefore, the head of the surge tank and penstock are initially subject to mass oscillations before the increase of active power, contrary to simulation results. Nevertheless, the water hammer effect at t=14 [min] is correctly represented as seen on the bottom plot of Figure 4.28 with a sudden variation of pressure. In addition, the mass oscillations induced in the surge

tank show good agreements according to the expectations.

Finally, the simulated stator current in Figure 4.30 shows a good agreement against the measurement despite an error of 10 [%] after the step of power, emphasized by the error of 1.19 [%] in the field current, observed in Figure 4.31.
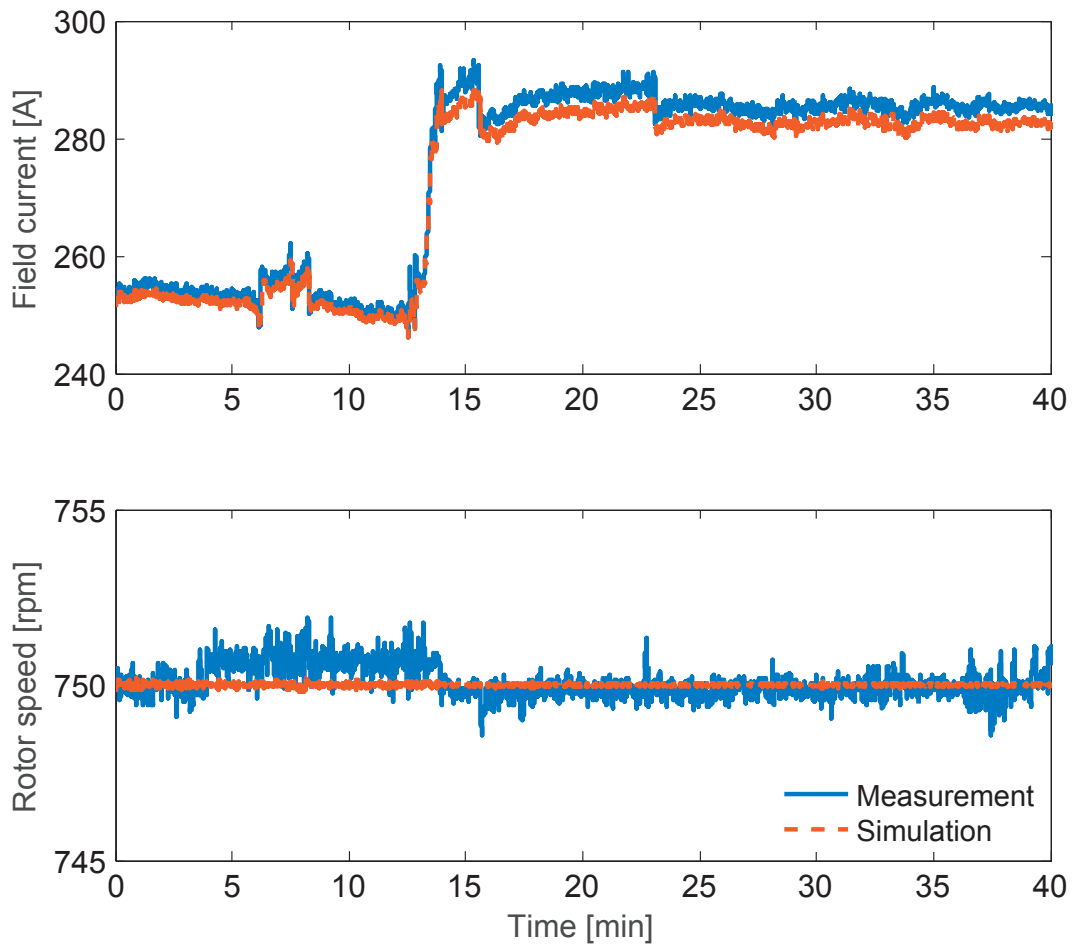
Figure 4.31: Field current (top); Rotor speed (bottom)

Variation of reactive power
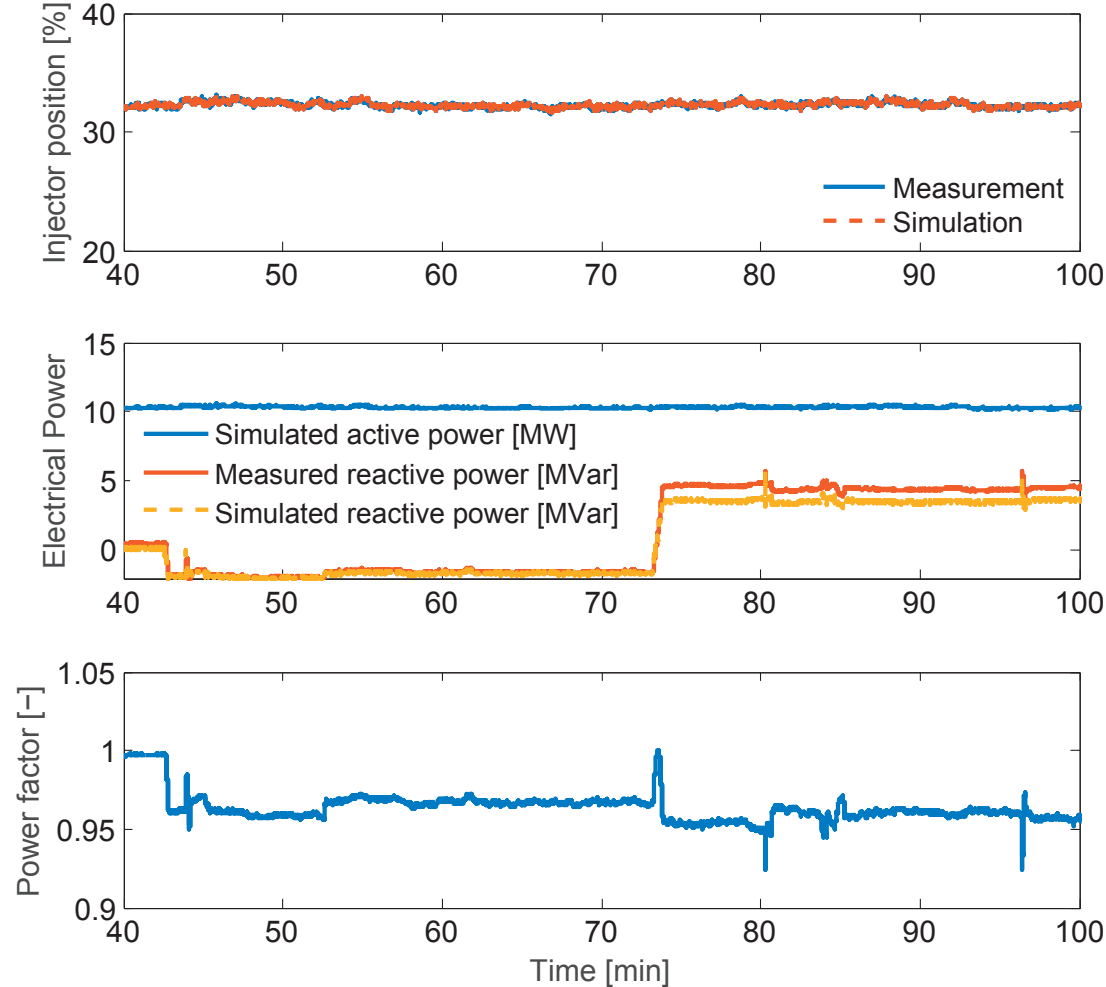
Figure 4.32: Second part of the test with variations of reactive power from 0 [MVar] to -3 [MVar] and from -3 [MVar] to 4.5 [MVar]; Injector position (top); Electric powers of the generator with measured reative power (middle); Estimated power factor from simulated powers (bottom)
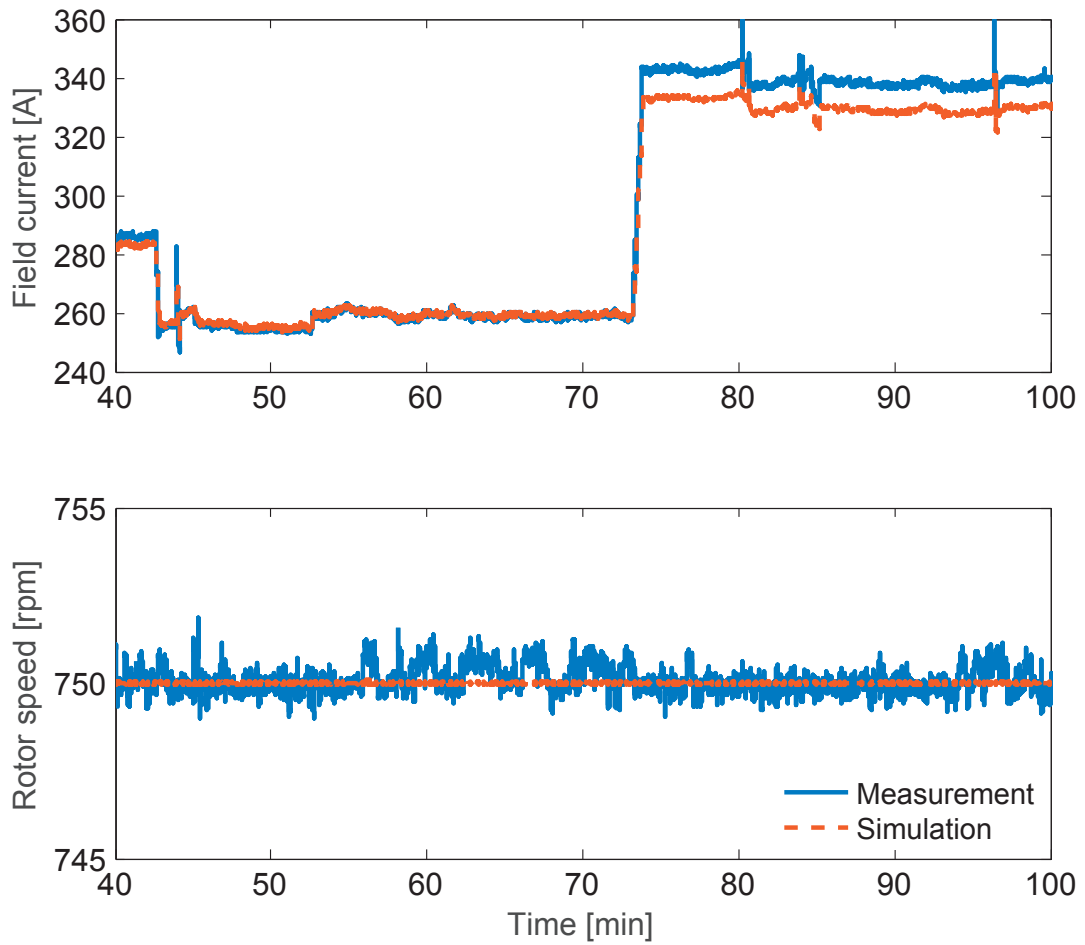
Figure 4.33: Comparison RT-simulation-measurement during the variation reactive power: Field current (top); Rotor speed (bottom)
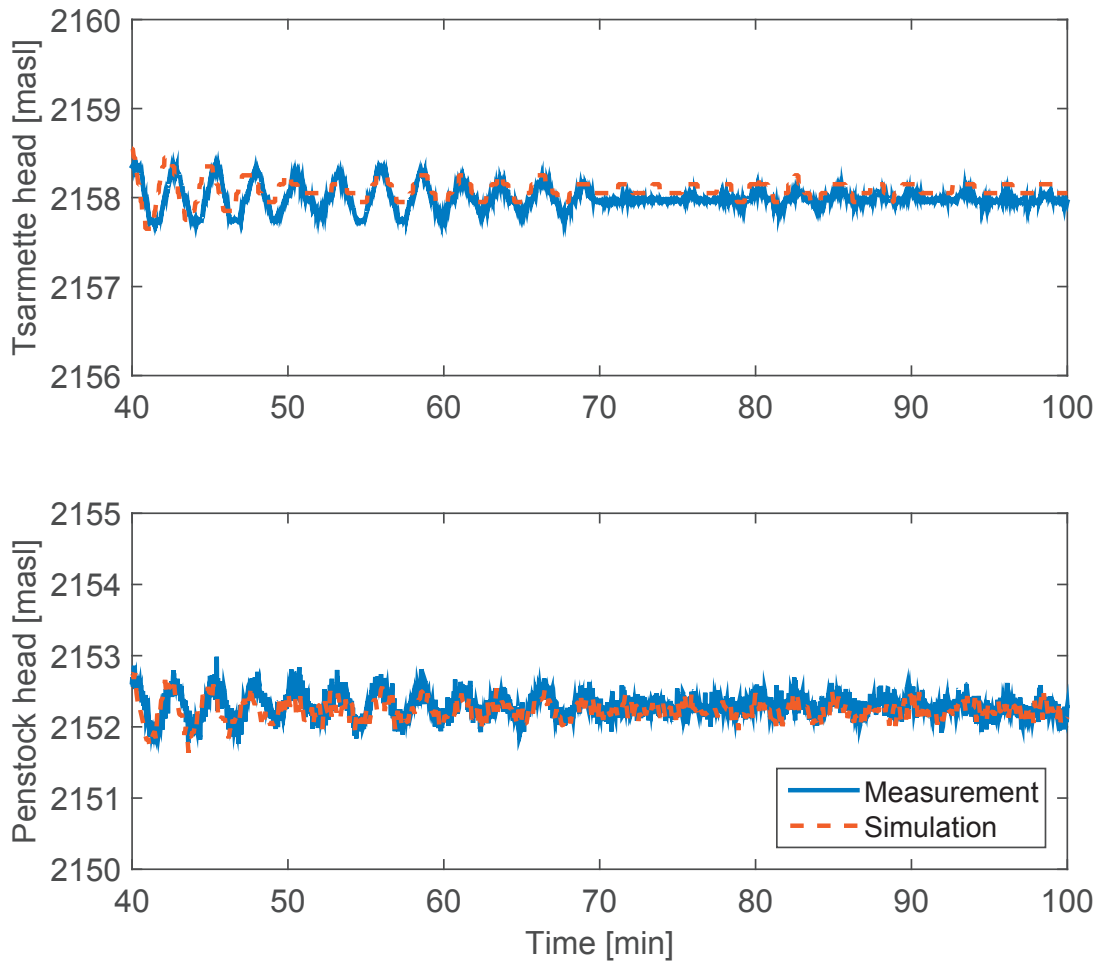
Figure 4.34: Comparison RT-simulation-measurement during the variation reactive power: Surge tank(top) and penstock(bottom) heads

The variation of reactive power is manually performed by modifying the power factor from 1 to 0.96 in an under-excited state of the generator, leading to an absorption of 3 [MVar]. Then, it is increased to 0.93 in the over-excited state which results to generation of 4 [MVar].

The field current shows a maximum discrepancy of 3 [%] at t=73.15 [min], inducing an error on the reactive power and stator current of 15 [%] and 12 [%], respectively.
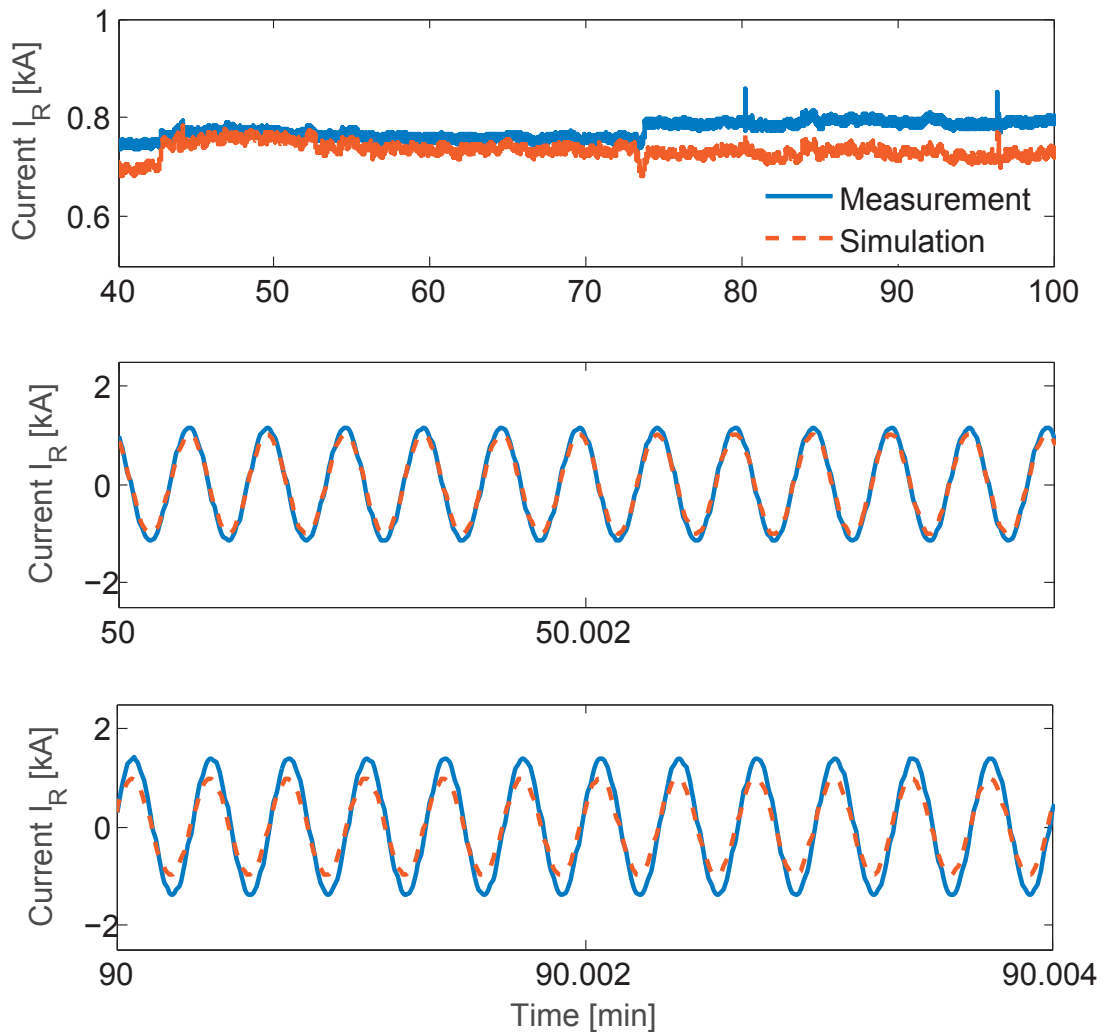
Figure 4.35: Stator current in the phase "R"; RMS-value of current (top); Zoom of the current when Q=-3 [MVar] (middle); Zoom of the current when Q= 4.5 [MVar] (bottom)

4.3.3 Conclusion

This second measurement campaign demonstrated the feasibility of real-time simulation with SIMSEN, as expected. The simulation model comprises the hydraulic model of Mottec power plant, which is interacting with the model of salient-pole synchronous generator connected to the power network. The real-time simulation operated in parallel under the same conditions as unit 3, where variations of active and reactive powers were achieved to assess the performance of the model. The results displayed good agreement in overall. Indeed, the dynamic behavior of the power plant was correctly represented with, in the first instance, the superposition of the water hammer and the mass oscillation in the penstock and mass oscillations in the surge tank after the opening of injectors. In the second instance, variations of powers were properly

simulated with a maximum error estimated to 10 [%] on the simulation outputs, that are the three-phase stator current.

Therefore, results indicate the possibility of implementing a model-based monitoring and fault detection as presented in section 3.5 on the basis of the presented simulation model. Additional tests case are available in appendix B.3.

5

Conclusion

5.1 Summary

The present thesis has presented a feasibility development of real-time(RT) simulations running in general-purpose computer, which will lead to a model-based monitoring application.

Chapter 2 reviewed applications with real-time simulators followed by a description of the time-domain simulation software SIMSEN. The numerical tool features a library with different electric and hydraulic models. It was followed by an investigation related to the real-time in SIMSEN enabled to assess the limit of time constraint for a given model and computer. This emphasized the issue related to the compromise between performance and accuracy with a short time step during a soft real-time simulation.

The test bench introduced in chapter 3 includes the modeling of a laboratory unit, which represents the motor-generator group in a reduced power scale. This latter simulates similar dynamic behavior as the real unit, and offers the possibility to achieve tests under off-design operations for development purpose. Identified parameters for the modeling and the assessment of real-time operation was accomplished by a comparative method and resulted to good agreements in both cases. As a conclusion, a dysfunction was carried out in order to

emphasize the capability of model-based fault detection process in the case of monitoring application.

Chapter 4 explained different and necessary steps for the implementation in the present hydroelectric power plant. Thanks to the contribution of numerous partners HEX, ALPIQ, PVE and HydroNET2, two measurements campaigns have taken place in order to validate the model of the power plant in the first stage. And in the second stage, performance of the model running in real-time was assessed with good results.

The main contribution of the present work consists of the application of a developed real-time system for hydroelectric power plants monitoring. In order to reach the objective, different steps were necessary:

- Feasibility study of real-time simulations running in a general purpose computer;

- Development of a small-scale test bench, where different tests have been carried out to validate the proposed approach;

- Optimization of the hydraulic model to satisfy real-time requirements and accuracy;

- Implementation and test of the system in a real 72 MW power plant, which represents an important contribution of the study.

Validations and performances of the developed model-based monitoring system have emphasized the following features: (i) Easy modeling of any energetic system topology and user-friendly real-time mode; (ii) Comparison of all accessible quantities in the simulation with the available measurements data in real-time; (iii) Low cost from hardware, i.e. acquisition card compared to hard real-time simulator.

5.2 Perspectives and improvements

The modular models in SIMSEN used in real-time as a complement, offer an interesting tool with a wide applications possibility. To improve such numerical tool, the implementation of the following suggestion would be interesting:

- A real-time initialization process that considers the current state of the quantity instead of a manual one, beforehand [55];

- A user-friendly and flexible user interface (UI), where it could be customizable and interacting with the model during a RT simulation;

- Data management procedure in case of long duration simulation. This mode would enable to relieve the display tool of the observed quantity by dividing data into different files or the use of modern technology such as stream-based method of storage [56];

- The complexity of models, such as introduced in chapter 4, requires computations costs even though technology performance increases. Consequently, accuracy must be sacrificed over the performance, by simplification process for example. Moreover, SIMSEN achieves numerical integration using a single CPU, thereby the full extension of a multi-core capacity is not exploited. Saying that, an alternative solution to this issue would be the division into different portions of the actual system model, which would be implemented in several SIMSENs in order to relieve the CPU. The models would run in parallel and would communicate using a share memory [57]. In other words, this would mean SIL simulations with different portions of model interacting to each other.

<div style="text-align: right; font-size: 4em;">*A*</div>

Appendix - Test bench modeling

A.1 Parameters identification for synchronous machine

The precise determination of machine parameters is an essential step for modeling. The various tests presented consecutively enable the identification of model parameters introduced in section 3.2.2, which are based on [58, 59].

A.1.1 Direct-axis reactance x_d

The direct synchronous reactance x_d is defined as Eq. A.1, the quotient of field currents $i_{f0,gap}$ and i_{fcc} in per unit. These latter parameters are respectively the no-load value and sustained short-circuited value of the field current, which are determined graphically, by means of the no-load and sustained short-circuit tests in the following subsections.

$$x_d = \frac{i_{fcc}}{i_{f0,gap}} = \frac{0.97}{0.83} = 1.21 \quad [p.u.] \tag{A.1}$$

Eq. A.1 is equivalent to the ratio between the voltage and current related to the same value of field current, where the pole of the rotor is aligned with the direct axis in order to have the components of the electric quantities on the same axis.

No-load test

The no-load test enables to obtain the characteristic of the counter electromotive force induced in the machine versus the field current (saturation curve). This quantity represents the internal voltage generated by the magnetic flux induced from the field current. Due to the voltage drop and armature reactions when current is circulating through the stator windings, the voltage can only be measured under no-load conditions, in other words the stator terminals of the machine must be opened.

The sequence of the test is conducted with the synchronous machine rotating at the nominal speed with the stator terminals opened throughout the test. A field current feeds the rotor circuit and is incrementally increased from 0 [p.u.] to 1.2 [p.u]. The line voltage of stator windings is measured at each stage of field current as in Figure A.1.
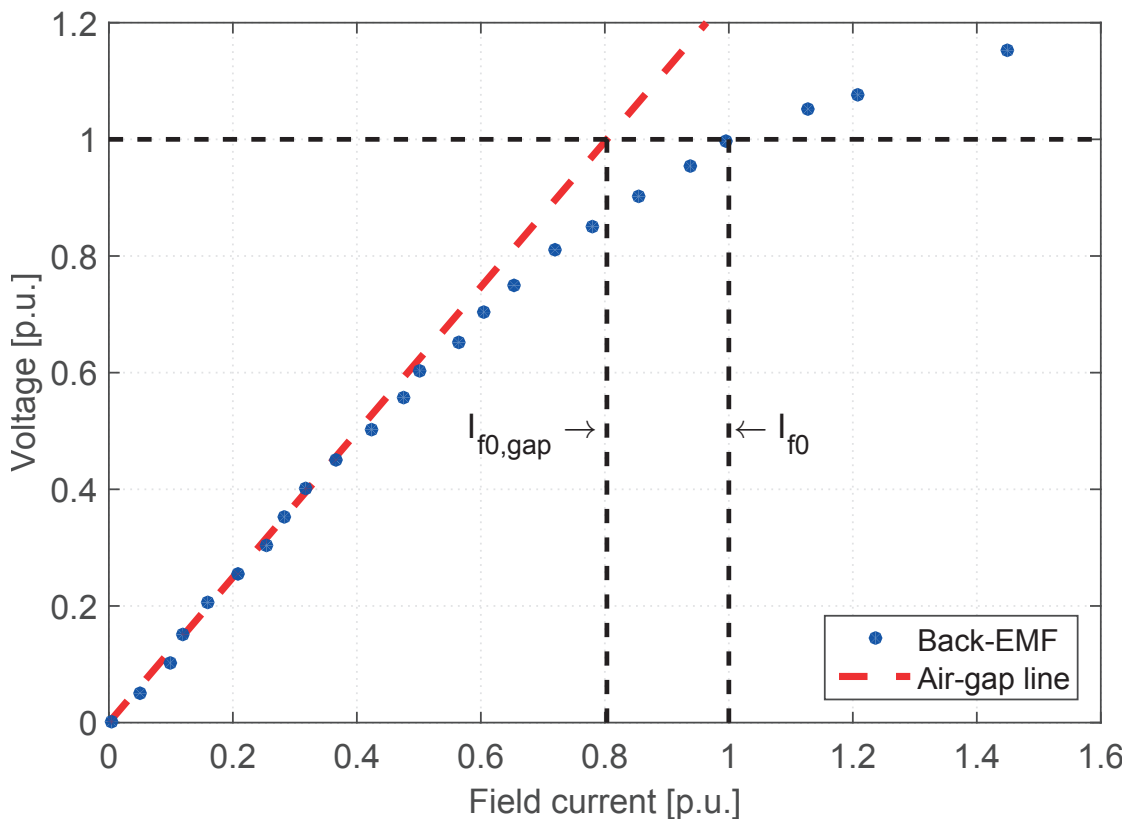
Figure A.1: Saturation curve

The saturation curve presented in Figure A.1 represents the voltage saturation characteristic of the synchronous machine introduced in section 3.1.2, displayed in per unit, versus the corresponding value of field current. A saturation occurs from i_f=0.5 [p.u.] and is emphasized by the air-gap line in red, which represents the internal voltage without any saturation. This

effect indicates the area where magnetic properties of the machine turns into a non-linear behavior, which induces additional core losses, resulting to a drop of efficiency.

In the model, it is assumed that the reactance x_d is a non-saturated parameter leading to choose $i_{f0,gap}$=0.83 [p.u.] to calculate Eq. A.1. In the case where the model is sustainably saturated, the value of i_{f0} is selected, yielding a field current i_{f0}=1 [p.u.]. Having said this, the saturation effect can be modeled in SIMSEN using the non saturated reactance, which is discussed in section 3.4.1.

Sustained short-circuit test

The sequence of the sustained short-circuit test is carried out with a machine rotating at the nominal speed with the stator terminals all short-circuited. From this point, a field current is applied and increase until inducing a stator current i_s = 1.1 [p.u.]. The short-circuit curve is achieved from the phase current of stator windings against the field current related to i_{f0}, in per unit as seen in Figure A.2.
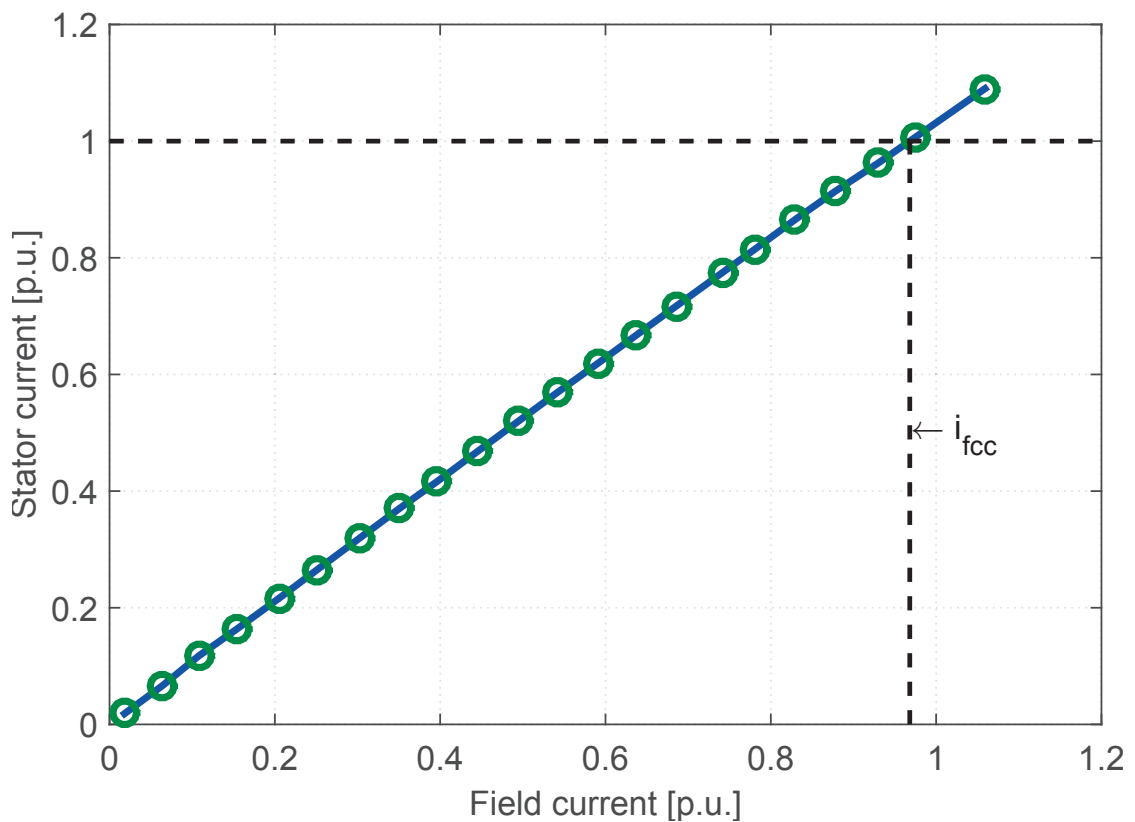
Figure A.2: Short-circuit curve

Unlike the saturation curve, the machine cannot saturate since due to the stator reaction. Indeed, the current induced in the stator windings generates a demagnetization flux, which weakens the linked flux produced by the rotor as a result. This flux weakening delays therefore the emergence of saturation, which means the machine cannot saturate throughout the whole test.

The second parameter i_{fcc}, necessary to Eq. A.1 corresponds to the value of field current when the nominal intensity of stator current is induced as showed in Figure A.2.

A.1.2   Quadrature-axis reactance x_q

The reactance x_q is determined with the maximum lagging current test where a pole slip is carried out. The variables in Eq. A.2, corresponds to the phase voltage v_R and phase current i_R of stator measured during the transient.

$$x_q = \frac{v_{R,RMS}}{i_{R,RMS}} = \frac{0.742}{0.982} = 0.76 \quad [p.u.] \tag{A.2}$$

Maximum lagging current test

The pole slip that occur during the test is achieved by weakening the remanent field of the pole. The test based on [58–60], follows the sequence described below:

- The synchronous machine is connected to the power grid and operates at p=0 [p.u.];

- The field current is brought down to i_f=0 [p.u.];

- The polarity of i_f is inverted and feeds again the rotor circuit, followed by an increase of amplitude until the emergence of the pole slip.

The field weakening increase the absorbed reactive power by the machine to maintain the magnetization of the rotor until the polarity change of the rotor. This is reflected by the stator current, which increases along the decrease of the field followed by the rapid current decrease after the slip.

Saying that, the moment when the pole slip occurs corresponds therefore to moment when the value of the stator current is maximum. Therefore, this moment is estimated at t=0.83 [p.u.] with a current intensity $i_{R,RMS}$=0.982 [p.u.] on Figure A.3. The voltage level of the power grid was lowered at $v_{RS,RMS}$=0.742 [p.u.], by means of a variable transformer in order to limit eventual saturation of the machine throughout the transient.
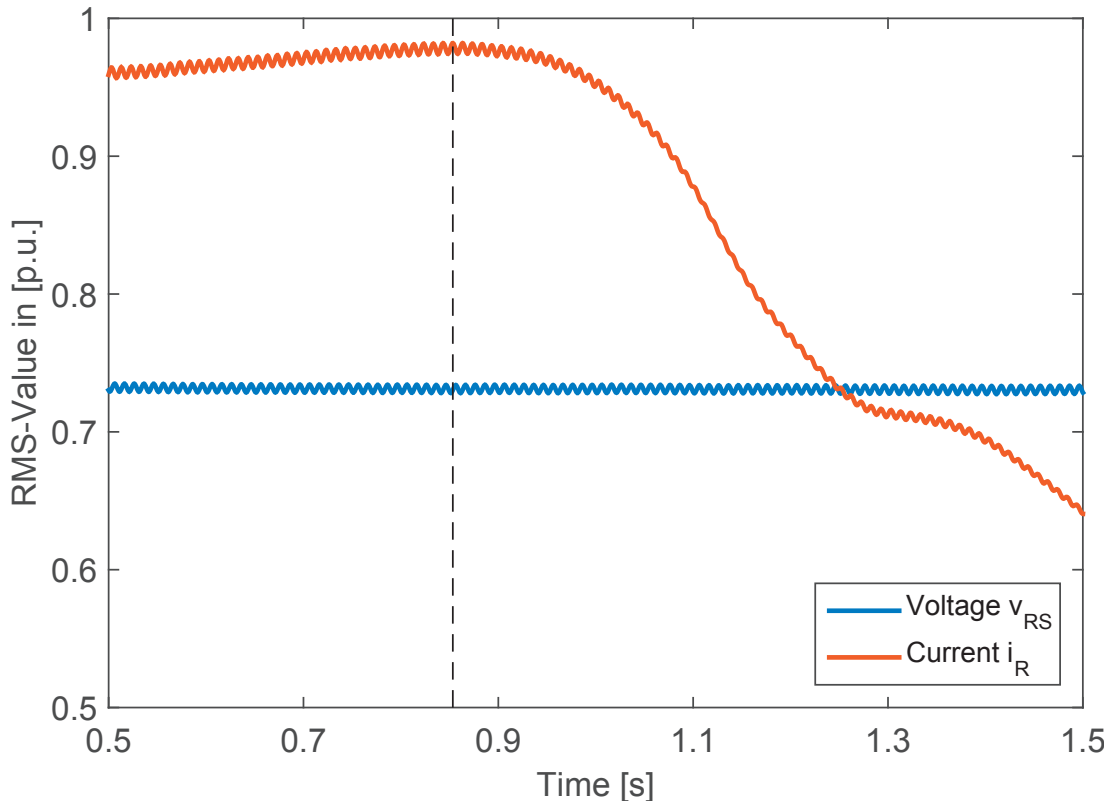
Figure A.3: Line voltage V_{RS} during the pole slipping

A.1.3 Potier Reactance x_p

An accurate determination of leakage reactance of stator windings $x_{\sigma s}$ is essential for the study of the behavior and the modeling of synchronous machines. In the literature, there is no experimental methods capable of accurately estimate this parameter since there is not any single method capable to measure directly a leakage flux unless it precisely calculated with numerical methods [61, 62]. In practice, the value of $x_{\sigma s}$ is approximated using the well-known method of Potier triangle using the saturation curve from the no-load and zero-power factor tests in section A.1.1 and in section A.1.3, respectively.

Zero-power factor test

The zero-power factor test consists of plotting the saturation curve under load conditions as seen in Figure A.4. The procedure of this test is realized with the synchronous machine connected to the nominal voltage level power network, operating with a field current inducing a nominal stator current and with a power factor $\cos(\phi)$, which is nil throughout the test. The voltage level is then reduced within a range from 0.6 [p.u.] to 1.0 [p.u.] with the current stator

maintained at the nominal value by modifying the field current.

The stability of the connected unit is no more ensured from 0.6 [p.u.] of voltage . However, [63–65] has experimentally verified and pointed out that the loaded characteristic curve is actually a parallel shift of the saturation curve in section A.1.1 which allows to extrapolate the incomplete part.

Construction of Potier triangle

The characteristic curves from the no-load and zero power factor tests are represented, in per unit, in Figure A.4 against the field current relative to i_{f0}. The triangle formed by the points "ABC" is referred as the "Potier triangle". This triangle is build following the sequence below:

- The point B corresponds to the nominal voltage under zero-power factor test and is considered as the starting point;

- The point A is determined from B with a horizontal shift of i_{fcc} from the section A.1.1;
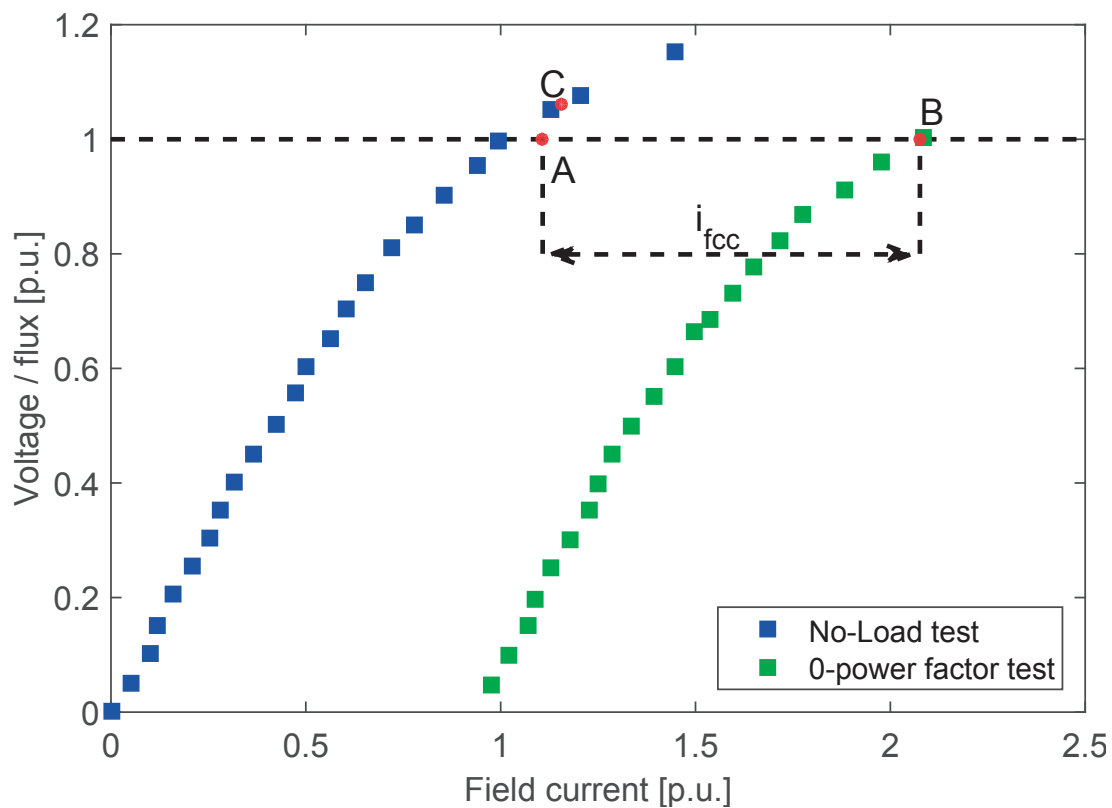
Figure A.4: Contruction of Potier triangle
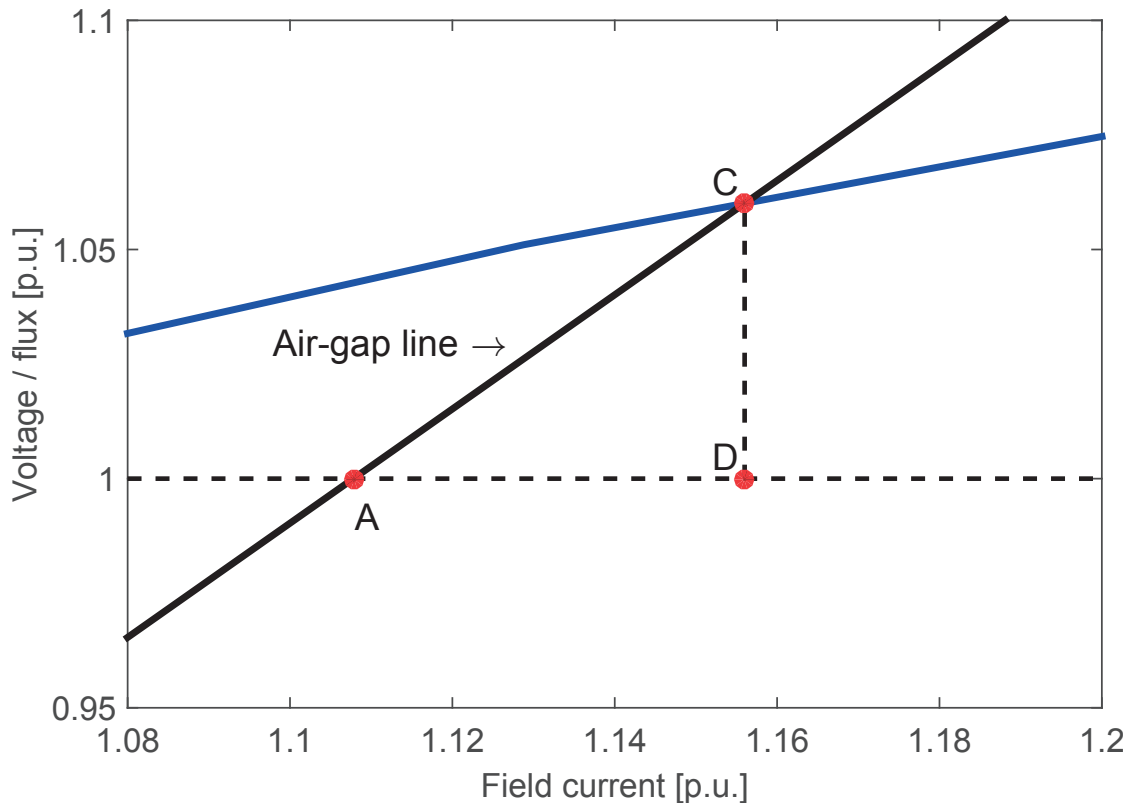
Figure A.5: Voltage drop of Potier reactance

- The point C corresponds to the the intersection between the no-load saturation curve and the air-gap line passing through A, as seen in Figure A.5.

The segment CD corresponds to the voltage drop u_p generated by the Potier reactance. This voltage is assigned to the Potier reactance in per unit since the stator current i_s equals to 1 [p.u.], which means

$$u_p = i_s \cdot x_p = 0.06 \quad \text{[p.u.]} \tag{A.3}$$

When all saturation is assumed to be on the armature, the Potier reactance is equal to the stator leakage reactance.

A.1.4 Determination of transient and sub-transient parameters

The determination of transient and sub-transient reactances are achieved by means of the "Sudden short-circuit test" and the "Applied voltage test with rotor in arbitrary position", respectively.

97

Sudden short-circuit test

The sudden short-circuit test is conducted following the sequences described below:

- The prime mover is settled to drive the synchronous machine at the nominal speed with
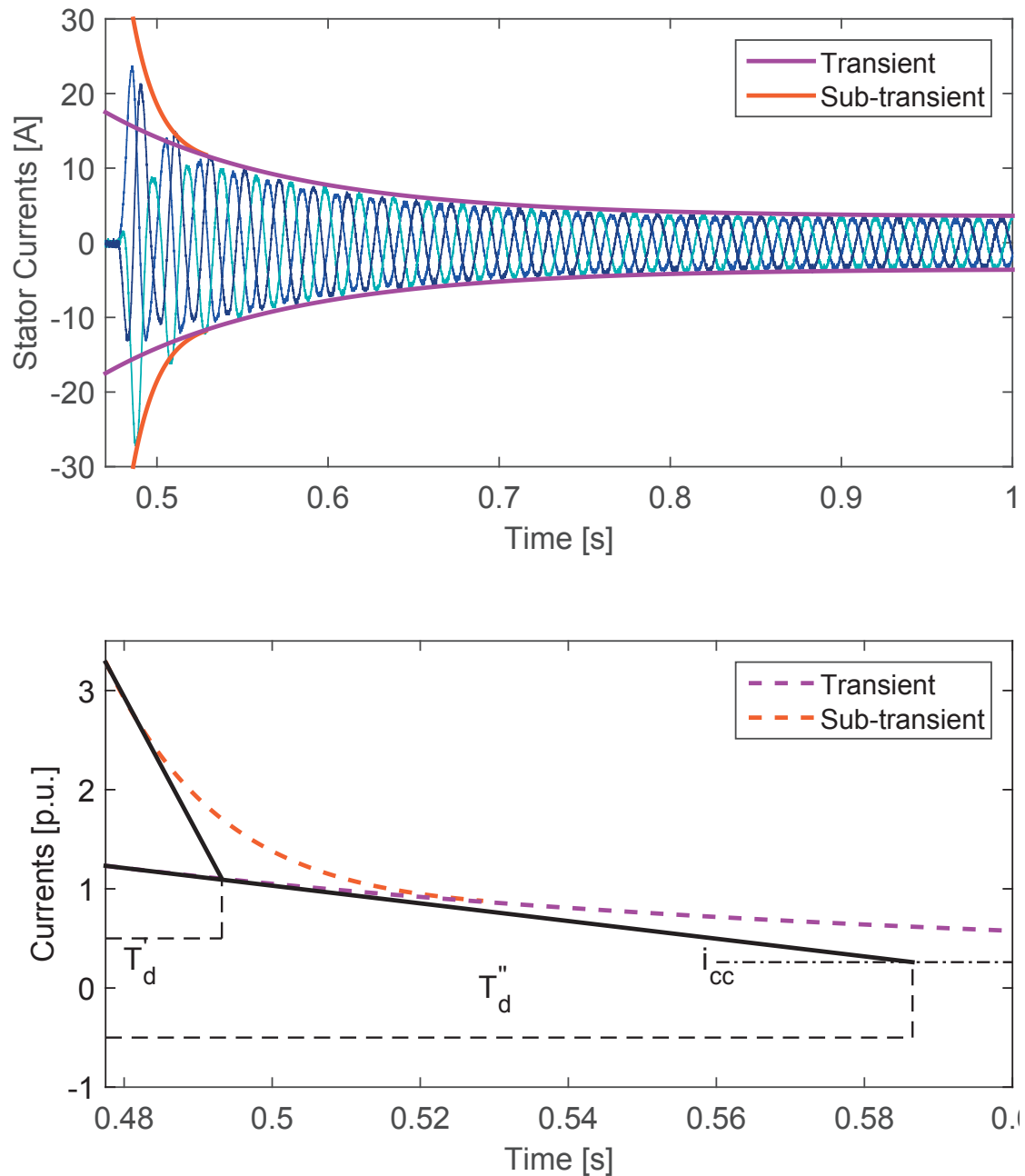
Figure A.6: Three-phase short-circuited stator current(top); Amplitude transient and sub-transient envelopes of the short-circuited currents(bottom)

the stator terminals opened;

- The power supply of the excitation circuit provides an amount of current yielding an induced voltage of 0.3 [p.u.];

- The three stator windings are then short-circuited in order to record the three-phase current and the field current with an oscilloscope.

The top plot of Figure A.6 contains the short-circuited currents including their envelopes characterized by T_d' and T_d'', whereas the bottom plot of the same figure depicts the amplitude of the envelopes in per unit. The decomposition of time constants into T_d' and T_d'' is as shown in Figure A.6, which were estimated to 110 [ms] and 16 [ms], respectively.

The test is carried out under reduced voltage conditions. The 0.3 [p.u.] voltage level is a recommendation of [58] in order to prevent harming the present synchronous machine. Even under such conditions, the amplitude of currents can reach peaks value in the order of 2-3 [p.u.] as seen in Figure A.6.
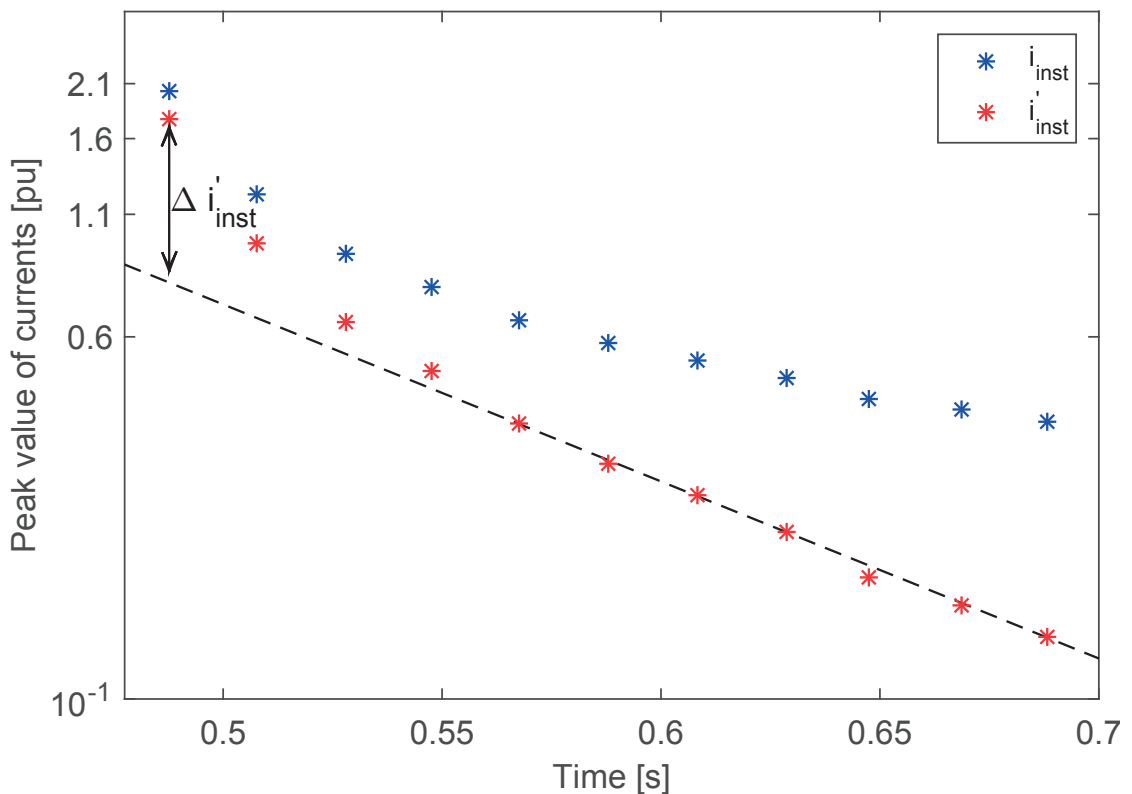
Figure A.7: Envelope amplitude of stator current with the transient component in a semi-log scale

The transient reactance x'_d is calculated using Eq. A.4

$$x'_d = \frac{u_s(t=0)}{i_{cc} + \Delta i'_{inst}(t=0)} = 0.16 \quad \text{[p.u.]} \tag{A.4}$$

with

$$i'_{inst} = i_{inst} - i_{cc} \tag{A.5}$$

The variable $\Delta i'_{inst}$ is graphically determined in Figure A.7. The envelope of Figure A.6 is displayed in semi-log plot. Its transient component is yielded by subtracting the continuous component i_{cc} as in Eq. A.5.

Applied voltage test with the rotor in arbitrary position

The sequences of this test are the following:

- The synchronous machine rotates at a very low speed with the short-circuited rotor circuit;
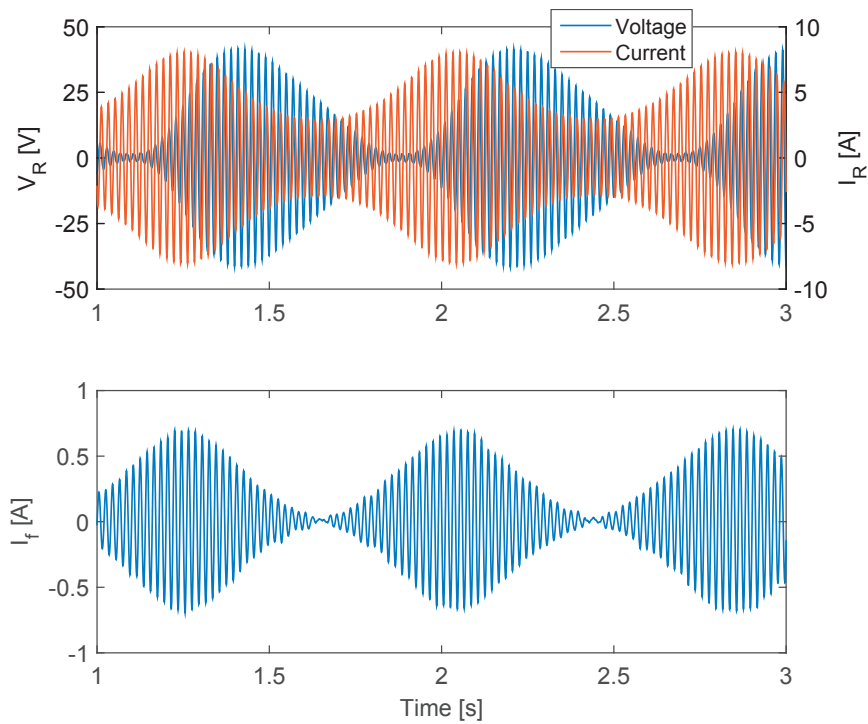
Figure A.8: Stator and rotor quantities related to position of rotor

- Two phases are supplied with a single-phase AC voltage source with a frequency of 50 [Hz];

- The voltage amplitude is settled to induce a current comprised between 0.2 [p.u] and 0.7 [p.u.];

- The voltage, current and field current v_{RS}, i_R and i_f are measured.

In this test, the objective consists of measuring the voltage and the induced current in the supplied phase and determine the sub-transient reactance for the direct and quadrature axes according to the rotor position. Its position is known with the current induced in the rotor circuit as seen in Figure A.8. Indeed, the direct axis corresponds to the instant when the amplitude of the latter current is maximal whereas the quadrature axis is assigned to the lowest amplitude.

Figure A.9 displays the measured current in Figure A.8 by only considering the amplitude modulation with power "P", an estimation from the stator quantities. The variation of reactance
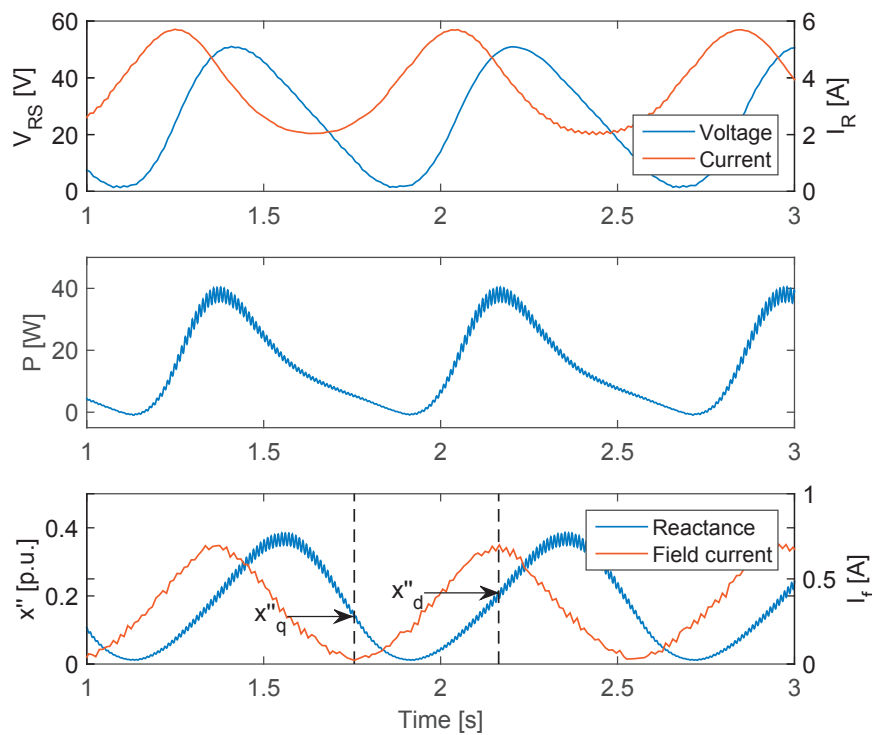
Figure A.9: Oscillation of RMS values according to the position of rotor

X'' in the figure is calculated from the instantaneous values, given by Eq. A.6.

$$X'' = \sqrt{\left(\frac{V_{RS}}{(2I_R)}\right)^2 - \left(\frac{P}{(2I_R^2)}\right)^2} \tag{A.6}$$

in per unit, one has:

$$x'' = \frac{X''}{Z_{Rated}} \tag{A.7}$$

The values resulting from the present test are $x_d'' = 0.13$ [p.u.] and $x_q'' = 0.22$ [p.u.].

A.1.5   Calculation of the Canay reactance x_c

The Canay reactance or characteristic reactance x_c is estimated from the field current measured from the sudden short-circuit test in section A.1.4. The method, introduced in [52], uses the top and bottom envelopes from the current oscillations as seen in Figure A.10, to determine the peak-to-peak amplitude. This amplitude is then plotted in a semi-log scale
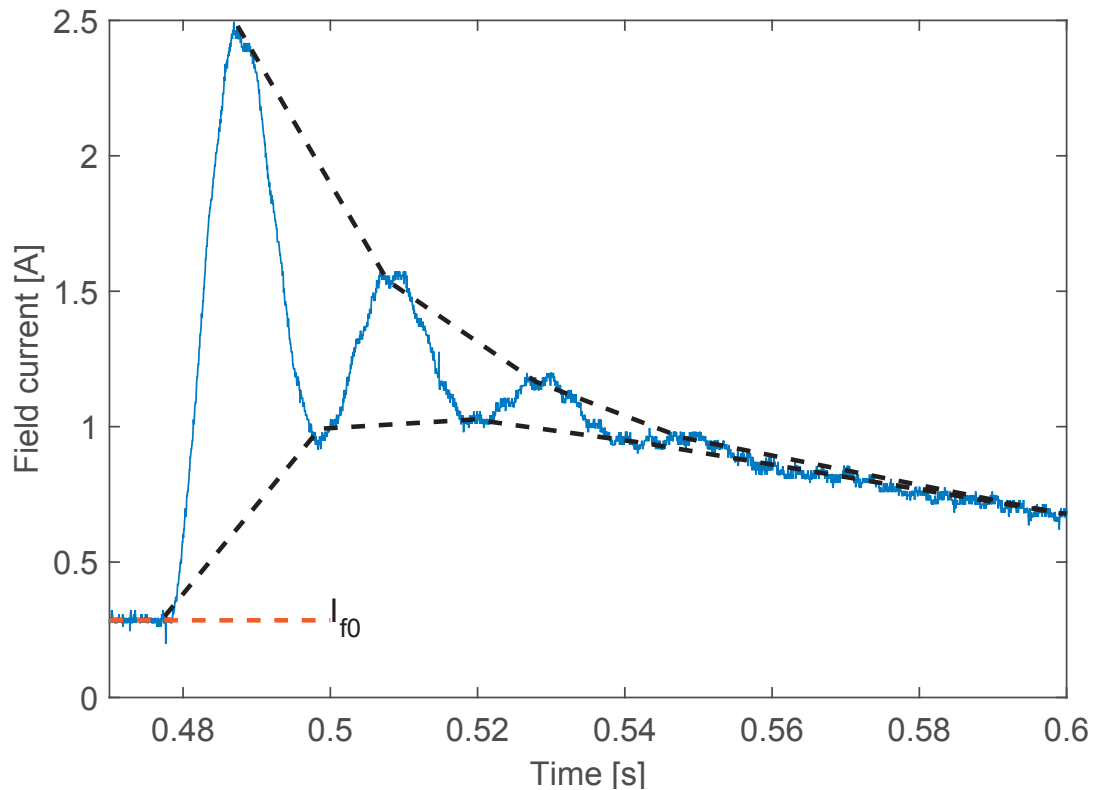
Figure A.10: Field current during the sudden three-phase short-circuit

graph, enabling a linear extrapolation of the values in order to estimate the initial amplitude at the time when the fault occurred. This initial amplitude corresponds to $2I_{f\sim}$ as seen in Figure A.11.

The parameter "a", necessary to calculate the reactance x_c, is defined as the ratio between the currents $I_{f\sim}$ and $I_{f,o}$ (Eq. A.8), where $I_{f,o}$ corresponds to the field current before the occurrence of the three-phase fault and which was measured at 0.3 [p.u.].
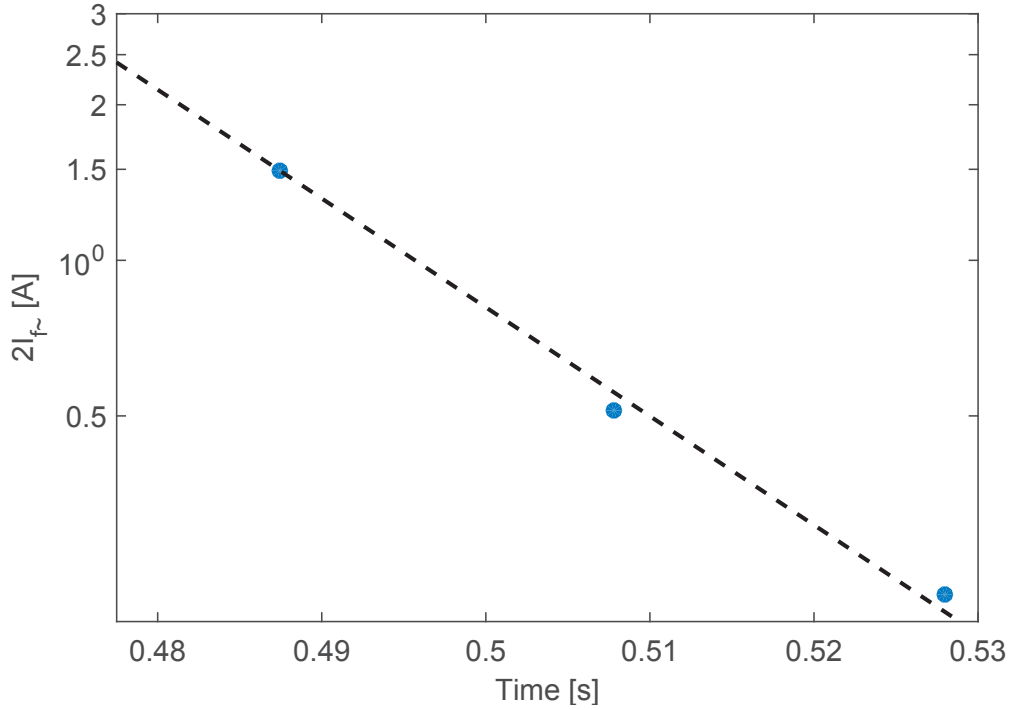
Figure A.11: Oscillations amplitude of the short-circuited field current

$$a = \frac{I_{f\sim}}{I_{fo}} = \frac{1.25}{0.3} = 4.166 \tag{A.8}$$

There are two possible approaches to calculate the Canay reactance x_c, which are introduced in the following subsections.

Iterative methodology

The method has the advantage of estimating x_c accurately. However, it requires the implementation of Eq. A.9 for numerical resolution with numerous iterations.

$$a = \frac{I_{f\sim}}{I_{f0}} = \left| \frac{1 + j\omega_n T''_{dc}}{(1 + j\omega_n T'_d)(1 + j\omega_n T''_d)} \right| \omega_n T'_{dc} \frac{(x_d - x_c)(x_d - x_c - x'_{dc})}{x_d x'_{dc}} \tag{A.9}$$

The solution from this method was estimated at

$$x_c = 0.1 \quad \text{[p.u.]} \tag{A.10}$$

Approximated methodology

The previous method produces an exact solution, however its use is not convenient for fast estimation of x_c without a tool with the algorithm pre-implemented. Consequently, another method is presented which approximate the solution without iterations. Considering a correction factor "c" defined in Eq. A.11,

$$c = \sqrt{1 + \left(\frac{x_d - x_d' - ax_d''}{a\omega_n x_d' T_d''}\right)^2} \tag{A.11}$$

which considers the ohmic influence of the damper circuit, the approximate solution of Eq. A.9 is replaced by in Eq. A.12.

$$x_c \approx x_d'' \left(1 - \frac{a\left(x_d' - x_d''\right)}{c\left(x_d - x_d'\right) - ax_d''}\right) = 0.0981 \quad \text{[p.u.]} \tag{A.12}$$

This methodology offers acceptable results and is suitable in practical cases. Moreover, further validation tests were investigated in [66], where the agreement of these solutions were emphasized by comparisons with a solution from finite element simulations.

A.1.6 Determination of inertia

The inertia J is an essential parameter characterizing the mechanical dynamic response described by Eq. A.13.

$$J\frac{d\omega}{dt} = \Sigma T \tag{A.13}$$

The conventional approach called "No-load retardation test" and recommended by [58] for the determination of J is not suitable for machines due to lack of robustness for small inertia. Therefore, an approach based on the same concept is introduced in the following subsection.

A.1.7 Inertia determination by load rejection

The generator is connected to the power network, providing an active power of 0.1 [p.u.] with a power factor equal to 1. Then, the generator is disconnected from the grid , inducing an

(a) Test 1   (b) Test 2
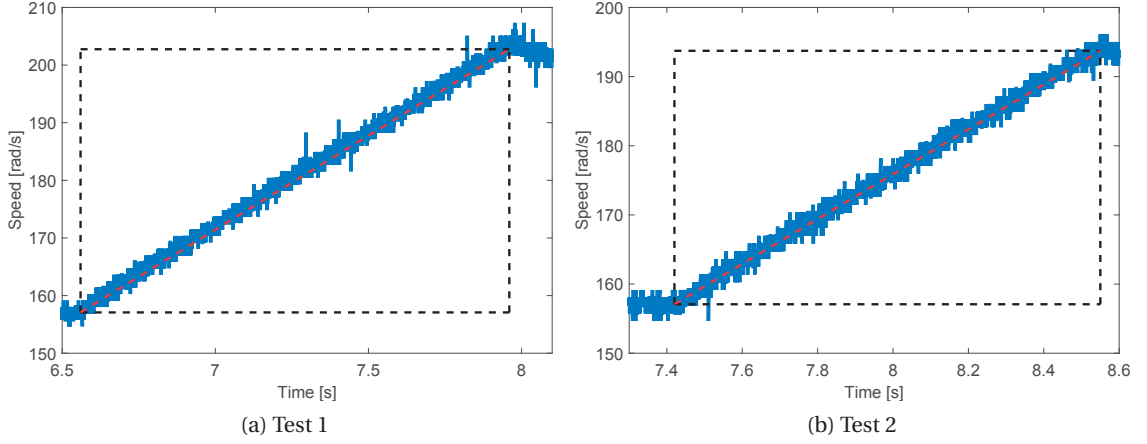
Figure A.12: Overspeed by load rejections

overspeed and followed by the standstill of the prime mover as soon as 10 [%] of the nominal speed is reached.

In this way, the motion equation Eq. refeq:Tmec is expressed as

$$T_{mec} = J\frac{d\omega}{dt} \tag{A.14}$$

with the initial conditions written in Eq. A.15, assuming the losses are negligible in the machine.

$$P_0 = \omega_0 \cdot T_{mec} \tag{A.15}$$

where T_{mec} and P_0 are respectively the mechanical torque and the active power before the load rejection. The substitution of Eq. A.14 into Eq. A.15 leads to

$$P_0 = J \cdot \omega_0 \frac{d\omega}{dt} \iff J = \frac{P_0 \Delta t}{\omega_0 \Delta \omega} \tag{A.16}$$

where $\Delta\omega$ and Δt corresponds to the variation of speed and time, determined from Figure A.12a and Figure A.12b. The introduced approach presents two advantages compared to the traditional method:

1. The measurement of torque is not necessary to determine the inertia as long as losses are neglected. In addition, this kind of device may be available on every machine due to the practical issue;

2. Once the rejection occurred, all the mechanical power provided by the prime mover is

Experiment 1			Experiment 2		
Quantity	Value	unit	Quantity	Value	unit
P_0	1254	[W]	P_0	1254	[W]
ω_0	157.08	$[\frac{rad}{s}]$	ω_0	157.08	$[\frac{rad}{s}]$
$\Delta\omega$	45.67	$[\frac{rad}{s}]$	$\Delta\omega$	36.65	$[\frac{rad}{s}]$
Δt	1.40	[s]	Δt	1.13	[s]
J_1	0.245	$[kgm^2]$	J_2	0.246	$[kgm^2]$

Table A.1: Estimation of parameters from the overspeed

stored under the form of kinetic energy. Consequently, the frictions become negligible, leading to a linear variation of speed.

The estimated inertia in Table A.1 illustrate the consistency of the test for machines with small inertia and can be performed on large power machines.

A.2 Circuit-breaker macro

In order to avoir meaningless results in the simulation when the model is connected to the grid, the macro in Figure A.13 of the model in Figure 3.5 verifies that all the requirements, i.e. frequency, voltage level and phase shift, are similar comparing both sides, power grid and machine, before applying the synchronization. Once these requirements are met, the trigger signal is sent to the circuit-breaker to connect the model of synchronous machine with the voltage source.

The sequence of verification are as follows: the three-phase network voltage is converted into Park components α_{net} and β_{net} in a fixed frame to estimate the network angle θ_s. At the same time, the three-phase stator voltage is also transformed into Park components α_{sm} and β_{sm} in a rotating frame using θ_s. They are afterward used in the logical functions given in Eq. A.17 and in Eq. A.18 to verify the voltage level and phase shift conditions, respectively.

$$\left| \sqrt{\alpha_{net}^2 + \beta_{net}^2} - \sqrt{\alpha_{sm}^2 + \beta_{sm}^2} \right| \leq \epsilon_1 \tag{A.17}$$

$$\left| \beta_{sm} \right| \leq \epsilon_2 \quad \& \quad \alpha_{sm} > 0 \tag{A.18}$$

ϵ_1 and ϵ_2 are the admitted tolerance threshold. The frequency is estimated from the rotor
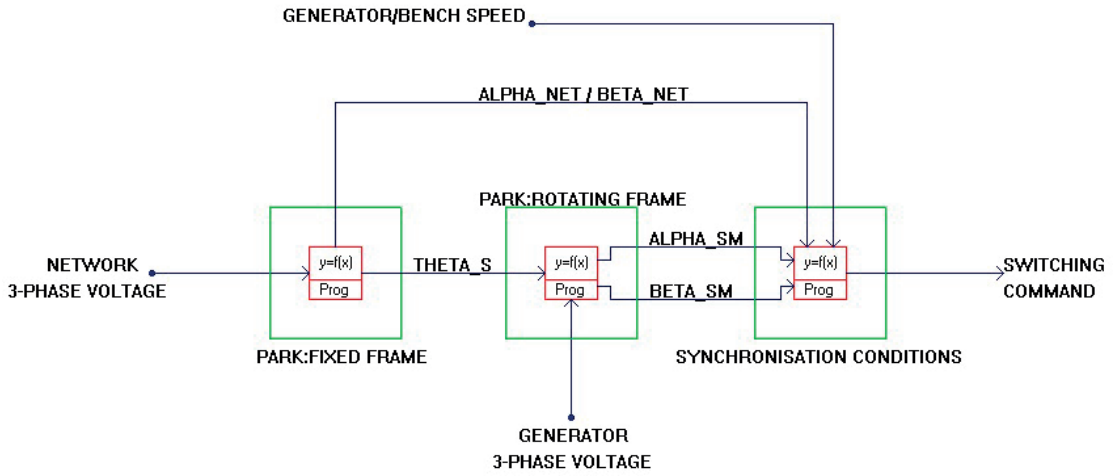
Figure A.13: Synchronization process

speed of the synchronous machine.

A.3 Digital Transient Torque Measurement

The Digital Transient Torque measuring device (Figure 4.15d) calculates in "real time" the electromagnetic torque in steady-state and transient conditions, from the three-phase voltage and current measured on the stator of the machine. Unlike the conventional device, which measures the torque on the shaft by means of strain gauges, the DTTM does not require any addition equipment. Indeed, the instantaneous values of phase voltages and currents are sampled and transferred to a microprocessor (DSP). This latter carries out the Park transformation on the phase values to convert them into Park values.

The electromagnetic torque is given by

$$T_{em} = \frac{3}{2} p \left(\Psi_d i_q - \Psi_q i_d \right) \qquad \text{[Nm]} \tag{A.19}$$

with Ψ_d, Ψ_d the total flux linkage of the stator in d and q axes. The estimation of magnetic flux is estimated from Eq A.20.

$$\Psi_{d,q} = \int \left(u_{d,q} - r \cdot i_{d,q} \right) dt \tag{A.20}$$

with

- i_d, i_q - stator currents in d and q axes;

- r - stator ohmic resistance;

- u_d, u_q - stator voltages in d and q axes;

B

Appendix - Hydroelectric power plant

B.1 Interface for PicoLog

The interface of Figure 4.25 is a passive circuit, which adapts the AC signals to unipolar inputs. The circuit scales the amplitude of the incoming signal and shifts the signal origin in the middle of the input range using an external DC signal. The scheme of the circuit is depicted in Figure B.1. The internal resistance of PicoLog corresponds to R_A=1[MΩ]. Using the superposition theorem, the output signal is given by

$$V_{out} = \frac{R_A\,(R_2\,R_3\,V_{IN} + R_1\,R_2\,V_{DC})}{R_1\,R_2\,R_3 + R_A\,(R_1\,R_2 + R_1\,R_3 + R_2\,R_3)} \tag{B.1}$$

The incoming signal is assumed sinusoidal with a peak amplitude of 10 [V], which must fit into the range of PicoLog that is 0-2.5 [V]. Therefore, the following conditions must be satisfied:

$$A_1 = \frac{V_{OUT}}{V_{IN}} = \frac{1}{8} = 0.125 \tag{B.2}$$

$$A_2 = \frac{V_{OUT}}{V_{DC}} = \frac{1}{2} = 0.5 \tag{B.3}$$
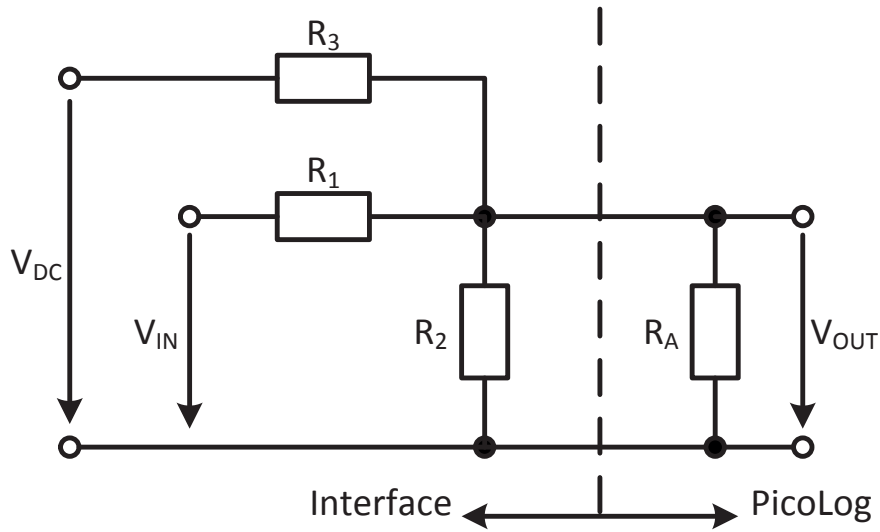
Figure B.1: Amplitude modulation and centering circuit for AC signal designed for PicoLog device

with A_1 the scaling gain of the signal and A_2 the shifting gain considering that the DC signal is 2.5 [V]. Comparing with Eq. B.1, they can be rewritten as

$$A_1 = \frac{R_A R_2 R_3}{R_1 R_2 R_3 + R_A (R_1 R_2 + R_1 R_3 + R_2 R_3)} \tag{B.4}$$

$$A_2 = \frac{R_1 R_2 R_A}{R_1 R_2 R_3 + R_A (R_1 R_2 + R_1 R_3 + R_2 R_3)} \tag{B.5}$$

By substituting B.4 into B.5, it results to

$$R_1 = \frac{A_2}{A_1} R_3 \tag{B.6}$$

which leads to

$$R_2 = \frac{A_2 R_3}{1 - A_1 - A_2} \tag{B.7}$$

The value of the resistances are reported in Table B.1, which was calculated assuming that R_3=15 [kΩ].

Resistance	R_1	R_2	R_3
Value [kΩ]	62	20	15

Table B.1: Resistances with normalized values

B.2 Off-Line test cases

B.2.1 Test case 1

The results presented in this subsection involve the variations of power factor, starting from $\cos(\phi)=1$ to $\cos(\phi)=0.75$ (under-excited mode) and ending at $\cos(\phi)=0.7$ (over-excited mode)
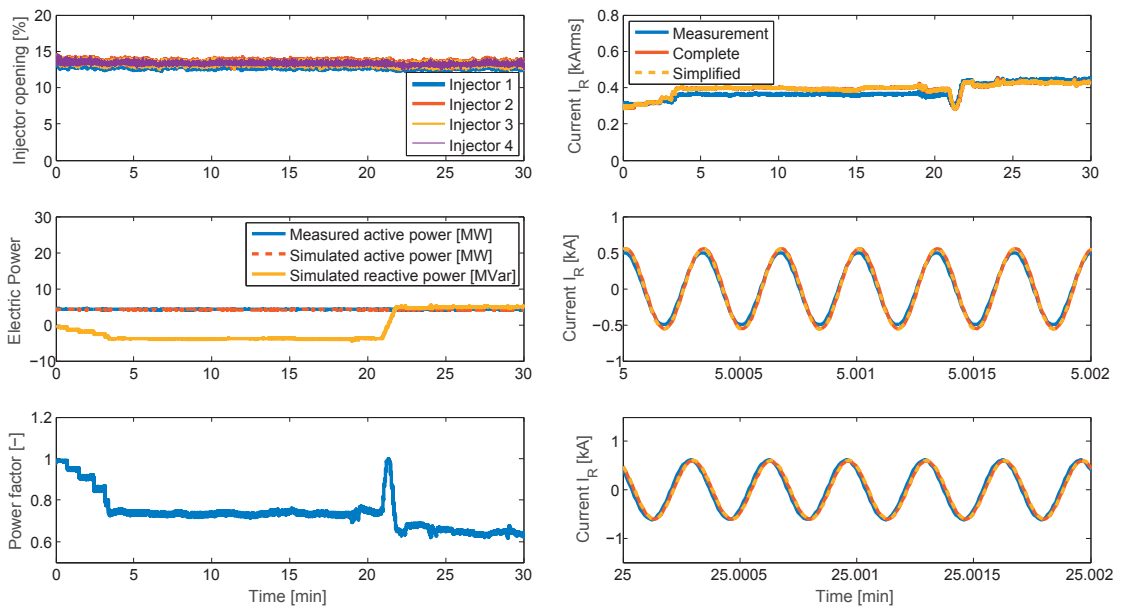
(a) Injectors position (top); Electric powers (middle); Estimated $\cos(\phi)$ from simulated powers (bottom)

(b) RMS-value of I_R (top); Zoom 1 of I_R (middle); Zoom 2 of I_R (bottom)
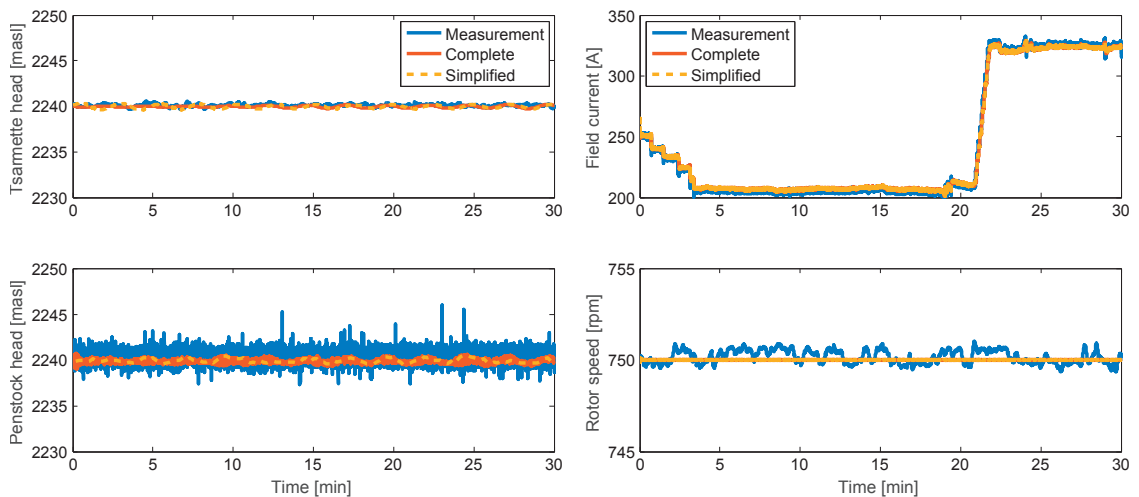
(c) Head of Tsarmette tank (top) and penstock (bottom)

(d) Field current (top); Shaft speed (bottom)

Figure B.2: Reactive power variation test with a constant active power

whereas the active power is fixed at P=4.5 [MW].

B.2.2 Test case 2

The achieved test in this test case comprises a rise of power active from P=9.6 [MW] to P=24 [MW] while the reactive power is maintained around Q=0 [MVar].
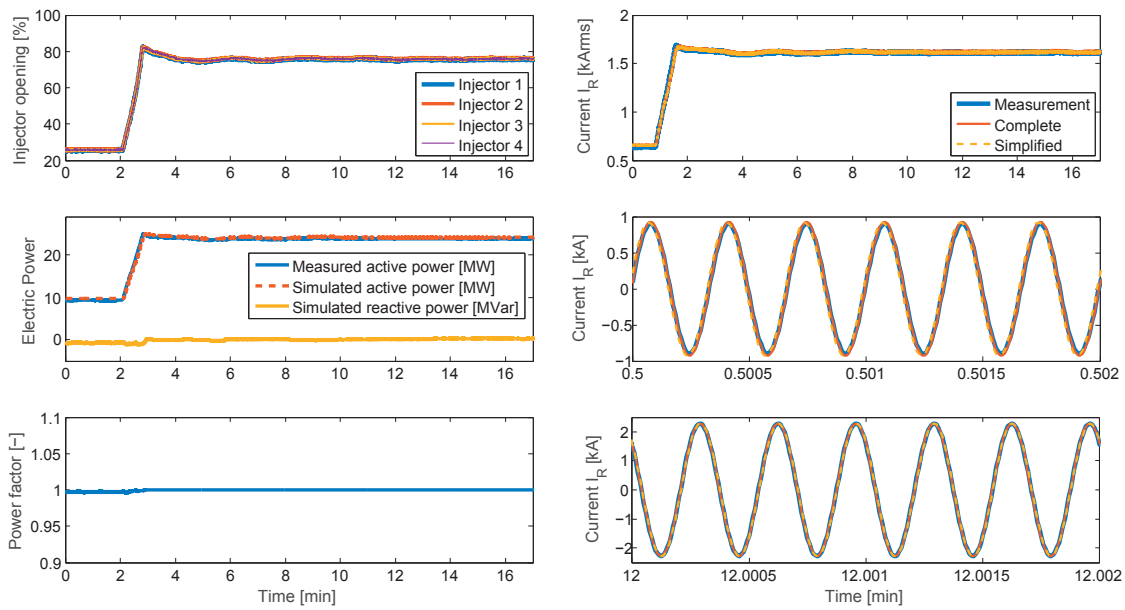
(a) Injectors position (top); Electric powers (middle); Estimated $\cos(\phi)$ from simulated powers (bottom)

(b) RMS-value of I_R (top); Zoom 1 of I_R (middle); Zoom 2 of I_R (bottom)
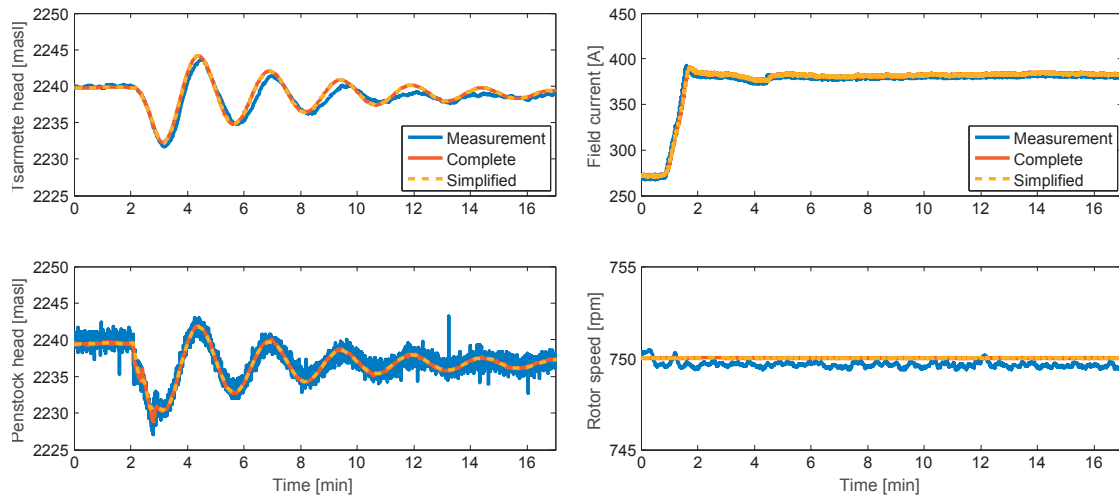
(c) Head of Tsarmette tank (top) and penstock (bottom)

(d) Field current (top); Shaft speed (bottom)

Figure B.3: Variation of active power with a power factor maintained at $\cos(\phi)$=1

B.3 On-line test cases

The real-time simulation is compared with the measurements. The sequence of the test is as follows: (i) Increase of reactive power from Q=-2 [MVar] to Q=5[MVar] with P=10 [MW]; (ii) Variation of active power P=10 [MW] to P=20 [MW] with Q=5 [MVar]; (iii) Decrease of reactive power from Q=5 [MVar] to Q=0[MVar] with P=20 [MW]
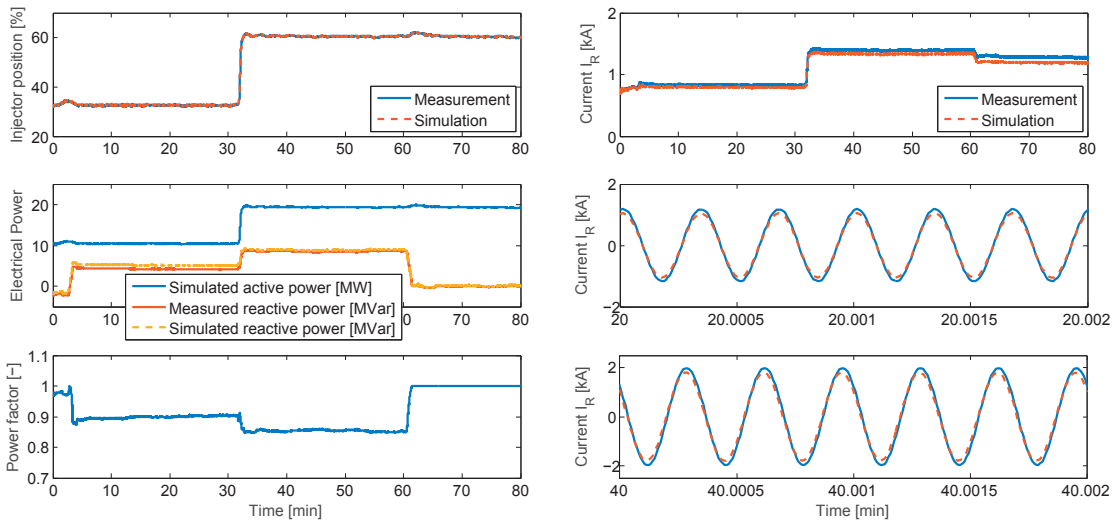
(a) Injectors position (top); Electric powers (middle); Estimated $\cos(\phi)$ from simulated powers (bottom)

(b) RMS-value of I_R (top); Zoom 1 of I_R (middle); Zoom 2 of I_R (bottom)
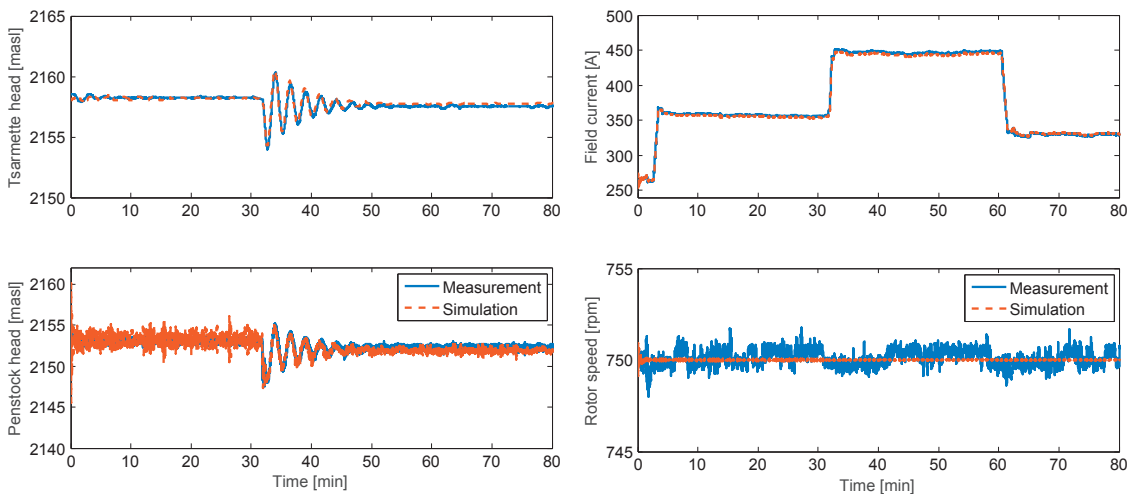
(c) Head of Tsarmette tank (top) and penstock (bottom)

(d) Field current (top); Shaft speed (bottom)

Figure B.4: Comparison of simulation-measurement from real-time simulation of Mottec

Bibliography

[1] I. E. Agency, "Energy and Climate Change," p. 200, 2015.

[2] W. E. Council, "2015 World Energy Issues Monitor."

[3] B. Prof. Burger, "Electricity production from solar and wind in Germany in 2014," Freiburg, Germany, Dec. 2014. [Online]. Available: http://www.ise.fraunhofer.de/en/downloads-englisch/pdf-files-englisch/data-nivc-/electricity-production-from-solar-and-wind-in-germany-2014.pdf/view

[4] J. Bélanger, P. Venne, and J.-N. Paquin, "The What, Where and Why of Real-Time Simulation," in *OPAL-RT Technologies*.

[5] A. Beguin, P. Allenbach, S. Keller, J. J. Simond, S. Brausewetter, and J. Koutnik, "Hardware-in-the-Loop Simulation Software for Regulator Tests and Optimization," in *Conference Record of the 2007 IEEE Industry Applications Conference, 2007. 42nd IAS Annual Meeting*, 2007, pp. 2422–2428.

[6] J. Chatelain, *Machines Électriques*, ser. Traité d'Électricité. Lausanne: Presses Polytechniques Romandes, 1989, vol. X.

[7] A. Robert, J.-P. Stucky, F. Panchaud, A. Hoeffleur, and H. Widmer, "L'aménagement hydro-électrique de la Gougra."

Bibliography

[8] C. Nicolet, "Hydroacoustic Modelling and Numerical Simulation of Unsteady Operation of Hydroelectric Systems," Thesis, EPFL, Lausanne, 2007.

[9] "SIMSEN," May 2015. [Online]. Available: http://simsen.epfl.ch/

[10] "Energy Vortex." [Online]. Available: http://www.energyvortex.com/

[11] P. Tavner, L. Ran, J. Penman, and H. Sedding, *Condition Monitoring of Rotating Electrical Machines*, ser. IET POWER AND ENERGY SERIES. London, United Kingdom: The Institution of Engineering, no. 56.

[12] R. Blackburn and C. D. Taylor, "On the Electromagnetic Fields from a Hybrid Type of EMP Simulator," *IEEE Transactions on Electromagnetic Compatibility*, vol. EMC-20, no. 1, pp. 240–247, Feb. 1978.

[13] L. N. Walker, G. Ott, A. L. Day, and D. T. Wong, "Modification and Performance Evaluation of the Faster-Than-Real-Time Hybrid Simulator," *IEEE Transactions on Power Apparatus and Systems*, vol. PAS-97, no. 5, pp. 1795–1804, Sep. 1978.

[14] H. Doi, M. Goto, T. Kawai, S. Yokokawa, and T. Suzuki, "Advanced power system analogue simulator," *IEEE Transactions on Power Systems*, vol. 5, no. 3, pp. 962–968, Aug. 1990.

[15] R. Kuffel, J. Giesbrecht, T. Maguire, R. Wierckx, and P. McLaren, "RTDS-a fully digital power system simulator operating in real time," in *, 1995 International Conference on Energy Management and Power Delivery, 1995. Proceedings of EMPD '95*, vol. 2, Nov. 1995, pp. 498–503 vol.2.

[16] N. Junod, P. Allenbach, S. Robert, B. Kawkabani, A. Hodder, and G. Banyai, "HIL Simulation of a mixed islanded power network with external DSP regulator," in *2010 XIX International Conference on Electrical Machines (ICEM)*, 2010, pp. 1–6.

[17] A. Hodder and B. Kawkabani, "An advanced teaching lab for the setting up of an islanded production unit," in *2012 XXth International Conference on Electrical Machines (ICEM)*, Sep. 2012, pp. 2046–2052.

[18] S. Phatanapherom, P. Uthayopas, and V. Kachitvichyanukul, "Fast simulation model for grid scheduling using HyperSim," in *Simulation Conference, 2003. Proceedings of the 2003 Winter*, vol. 2, Dec. 2003, pp. 1494–1500 vol.2.

[19] M. Ourari, L.-A. Dessaint, and V. Q. Do, "Integration of Dynamic Equivalents in Hypersim Power System Simulator," in *IEEE Power Engineering Society General Meeting, 2007*, Jun. 2007, pp. 1–6.

[20] "EMTP-RV," Jul. 2015. [Online]. Available: http://emtp.com/

[21] "Simulink," Jul. 2015. [Online]. Available: http://ch.mathworks.com/products/simulink/

[22] M. Matar and R. Iravani, "FPGA Implementation of the Power Electronic Converter Model for Real-Time Simulation of Electromagnetic Transients," *IEEE Transactions on Power Delivery*, vol. 25, no. 2, pp. 852–860, Apr. 2010.

[23] R. Razzaghi, F. Colas, X. Guillaud, M. Paolone, and F. Rachidi, "Hardware-in-the-Loop Validation of an FPGA - Based Real-Time Simulator for Power Electronics Applications," *IPTS International Conference on POwer System Transients*, 2015.

[24] S.-M. Baek, S. Nam, J. Song, J. Lee, T. Kim, and J. Shin, "Design of Advanced Voltage Management System Including Manual Operation Mode via Real-Time Digital Simulator," *IEEE Transactions on Industry Applications*, vol. 49, no. 4, pp. 1817–1826, Jul. 2013.

[25] A. Ahmidi, X. Guillaud, Y. Besanger, and R. Blanc, "A Multilevel Approach for Optimal Participating of Wind Farms at Reactive Power Balancing in Transmission Power System," *IEEE Systems Journal*, vol. 6, no. 2, pp. 260–269, Jun. 2012.

[26] O. Richardot, A. Viciu, Y. Besanger, N. HadjSaid, and C. Kieny, "Coordinated Voltage Control in Distribution Networks Using Distributed Generation," in *Transmission and Distribution Conference and Exhibition, 2005/2006 IEEE PES*, May 2006, pp. 1196–1201.

[27] A. Roscoe, A. Mackay, G. Burt, and J. McDonald, "Architecture of a Network-in-the-Loop Environment for Characterizing AC Power-System Behavior," *IEEE Transactions on Industrial Electronics*, vol. 57, no. 4, pp. 1245–1253, Apr. 2010.

[28] A. Teninge, Y. Besanger, F. Colas, H. Fakham, and X. Guillaud, "Real-time simulation of a medium scale distribution network: Decoupling method for multi-CPU computation," in *Complexity in Engineering (COMPENG), 2012*, Jun. 2012, pp. 1–6.

[29] S. Sun, M. Dong, and B. Liang, "Real-Time Power Balancing in Electric Grids With Distributed Storage," *IEEE Journal of Selected Topics in Signal Processing*, vol. 8, no. 6, pp. 1167–1181, Dec. 2014.

[30] C. Dufour, J. Mahseredjian, and J. Belanger, "A Combined State-Space Nodal Method for the Simulation of Power System Transients," *IEEE Transactions on Power Delivery*, vol. 26, no. 2, pp. 928–935, Apr. 2011.

[31] C. Dufour, H. Saad, J. Mahseredjian, and J. Bélanger, "Custom-Coded Models in the State Space Nodal Solver of ARTEMiS," in *Proc. IPST*, Vancouver, BC, Canada, 2013.

Bibliography

[32] S. Sarri, M. Paolone, R. Cherkaoui, A. Borghetti, F. Napolitano, and C. Nucci, "State estimation of Active Distribution Networks: Comparison between WLS and iterated kalman-filter algorithm integrating PMUs," in *2012 3rd IEEE PES International Conference and Exhibition on Innovative Smart Grid Technologies (ISGT Europe)*, Oct. 2012, pp. 1–8.

[33] L. Vanfretti, S. Bengtsson, V. Peric, and J. Gjerde, "Spectral estimation of low-frequency oscillations in the Nordic grid using ambient synchrophasor data under the presence of forced oscillations," in *PowerTech (POWERTECH), 2013 IEEE Grenoble*, Jun. 2013, pp. 1–6.

[34] R. Majumder, B. Pal, C. Dufour, and P. Korba, "Design and real-time implementation of robust FACTS controller for damping inter-area oscillation," *IEEE Transactions on Power Systems*, vol. 21, no. 2, pp. 809–816, May 2006.

[35] A. Domahidi, B. Chaudhuri, P. Korba, R. Majumder, and T. Green, "Self-tuning flexible ac transmission system controllers for power oscillation damping: a case study in real time," *IET Generation, Transmission Distribution*, vol. 3, no. 12, pp. 1079–1089, Dec. 2009.

[36] A. Yamane, W. Li, J. Belanger, T. Ise, I. Iyoda, T. Aizono, and C. Dufour, "A Smart Distribution Grid Laboratory," in *IECON 2011 - 37th Annual Conference on IEEE Industrial Electronics Society*, Nov. 2011, pp. 3708–3712.

[37] C. Dufour and J. Belanger, "Real-Time Simulation of Fuel Cell Hybrid Electric Vehicles," in *International Symposium on Power Electronics, Electrical Drives, Automation and Motion, 2006. SPEEDAM 2006*, May 2006, pp. 930–936.

[38] C. Dufour, T. Ishikawa, S. Abourida, and J. Bélanger, "Modern Hardware-In-the-Loop Simulation Technology for Fuel Cell Hybrid Electric Vehicles," in *IEEE Vehicle Power and Propulsion Conference, 2007. VPPC 2007*, Sep. 2007, pp. 432–439.

[39] A. Myaing, M. Faruque, V. Dinavahi, and C. Dufour, "Comparison of insulated gate bipolar transistor models for FPGA-based real-timesimulation of electric drives and application guideline," *IET Power Electronics*, vol. 5, no. 3, pp. 293–303, Mar. 2012.

[40] H. Tiegna, Y. Amara, and G. Barakat, "New line-starting method of a class of synchronous motors," in *Electric Machines Drives Conference (IEMDC), 2013 IEEE International*, May 2013, pp. 1471–1476.

[41] J.-N. Paquin, W. Li, J. Belanger, L. Schoen, I. Peres, C. Olariu, and H. Kohmann, "A modern and open real-time digital simulator of All-Electric Ships with a multi-platform co-simulation approach," in *IEEE Electric Ship Technologies Symposium, 2009. ESTS 2009*, Apr. 2009, pp. 28–35.

[42] K.-C. Lee, j.-W. Jeon, D.-H. Hwang, and Y.-J. Kim, "Comparison between software simulation and HIL simulation of antiskid brake system for aircrafts," in *31st Annual Conference of IEEE Industrial Electronics Society, 2005. IECON 2005*, Nov. 2005, pp. 6 pp.–.

[43] F. Blanquez, E. Rebollo, F. Blazquez, and C. Platero, "Real time power plant simulation platform for training on Electrical Protections and Automatic Voltage Regulators," in *2013 12th International Conference on Environment and Electrical Engineering (EEEIC)*, May 2013, pp. 150–155.

[44] M. Han, A. Beguin, C. Nicolet, and B. Kawkabani, "Advanced condition monitoring system for synchronous machines based on real-time simulation," in *2014 International Conference on Electrical Machines (ICEM)*, Sep. 2014, pp. 1485–1491.

[45] A. Sapin, "Logiciel Modulaire pour la simulation et l'étude des systèmes d'entraînement et des réseaux électriques," Ph.D. dissertation, EPFL, Lausanne, 1995.

[46] "SORCUS," May 2015. [Online]. Available: http://www.sorcus.com/

[47] P. Kundur, *Power System Stability and Control*, 1994.

[48] A. Fitzgerald, C. Kingsley Jr., and S. D. Umans, *Electric Machinery 6th Ed.*, ser. McGraw-Hill Higher Education, 2003, no. McGraw-Hill series in electrical engineering. Power and energy.

[49] S. J. Chapman, *Electric Machinery Fundamentals 4th Ed.* McGraw-Hill Higher Education, 2005.

[50] M. Jufer, *Électromécanique*, ser. Traité d'Électricité. Lausanne: Presses Polytechniques Romandes, 1995, vol. IX.

[51] R. Park, "Two-reaction theory of synchronous machines generalized method of analysis-part I," *American Institute of Electrical Engineers, Transactions of the*, vol. 48, no. 3, pp. 716–727, Jul. 1929.

[52] I. M. Canay, "Determination of model parameters of synchronous machines," *Electric Power Applications, IEE Proceedings B*, vol. 130, no. 2, pp. 86–94, 1983.

[53] R. Patton, "Fault detection and diagnosis in aerospace systems using analytical redundancy," in *IEE Colloquium on Condition Monitoring and Fault Tolerance*, Nov. 1990, pp. 1/1–120.

[54] R. Patton and S. Kangethe, "Robust fault diagnosis using the model-based approach," in *IEE Colloquium on Condition Monitoring and Failure Diagnosis - Part 1*, Nov. 1988, pp. 2/1–213.

[55] F. Gonzalez and W. J. Davis, "Initializing on-line simulations from the state of a distributed system," in *Simulation Conference Proceedings, 1998. Winter*, vol. 1, Dec. 1998, pp. 507–513 vol.1.

[56] Y. Sun, J. Fang, and Y. Han, "A Distributed Real-Time Storage Method for Stream Data," in *Web Information System and Application Conference (WISA), 2013 10th*, Nov. 2013, pp. 314–317.

[57] W. Ma, Y. Chen, and D. Yao, "PC-based real-time simulator and its application on testing of power plant auxiliary system control," in *2010 International Conference on Power System Technology (POWERCON)*, Oct. 2010, pp. 1–4.

[58] I. E. Commission, "Methods for determining synchronous machine quantities from tests," *IEC 60034*, vol. 4, pp. 1–158, 2008.

[59] "IEEE Guide for Test Procedures for Synchronous Machines, Part I - Acceptance and Performance Testing, Part II - Test Procedures and Parameter Determination for Dynamic Analysis," *IEEE Std 115-2009 (Revision of IEEE Std 115-1995)*, pp. 1–219, May 2010.

[60] R. V. Shepherd and C. E. Kilbourne, "The quadrature synchronous reactance of salient-pole synchronous machines," *Electrical Engineering*, vol. 62, no. 11, pp. 684–689, Nov. 1943.

[61] L. Yanping and C. Weihua, "Numerical calculation of stator end-leakage reactance of large turbogenerator," in *Proceedings of the Fifth International Conference on Electrical Machines and Systems, 2001. ICEMS 2001*, vol. 1, 2001, pp. 170–173 vol.1.

[62] T. Cox, F. Eastham, and J. Proverbs, "End Turn Leakage Reactance of Concentrated Modular Winding Stators," *IEEE Transactions on Magnetics*, vol. 44, no. 11, pp. 4057–4061, Nov. 2008.

[63] S. Beckwith, "Approximating Potier Reactance," *Electrical Engineering*, vol. 56, no. 7, pp. 813–818, Jul. 1937.

[64] S. L. Mikhail, "Potier reactance for salient-pole synchronous machines," *American Institute of Electrical Engineers, Transactions of the*, vol. 69, no. 1, pp. 235–238, Jan. 1950.

[65] T. Hikihara and T. Okajima, "Physical meaning of the Potier triangle based on the analysis of magnetic flux saturation," *IEEE Transactions on Magnetics*, vol. 24, no. 5, pp. 2186–2193, 1988.

[66] R. de Carbalho Padilha, "Effect of the damper winding on transient behavior of salient pole synchronous machines," Master thesis, EPFL, Lausanne, Mar. 2015.

List of Symbols

Acronyms

ABS	Anti skid Brake System
AD/DA	Analog-Digital/Digital-Analog
CO_2	Carbon dioxide
COTS	Commercially Off-The-Shelf
CPU	Central Processing Unit
DCT	Dual-Clutch Transmission
DLL	Dynamic-Link Library
DSP	Digital Signal Processor
EMT	Electromagnetic Transient
EPFL	École Polytechnique Fédérale de Lausanne
FACTS	Flexible AC Transmission System
FPGA	Field-Programmable Gate Array
HIL	Hardware-in-the-Loop

List of Symbols

I/O   Input/Output

IGBT   Insulated-Gate Bipolar Transistor

IKF   Iterative Kalman Filter

LMI   Linear Matrix Inequalities

MMT   Multi-Media Timer

OECD   Organization for Economic Cooperation and Development

OS   Operating System

PC   Personal Computer

PCI   Peripheral Component Interconnect

PHIL   Power Hardware-in-the-Loop

PSS   Power System Stabilizer

PV   Photo Voltaic

RCP   Rapid Control Prototyping

RMS   Root Mean Square

RT   Real-Time

SIL   Software-in-the-Loop

SIMSEN   Simulation Modulaire pour Système Energétique

SSN   State-Space-Nodal

SVC   Secondary Voltage Controller

UI   User Interface

Greek

λ Local loss coefficient   [–]

ϕ Phase angle between the current and voltage   [rad]

ω_m Nominal pulsation of the shaft   [rad/s]

ω_n	Nominal pulsation of the power network	[rad/s]

Latin

A	Cross section of a pipe	[m^2]
a	Wave speed of the water in a pipe	[m/s]
C_{ST}	Surge tank equivalent capacitance	[m^2]
C	Hydraulic capacitance	[H/m]
D_{ref}	Turbine wheel average diameter	[m]
D	Diameter of a pipe	[m]
f_0	Electro-mechanical local mode	[Hz]
f	Frequency	[Hz]
g	Gravitational acceleration ($g \simeq 9.81$ m/s^2)	[m/s^2]
h_c	Surge tank piezometric head	[mWC]
H_d	Surge tank head losses	[mWC]
H_{ST}	Surge tank total head	[mWC]
H_v	Valve piezometric head	[mWC]
H	Turbine head drop	[mWC]
h	Piezometric head	[mWC]
i_D	Current of the damper winding in the direct-axis	[pu]
i_d	Current in the direct-axis	[pu]
I_f	Current of the excitation circuit	A
i_f	Current of the excitation circuit	[pu]
i_o	Zero phase-sequence current	[pu]
i_Q	Current of the damper winding in the quadrature-axis	[pu]
i_q	Current in the quadrature-axis	[pu]

List of Symbols

J	Inertia of the rotor	$[kgm^2]$
K_d	Surge tank head loss coefficient	[–]
K_t	Turbine head loss coefficient	[–]
K_v	Valve head loss coefficient	[–]
L	Hydraulic inductance	[H/m]
N_{11}	Pelton turbine speed factor	[rpm·m$^{1/2}$]
N	Speed	[rpm]
P	Active power	[W]
p	Pair pole	[–]
Q_c	Surge tank stored discharge	[m^3/s]
Q_{11}	Pelton turbine discharge factor	[m$^{1/2}$/s]
Q_{inj}	Discharge of injector	[m^3/s]
Q_{tot}	Total discharge in the turbine	[m^3/s]
Q	Reactive power	[Var]
Q	Water discharge	[m^3/s]
R_d	Surge tank equivalent resistance	[s/m^2]
R_t	Pelton turbine equivalent resistance	[s/m^2]
r_D	Resistance of the damper winding in the direct-axis	[pu]
R_{inj}	Resistance of injector	[s/m^2]
r_Q	Resistance of the damper winding in the quadrature-axis	[pu]
r_s	Resistance of the armature winding	[pu]
R_v	Valve hydraulic resistance	[H/m]
R	Hydraulic resistance	[H/m]
T_{11}	Pelton turbine torque factor	[N/m^3]
T_{add}	Communication time with external devices	[s]

124

T'_{do}	Opened-circuit transient time constant in the direct–axis	[s]
T''_{do}	Opened-circuit sub-transient time constant in the direct–axis	[s]
T'_d	Short-circuit transient time constant in the direct–axis	[s]
T''_d	Short-circuit sub-transient time constant in the direct–axis	[s]
T_{em}	Electromagnetic torque	[Nm]
T_{int}	Integration time	[s]
T_n	Time reference	[s]
T''_q	Sub-transient time constant in the quadrature–axis	[s]
T_{step}	Simulation time step	[s]
T	Turbine mechanical torque	[Nm]
u_d	Voltage in the direct-axis	[pu]
u_f	Voltage of the excitation circuit	[pu]
u_o	Voltage in the zero-axis	[pu]
u_q	Voltage in the quadrature-axis	[pu]
$x_{\sigma Df}$	Exclusive mutual reactance between excitation circuit and damper winding	[pu]
$x_{\sigma D}$	Leakage reactance of the damper winding in the direct-axis	[pu]
$x_{\sigma d}$	Leakage reactance in the direct–axis	[pu]
$x_{\sigma f}$	Leakage reactance of the excitation circuit in the direct-axis	[pu]
$x_{\sigma Q}$	Leakage reactance of the damper winding in the quadrature-axis	[pu]
$x_{\sigma q}$	Leakage reactance in the quadrature-axis	[pu]
x_σ	Leakage reactance of stator winding	[pu]
x_{ad}	Magnetizing reactance in the direct–axis	[pu]
x_{aq}	Magnetizing reactance in the quadrature-axis	[pu]
x_c	Canay reactance	[pu]
x_d	Synchronous reactance in the direct–axis	[pu]

List of Symbols

x'_d	Transient reactance in the direct–axis	[pu]
x''_d	Sub-transient reactance in the direct–axis	[pu]
x_o	Magnetizing reactance in the in the zero-axis	[pu]
x_p	Potier reactance	[pu]
x_q	Synchronous reactance in the quadrature–axis	[pu]
x'_q	Transient reactance in the quadrature–axis	[pu]
x''_q	Sub-transient reactance in the quadrature–axis	[pu]
y_{inj}	Nozzle position of injector	[–]

Matrices and Vectors

A	Global matrix	
B	Auxiliary matrix	
C	Boundary conditions vector	
X	State vector	

Michel HAN | Curriculum Vitæ

michel.han@a3.epfl.ch

• Date of birth:26.02.1986 • Nationality:Switzerland

Education

Swiss Institute of Technology	**Lausanne**
Ph.D. in Electrical Engineering, Energy Doctorate School	*2012–2015*
Swiss Institute of Technology	**Lausanne**
M.Sc. in Electrical Engineering, Power and Energy Orientation	*2009–2011*
Swiss Institute of Technology	**Lausanne**
B.Sc. in Electrical Engineering	*2005–2009*

Professional Experience

Vocational..

EPFL   **Lausanne**

Teaching and Research Assistant   *2012–2015*

- Investigation of real-time simulation in SIMSEN with a general-purpose computer
  for a model-based monitoring application.
- Teaching assistant in the courses : "Electromechanical Energy Conversion", "Electrical Machines",
  "Transients of Electrical Machines" and "laboratory of Electrical Machines".

JTEKT   **Nara**

Internship   *2011–2012*

Development of control system for an all-mechanical valve in piston engine

ETRI   **Daejeon**

Internship   *2009*

Research and literature archiving of Linux bounding Driver

Miscellaneous...

ADELE   **Lausanne**

Committee   *2005–2009*

Student association in electrical engineering
Member of committee (2005-2007) and president of committee (2007-2009)

LUC Badminton   **Lausanne**

Nuit du Badminton   *2013–2015*

Sport event to promote the badminton (president of organization)
http://www.lucbadminton.ch/nuit

Languages

French: Native

English: Fluent reading, writing, speaking

Korean: Mother tongue
Japanese: Fair speaking, writing, reading
German: Basic knowledge

Computer skills

Simulation tool: Matlab, SIMSEN
Programming language: Visual Basic, C/C++
Office tool: MS office, MS Visio, Latex

Publications

[1] M. Han, A. Beguin, C. Nicolet, and B. Kawkabani. Advanced condition monitoring system for synchronous machines based on real-time simulation. In *2014 International Conference on Electrical Machines (ICEM)*, pages 1485–1491, September 2014.

[2] M. Han, B. Kawkabani, and J.-J. Simond. Eigenvalues analysis applied to the stability study of a variable speed pump turbine unit. In *2012 XXth International Conference on Electrical Machines (ICEM)*, pages 907–913, September 2012.